

Spring 2012

Observational studies of scatterometer ocean vector winds in the presence of dynamic air-sea interactions

Amanda Michael Plagge
University of New Hampshire, Durham

Follow this and additional works at: <https://scholars.unh.edu/dissertation>

Recommended Citation

Plagge, Amanda Michael, "Observational studies of scatterometer ocean vector winds in the presence of dynamic air-sea interactions" (2012). *Doctoral Dissertations*. 656.
<https://scholars.unh.edu/dissertation/656>

This Dissertation is brought to you for free and open access by the Student Scholarship at University of New Hampshire Scholars' Repository. It has been accepted for inclusion in Doctoral Dissertations by an authorized administrator of University of New Hampshire Scholars' Repository. For more information, please contact nicole.hentz@unh.edu.

**OBSERVATIONAL STUDIES OF SCATTEROMETER
OCEAN VECTOR WINDS IN THE PRESENCE OF
DYNAMIC AIR-SEA INTERACTIONS**

BY

AMANDA MICHAEL PLAGGE

Bachelor of Arts, Dartmouth College, 2003
Bachelor of Engineering, Thayer School of Engineering, 2004
Master of Science, Dartmouth College, 2006

DISSERTATION

Submitted to the University of New Hampshire
in partial fulfillment of
the requirements for the Degree of

Doctor of Philosophy

in

Earth and Environmental Science: Oceanography

May 2012

UMI Number: 3525064

All rights reserved

INFORMATION TO ALL USERS

The quality of this reproduction is dependent upon the quality of the copy submitted.

In the unlikely event that the author did not send a complete manuscript and there are missing pages, these will be noted. Also, if material had to be removed, a note will indicate the deletion.

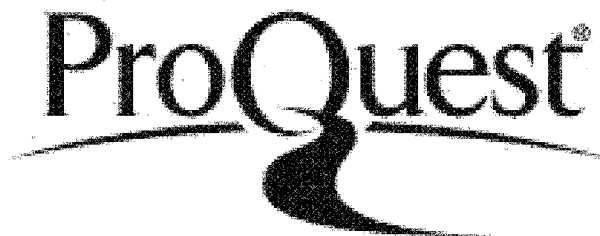


UMI 3525064

Published by ProQuest LLC 2012. Copyright in the Dissertation held by the Author.

Microform Edition © ProQuest LLC.

All rights reserved. This work is protected against
unauthorized copying under Title 17, United States Code.

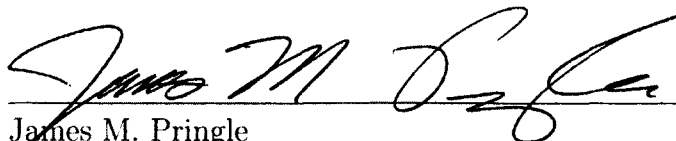


ProQuest LLC
789 East Eisenhower Parkway
P.O. Box 1346
Ann Arbor, MI 48106-1346

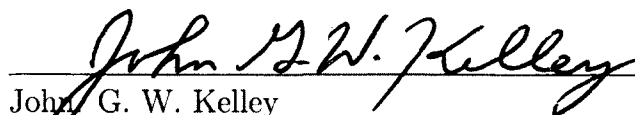
This dissertation has been examined and approved.



Dissertation Director: Douglas Vandemark
Research Associate Professor of Earth Sciences
Institute for the Study of Earth, Oceans, and Space
University of New Hampshire



James M. Pringle
Associate Professor of Earth Sciences
Institute for the Study of Earth, Oceans, and Space
University of New Hampshire



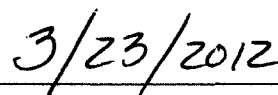
John G. W. Kelley
Affiliate Assistant Professor of Ocean Engineering
University of New Hampshire &
NOAA National Ocean Service



John R. Moisan
Research Oceanographer
NASA Goddard Space Flight Center



Bertrand Chapron
Director, Spatial Oceanography Lab
IFREMER, France



Date

ACKNOWLEDGMENTS

I would like to thank my friends, colleagues, and professors at UNH for their support in my pursuance of this doctorate and an academic career. First and foremost, without the encouragement, guidance, and patience of my advisor, Doug Vandemark, none of this would have been possible. The other members of my committee – Bertrand Chapron, John Kelley, John Moisan, and James Pringle – have been extremely flexible and helpful throughout the process, especially during the last few months of complications. My fellow graduate students have provided solace, reassurance, and laughter at the most crucial moments, and helped make my entire time at UNH rewarding on many levels. Special thanks also to Jen Bourgeault in the NRESS office and Dovev Levine in the Graduate School office, who have greatly assisted me with the practical details of completing a degree and a dissertation.

Outside of UNH, I have been extremely fortunate in my collaborators, and would like to thank all of them, including Dr. David Long at Brigham Young University, Dr. Ernesto Rodriguez and colleagues at JPL, and most especially Dr. Jim Edson at the University of Connecticut, without whose help I (and Chapter 4) would have been lost.

My thanks also go out to my family – immediate, extended, and adopted – for believing in me and in my insistence in completing what must have seemed like far too many years of school. Most crucially, thank you to my husband Jordan, for everything.

This research was supported by a NASA/UNH Research and Discover Fellowship (2006-2008), a NH Space Grant Fellowship (2008-2009), and a NASA Graduate Student Research Program Fellowship (2009-2012). Non-financial support for 2010-2012 was also provided through NASA's Ocean Vector Winds Science Team.

TABLE OF CONTENTS

ACKNOWLEDGMENTS	iii
LIST OF TABLES	vii
LIST OF FIGURES	viii
ABSTRACT	xiii
1 Introduction	1
1.1 Statement of Problem	2
1.1.1 Scatterometer “wind”?	2
1.1.2 Equivalent neutral wind	3
1.1.3 Accuracy of scatterometer winds	4
1.1.4 Investigation of differences	5
1.1.5 Oceanic effects: Currents	6
1.1.6 Atmospheric case: Stability	7
1.1.7 Questions to answer	9
1.2 Objectives and overview of dissertation organization	9
2 Coastal Validation of Ultra-High Resolution Wind Vector Retrieval from QuikSCAT in the Gulf of Maine	15
2.1 Prologue	15
2.2 Abstract	15
2.3 Introduction	16
2.4 Methods	18
2.4.1 Data	18
2.4.2 Statistical analysis	19
2.4.3 Ambiguity re-selection	20
2.5 Results	22

2.5.1	Speed and direction	22
2.5.2	Near-shore coverage	26
2.5.3	Illustration of one potential UHR-RS benefit	27
2.6	Conclusion	28
3	Examining the impact of surface currents on satellite scatterometer and altimeter ocean winds	31
3.1	Prologue	31
3.2	Abstract	31
3.3	Introduction	32
3.4	Data and Methods	36
3.5	Results	42
3.6	Discussion	50
3.7	Conclusions	56
3.8	Acknowledgments	57
3.9	Appendix	58
3.9.1	Directional Impacts	58
3.9.2	Spatial Case Study Challenges	59
4	A note on the interpretation of scatterometer winds near sea surface temperature fronts	66
4.1	Prologue	66
4.2	Abstract	66
4.3	Introduction	67
4.3.1	Marine Atmospheric Boundary Layer Dynamics and Monin-Obukhov Similarity Theory	68
4.3.2	Overview of Scatterometry	72
4.3.3	Scatterometry and SST Fronts	74
4.3.4	Hypotheses and Approach	75
4.4	Data and Methods	76
4.4.1	Overview of CLIMODE and <i>In Situ</i> Data	76

4.4.2	Scatterometer Data	80
4.5	Results	81
4.5.1	Surface Layer Adjustment	81
4.5.2	Boundary Layer Adjustment	83
4.5.3	Stress Perturbations	86
4.6	Discussion	86
4.6.1	Importance of SLA in Causing Wind Changes Across SST Fronts . .	86
4.6.2	Boundary Layer Adjustment Shown with ΔT and with SST Perturbation	89
4.6.3	Validation of Baroclinic Effects	91
4.6.4	Additional Effects of SST on Scatterometry	92
4.7	Conclusions	93
5	Overall Conclusions	100
5.1	Summary	100
5.2	Future work and implications	101
5.2.1	Support for further scatterometer missions	101
5.2.2	Ocean Modeling: wind work and curl of wind stress	102
5.2.3	Offshore wind resource for power generation	103
5.2.4	Equivalent neutral wind versus wind stress	103

List of Tables

2.1	Data summary for 2006; $ U $ indicates magnitude residuals, ϕ indicates directional residuals, “NS” and “OS” are nearshore and offshore respectively.	25
3.1	Slopes, intercepts, and their uncertainties for the weighted least squares fit of wind speed residuals (m s^{-1}) versus u_p for different QuikSCAT resolutions and for different buoys.	45
3.2	Statistics from the same weighted least squares fit of wind residuals versus currents as for Table 3.1 but after filtering for different air-sea interface conditions. Significant wave height and the Monin-Obukov stability length scale parameter (L) come from buoy observations; stability of boundary layer is based on definitions in Large and Pond (1982). Results are for combined buoy L and N datasets.	47

List of Figures

2-1	Buoy network in the Gulf of Maine. <i>Acknowledgments: NOAA's National Data Buoy Center and the Gulf of Maine Ocean Observing System</i>	19
2-2	UHR and buoy wind magnitude for Jan 16, 2006; sub-sampled (every 4th) unit wind vectors shown in black; buoy speeds in circles ("x" indicates no data).	20
2-3	L2B 12.5 km and buoy wind magnitude for Jan 16, 2006; sub-sampled (every 10th) unit wind vectors shown in black buoy speeds in circles ("x" indicates no data).	21
2-4	Pixel-level comparison of UHR speed and direction before and after re-selection routine. Pixel color indicates direction in degrees. Arrows on rose show wind vectors from the UHR pixels (blue) and a nearby buoy (bold black).	22
2-5	Summary of scatterometer-minus-buoy residuals for 2006, plotted according to buoy wind speed. Green indicates 25 km data, red 12.5 km, and blue UHR-RS.	23
2-6	Summary of scatterometer-minus-buoy residuals for 2006, plotted according to buoy station (arranged according to distance from shore). Green indicates 25 km data, red 12.5 km, and blue UHR-RS.	24
2-7	Cummulative pixel center locations in January 2006: 3 types of QuikSCAT data.	26
2-8	Evidence of roll vortices during northwest flow event, January 16, 2006. White arrow shows prevailing wind direction.	27
3-1	Map of the Gulf of Maine region in the northeast US and Canada including bathymetry and with the inset showing the study site. Star symbols indicate regional observing system buoys (black) with this study's surface current and wind measurement time series nodes, buoys N and L, shown in white.	36

3-2	Histogram of observed surface current magnitude for both buoys within the collocated datasets.	37
3-3	Histogram of observed wind and surface current direction for both buoys L and N (upper panel) and the directional difference between the wind and the current (lower). Both are provided using meteorological convention (direction from which the fluid arrives) and both are derived from the datasets used in Fig. 3-2.	38
3-4	Wind speed measurement comparisons between the earth-relative buoy and collocated QuikSCAT observations at a) buoy L, b) buoy N, and c) data for both sites. Panels across each row represent the differing QuikSCAT wind products with highest resolution UHR data on the left, the 12.5 km product in the middle, and the 25 km on the right. A dashed line provides the result from a linear regression fit; this fit and the correlation coefficient are noted in the upper left of each panel.	41
3-5	Wind speed differences (QuikSCAT - buoy) versus the projected surface current velocity u_p with results provided for each QuikSCAT wind product. Data represent all wind, wave, and current conditions within the datasets at buoys L and N. The sample population (N) is noted in each panel.	43
3-6	Bin-averaged wind speed differences (QuikSCAT - buoy) versus u_p (10 cm s^{-1} bins) for the same datasets in Fig. 3-5. Error bars represent standard error within each bin. The black dashed curve represents a -1:1 line while the gray dot-dashed is the result from a weighted linear regression (see text). Sample population is noted on each panel.	44
3-7	Binned wind speed residuals (QuikSCAT minus buoy) versus the effective surface current for the conditions chosen to show the best correlation: moderate wind speed and neutral atmospheric stability. This and all subsequent binned figures follow the methodology of Fig. 3-6).	46
3-8	Binned wind speed residuals (QuikSCAT minus buoy) versus the effective surface current for conditions giving worst correlation: light wind and unstable boundary layer.	48

3-9	Wind speed differences (ASCAT - buoy) versus the projected surface current velocity u_p with results provided for each ASCAT wind product. Data represent all wind, wave, and current conditions within the dataset at buoy N, 2007-2011.	49
3-10	Wind speed differences (ASCAT minus buoy) binned according to u_p (see Fig 3-9 for correlations).	50
3-11	Wind speed differences (Altimeter - buoy) versus projected surface current velocity u_p . Data represent all wind, wave, and current conditions within the collocated dataset at buoy N, 2004-2011.	51
3-12	Residuals for altimeter minus buoy N wind speeds, binned according to u_p	51
3-13	Spatial view of surface current effects on a QuikSCAT pass from 23:01 UTC Dec. 26, 2008, for the region southwest of Nova Scotia, depicted as a black box in Fig. 3-1. (a) FVCOM surface current magnitude (grayscale) and vectors (black arrows) from a run at 22:58 UTC Dec. 26, 2008. (b) WRF wind speed from a model run at 00:00 UTC Dec. 27, 2008 with white arrows showing subsampled WRF wind vectors. (c) 12km QuikSCAT wind speed; here white arrows show subsampled QuikSCAT wind vectors. (d) Windspeed residual (scatterometer minus model), including an offset determined by the mean wind speed difference and the mean current speed within the ROI.	55
3-14	Bin-averaged wind speed differences (QuikSCAT - buoy) versus u_p (10 cm s ⁻¹ bins) for the same datasets used in Figs. 3-5 and 3-6. Error bars represent standard error within each bin. The gray dot-dashed line is the result from a weighted linear regression (see text). Sample populations and correlation coefficients are noted on each panel.	59
4-1	Map of the eastern coast of the US, showing SST from the AVHRR sensor. Buoy location indicated by circle. Acknowledgements to the Ocean Remote Sensing Group of Johns Hopkins University Applied Physics Laboratory.	77

4-2	Surface pressure, winds and latent heat flux at 12 UTC on 27 January 2006 showing a cyclone to the north of Newfoundland drawing cold, dry air over the Gulf Stream. From Marshall et al. (2009).	78
4-3	The 2.8 m discus mooring deployed from November 2005 to November 2006. It was replaced by an identical discus buoy that broke free of its mooring in February 2007.	79
4-4	Scatterplot showing collocated QuikSCAT wind speeds vs. buoy neutral winds for entire dataset ($N = 586$).	80
4-5	Plot of neutral wind speed difference (QuikSCAT wind speed minus buoy neutral wind speed) vs. z/L . Larger, bold circles indicate the average for each z/L bin; errorbars indicate standard error (SE, or standard deviation divided by the square root of the number of points in each bin)	81
4-6	Plot of speed difference from measured wind vs. z/L . Black dots indicate buoy neutral winds minus buoy measured winds; gray circles indicate scatterometer wind minus buoy measured wind. Binned averages for black dots are connected with the black line, and binned averages for the gray circles are indicated by larger, bold gray circles with errorbars indicating SE. . . .	82
4-7	Wind speed perturbations (means calculated for each 30-day period) binned according to ΔT ; black squares show measured buoy speed perturbations, black diamonds show buoy neutral wind perturbations, and gray circles show scatterometer wind perturbations; for each case, errorbars show SE.	83
4-8	Wind speed perturbations binned according to ΔT for instances of unstable atmosphere and cold air advection only; plot uses same methodology as in Fig. 4-7	84
4-9	Wind speed perturbations binned according to ΔT for instances of stable atmosphere and warm air advection only; plot uses same methodology as in Fig. 4-7	85
4-10	Histograms showing distribution of buoy wind direction, for all data and for limited “stable WAA” and “unstable CAO” cases.	86

4-11	Buoy direct-covariance wind stress perturbations binned according to ΔT for instances of unstable atmosphere and cold air advection only; plot uses same methodology as in Fig. 4-7	87
4-12	Buoy direct-covariance wind stress perturbations binned according to ΔT for instances of stable atmosphere and warm air advection only; plot uses same methodology as in Fig. 4-7	88
4-13	Plot of speed ratios to measured wind vs. z/L . Buoy neutral-to-measured wind ratios (U_{10N}/U_{10}) are shown as black dots with the bin-averaged values joined by a black line as in Fig. 4-6. The ratios of scatterometer-to-measured-buoy wind are shown in gray circles (U_{QS}/U_{10}), with bin-averaged values indicated by larger heavy gray circles with SE errorbars.	89
4-14	Buoy wind speed perturbations from U_{10} binned according to ΔT for instances of unstable atmosphere and cold air advection only; slopes indicated were determined using linear least squares fit and errorbars show SE. . . .	90
4-15	Wind speed perturbations binned according to ΔT_{sea} , methodology as in Fig. 4-7. Slope of 0.27 corresponds to the coupling coefficient given for the Gulf Stream in O'Neill et al. (2010a).	91
4-16	Wind speed perturbations binned according to ΔP_{air} , methodology as in Fig. 4-7. Slope of -0.27 corresponds to the opposite of the coupling coefficient given for the Gulf Stream in O'Neill et al. (2010a).	92

ABSTRACT
OBSERVATIONAL STUDIES OF SCATTEROMETER OCEAN
VECTOR WINDS IN THE PRESENCE OF DYNAMIC AIR-SEA
INTERACTIONS

by

Amanda Michael Plagge

University of New Hampshire, May, 2012

Ocean vector wind measurements produced by satellite scatterometers are used in many applications across many disciplines, from forcing ocean circulation models and improving weather forecasts, to aiding in rescue operations and helping marine management services, and even mapping energy resources. However, a scatterometer does not in fact measure wind directly; received radar backscatter is proportional to the roughness of the ocean's surface, which is primarily modified by wind speed and direction. As scatterometry has evolved in recent decades, highly calibrated geophysical model functions have been designed to transform this received backscatter into vector winds. Because these products are used in so many applications, it is crucial to understand any limitations of this process. For instance, a number of assumptions are routinely invoked when interpreting scatterometer retrievals in areas of complex air-sea dynamics without, perhaps, sufficient justification from supporting observations.

This dissertation uses satellite data, *in situ* measurements, and model simulations to evaluate these assumptions. Robustness is assured by using multiple types of satellite scatterometer data from different sensors and of different resolutions, including an experimental ultra-high resolution product that first required validation in the region of study. After this validation survey, a subsequent investigation used the multiple data resolutions to focus on the influence of ocean surface currents on scatterometer retrievals. Collocated scatterometer and buoy wind data along with buoy surface current measurements support the theory that scatterometer winds respond to the relative motion of the ocean surface; in other words, that they can effectively be considered current-relative, as has been generally assumed. Another major control on scatterometer retrievals is atmospheric stability, which

affects both surface roughness and wind shear. A study using wind, stress, temperature, and pressure measurements at a mooring in the Gulf Stream as well as collocated scatterometer data proved that the scatterometer responds as expected to changes in stability. Therefore, scatterometer retrievals can effectively be used to evaluate changes in wind due to speed adjustment over temperature fronts. Given the conclusions of these individual studies, this work collectively solidifies decades of theory and validates the use of scatterometer winds in areas of complex air-sea interaction.

CHAPTER 1

Introduction

Satellite scatterometry has become a vital part of both scientific research and operational forecasting systems across the globe, providing vector winds over the global ocean, twice daily and in all weather¹. Ocean vector winds are used to force ocean circulation models, help marine management services, improve weather forecasts, aid in rescue operations, and even map energy resources. NASA’s most recent scatterometer, the SeaWinds sensor on the QuikSCAT satellite (“QuikSCAT”), was an active, Ku-band (at 13.4 GHz) scanning radiometer. For over ten years, it covered 90% of the globe in 24 hours, and the ocean wind data have been provided at spatial resolutions of 25, 12.5, and 2.5 km.

In the most general terms, the scatterometer wind retrieval process begins by measuring the reflectance of the radar signal off of the ocean’s surface (normalized radar cross-section, “backscatter”, or σ^0): the power received will be a function of the roughness of the surface. This roughness in turn is primarily determined by the strength of the wind blowing across the surface. Basically, this inversion from backscatter to wind vector works as follows: for a given set of σ^0 measurements, a geophysical model function (GMF) is inverted to provide multiple maximum likelihood estimates of wind speed and direction. More than one estimate is created because, although the first order response of backscatter is as a power law in wind speed, the response is modulated by direction, creating harmonics related to the relative azimuthal angle between wind and antenna directions [Hoffman and Leidner (2005)]. Normalized radar cross-section therefore contains information about the vector winds at the surface of the ocean.

¹Despite the purported “all weather” capability of scatterometers, many studies have shown that retrievals can be contaminated by moderate to heavy rainfall. Rain influences backscatter in two ways: by changing the surface roughness of the water, and by attenuating and scattering the radar signal as it passes through the droplets in the atmosphere (especially at QuikSCAT’s Ku-band frequency) [Chelton and Freilich (2005)]. Rain flags have been included in QuikSCAT data since 2002, and because these effects have been so well studied, they will not be discussed further here.

1.1 Statement of Problem

1.1.1 Scatterometer “wind”?

Although it is common to refer to scatterometer “winds,” the radar measures no such thing directly. As discussed above, radar backscatter can be interpreted to provide information about wind speed and direction using empirically formulated relationships. However, backscatter is actually directly related to the surface wave field which is itself dependent on many physical processes including wind. Given the radiation wavelength and angle of incidence of the QuikSCAT radar (about 2cm and 45 degrees), the sea-state can be neglected and the important waves are those of 2 to 20 cm [Nghiem et al. (1997)]. According to Phillips (1977), these capillary and short gravity waves are maintained through a combination of physical processes, including (but not limited to):

- the direct effect of surface pressure variations being due to air flow over waves, i.e., wind,
- resonance with atmospheric turbulence pressure fluctuations, and
- second order wave-wave interactions transferring energy between spectral components.

Therefore, although for a given σ^0 measurement the scatterometer’s geophysical model function has been designed to provide equivalent neutral wind (see next section), the received signal is also influenced by these other processes. In certain regions, such as coastal areas and western boundary currents, many of the other processes that affect the surface wave field– and therefore backscatter– are present to a greater degree than in most of the global ocean. Land-ocean and atmosphere-ocean coupling complicate the dynamics; along with orographic effects on wind and multi-scale weather patterns, strong air-sea temperature differences, fetch, strong currents and current gradients, breaking waves, and tidal signals all affect the wave field. **How do these dynamics affect scatterometer retrieval of wind speed and direction?**

1.1.2 Equivalent neutral wind

The geophysical product provided from QuikSCAT is equivalent neutral wind (ENW) at a reference height of 10 m [Ebuchi et al. (2002); Freilich and Dunbar (1999), etc]. Scatterometer studies have been performed for decades, using tower-based [Colton et al. (1995)], airborne [Weissman (1990); Weissman et al. (1997)] and previous spaceborne [Freilich and Dunbar (1999); Verschell et al. (1999); Weissman and Graber (1999)] sensors. Through those experiments, it was determined that the gravity-capillary waves on the surface of the ocean to which the radar backscatter responds are controlled by – are in equilibrium with – the wind stress at the ocean surface, τ [Liu and Tang (1996), e. g.]. Surface wind stress can be described as the vertical transfer of horizontal momentum through the air-sea interface, written as

$$|\tau| = \rho_a u_{*a}^2 \quad (1.1)$$

where ρ_a is air density, and u_{*a} is the friction velocity of air, or the magnitude of the velocity fluctuations in a turbulent atmospheric boundary layer flow [Jones and Toba (2001)]. This turbulent-driven momentum flux is generated by wind shear and buoyancy caused by vertical density gradients. Therefore, the relationship between wind stress and wind shear depends on the density stratification (stability) of the atmosphere [Liu and Tang (1996)]. This means that for a given backscatter measurement, the wind speed at a given reference level varies according to changing atmospheric conditions (vertical profiles of humidity and temperature). The actual wind (u) is thus not uniquely related to scatterometer measurements [Liu and Tang (1996)], but the construct of equivalent neutral wind (ENW), the wind that should exist at a given height in neutral atmospheric stability conditions, should be. For this reason, QuikSCAT's GMF has been tuned to relate measurements of backscatter to ENW at 10 m above the ocean surface.

The physical components of ENW can be explored through the following first-order model for the vertical profile of wind in the marine atmospheric boundary layer [Bourassa (2006); Kara et al. (2008)]:

$$\mathbf{U}(z) - \mathbf{U}_s = \frac{\mathbf{u}_{*a}}{\kappa} \left[\ln \frac{z}{z_0} + \phi(z, z_0, L) \right] \quad (1.2)$$

This expression takes into account the effects of atmospheric stability (as discussed above), but also includes the potential motion of the surface, i.e., ocean currents. $U(z)$ is the wind speed as a function of height and U_s is the surface current speed; together they give the wind speed relative to the surface (this will be discussed in more detail later). The parameter κ is the Von Karman's constant (0.4), and the term $\ln z/z_0$ refers to the approximately logarithmic increase in wind speed with height, and depends not only on height off of the ground (z) but on the properties of the surface (roughness length, z_0). The last term is a representation of the flow modification due to atmospheric stratification, given by the Monin-Obukhov parameter L , which will be described in greater detail in Chapter 4. If the atmosphere is stable, the ENW is relatively weaker than the wind that would be measured by an *in situ* anemometer. For unstable atmospheric stratification, the ENW would be stronger than an anemometer-measured wind at the same height (AMW). When there is no stratification (i.e., neutral stability, $z/L = 0$), the stability term given by ϕ is zero, ENW should equal anemometer wind, and the relationship between friction velocity and ENW is given by the drag coefficient, C_D :

$$\sqrt{C_D} = \frac{u_{*a}}{U_z} = \frac{\kappa}{\ln z/z_0} \quad (1.3)$$

Even the drag coefficient is not easy to parameterize, and is influenced by wind speed, the steadiness of the wind, atmospheric stability, sea-state, and changing fetch, to name just a few [Jones and Toba (2001); Kara et al. (2007)]. This will also be discussed further in Chapter 4.

1.1.3 Accuracy of scatterometer winds

Given this discussion, **how well do scatterometer-derived equivalent neutral winds represent surface ocean vector winds?** This is not a simple question, as the answer depends both on local air-sea conditions and on how the scatterometer winds will be applied: are they intended to represent anemometer winds, or wind stress? Many of the QuikSCAT wind model validation studies used anemometer-measured winds from buoy arrays. To compare scatterometer-retrieved ENW with buoy AMW, it is necessary to use a model to adjust the measured wind at an observed height to the equivalent neutral wind

at a standard height of 10 m. Many scatterometer studies use the Liu-Katsaros-Businger (or LKB) method as described in Liu et al. (1979) [Ebuchi et al. (2002); Freilich and Dunbar (1999)]. When compared with buoy data in open ocean areas, standard resolution QuikSCAT wind vectors satisfy the instrument science requirements of ± 2 m/s and 20° [Tang et al. (2004)]. A buoy comparison study by Chelton and Freilich (2005) indicates vector errors of 0.75 m/s alongwind and 1.5 m/s crosswind, and a similar study by Tang et al. (2004) gives a bias and RMS difference of 0.2, 0.95 m/s in speed and 4.83° , 17.41° in direction. Another buoy comparison for deep water indicates RMS differences of 1.01 m/s and 23° , and indicates that other than significant wave height, there is no dependence of the wind residuals on oceanographic and atmospheric parameters [Ebuchi et al. (2002)]. However, other studies show that in the coastal ocean, QuikSCAT winds of all resolutions are significantly different from *in situ* measurements [Pickett et al. (2003); Tang et al. (2004)]. According to Tang et al. (2004), this is indicative of the “difficulty in remotely measuring the vector wind in coastal regions, where ocean-atmosphere interactions are modified by land.”

1.1.4 Investigation of differences

Complex ocean-atmosphere dynamics take place in many regions of the globe, including coastal areas, where processes include but wave fetch limitation, coastal currents, ocean tides, land and sea breezes, strong air-sea temperature differences, atmospheric boundary layer transitions, and orographic effects [Accadia et al. (2007); Davidson et al. (1992)]. Given the relationships between backscatter, surface roughness, and wind speed/direction, it is quite clear that local meteorology and oceanography will modify the wave spectrum and therefore backscatter and ENW. For instance, winter offshore wind flow in a coastal ocean, like the Gulf of Maine, can result in a very cold air mass moving over warmer water, causing strong atmospheric instability which therefore affects the ϕ term in the ENW equation. Alternatively, strong tidal signals, as in the Bay of Fundy, will cause the surface water to be moving relative to the wind, affecting the left-hand side of the equation. These types of interactions are also typical near western boundary currents, known for both strong surface velocities and strong air-sea temperature gradients. Because the dynamics can be

complex, both between the ocean and atmosphere and between the surface interface and radar backscatter, attempting to quantify all processes that affect ENW in either of these regions can be extremely difficult. However, by choosing specific cases (geophysical regimes, or locations, or both) to investigate the effects of a given process while minimizing the effects of the other terms in the equation, it may be possible to better quantify the controls on equivalent neutral wind from scatterometer.

1.1.5 Oceanic effects: Currents

Ocean surface currents combine with wind to modulate the surface wave spectrum and therefore backscatter and retrieved wind from a scatterometer [Kudryavtsev et al. (2005); Quilfen et al. (2001)]. As noted in Quilfen et al. (2001), surface currents directly influence the short-wave growth, distorting the direct action of the wind and changing the reference frame “in a vector sense.” This idea is borne out in Kudryavtsev et al. (2005) as well, where the authors suggest that the effect of a surface current results in an anisotropy of short wind waves (see also Zhang et al. (2009)). These effects on the wave spectrum could skew the assumed relationship between backscatter pattern and wind direction, as well as affecting derived wind magnitude.

In addition to actual wave field modification, an artificial bias is created between ENW and AMW. As shown in Equation 3.1, the retrieved ENW is relative to the moving ocean surface; on the other hand, AMW is not. If the winds are blowing in the same direction as the current, the satellite-retrieved wind would be less than the wind measured by anemometer, even with the AMW corrected for stability and height. Likewise, for a current opposing the wind, the scatterometer ENW would indicate a stronger wind than the corrected AMW.

Several current-relative wind studies have used scatterometer retrievals in the open ocean, most focusing on this difference between AMW and ENW. Kelly et al. (2001), for instance, compares winds from the NASA Scatterometer (NSCAT, QuikSCAT’s predecessor) with wind and current data from the Tropical Atmosphere-Ocean (TAO) moored

instrument array. Their results indicate that the primary differences between anemometer and scatterometer zonal winds (in this region) are due to ocean currents. As it focused on an El Niño event, this particular study had a very strong signal to work with, and showed that (compared with AMW) the NSCAT winds were “too low” by about 0.5 m/s before the equatorial currents reversed, and “too high” after reversal. A similar 3-year study [Kelly et al. (2005)] used the TAO array but with QuikSCAT wind vectors and additional current information from radar altimetry and climatological currents and also showed a difference of about 0.5 m/s between TAO and scatterometer winds. Quilfen et al. (2001) compared ERS scatterometer retrievals to the TAO array and also concluded that the current signature was apparent in their wind residual analysis, with significant correlation coefficients.

Given these effects, **how does the presence of surface currents affect retrieved backscatter, and therefore derived speed and direction, in the coastal zone? Are wind speed differences between buoy and scatterometer measurements greater in regions/times of significant surface current? Is this true of differences in wind direction?** Chelton et al. (2004) indicates that a moderate surface current of 0.3 m/s flowing parallel or anti-parallel to a 6 m/s wind will cause a 10% modification in ENW-derived wind stress, and that a strong current such as the Gulf Stream could change the stress estimate by as much as 20%. Can these effects be observed in the Gulf of Maine? Chapter 3 of this dissertation investigates these questions using the existing buoy network and the persistent coastal currents and strong tides of the Gulf of Maine. If there are large differences between scatterometer ENW and buoy wind speed near currents, this could indicate the importance of incorporating surface current information into modeled air-sea coupling investigations, and large direction differences would indicate that the use of scatterometer-derived wind stress curl near strong currents could be quite complicated.

1.1.6 Atmospheric case: Stability

Laboratory experiments, models, and small-scale real-world tests have shown that stability directly affects the generation of surface ripples [Wu (1991); Colton et al. (1995);

Kudryavtsev et al. (2005), etc]. Some studies proposed model functions relating radar backscatter directly to u_* to capture this stability dependence [Weissman (1990); Weissman et al. (1994)]. The existing QuikSCAT GMF includes a parameterization for stability effects on backscatter. Atmospheric stability effects on winds have been investigated using scatterometer retrievals in the open ocean, particularly with respect to sea surface temperature (SST) fronts and enhanced air-sea coupling [Chelton et al. (2001); Chelton et al. (2004); Chelton et al. (2006); Song et al. (2006)]. Chelton et al. (2001) used standard resolution 25 km QuikSCAT surface wind vectors (relating the scatterometer ENW to surface stress with the neutral stability drag coefficient) and SST from the eastern Tropical Pacific to investigate ocean-atmosphere coupling. Results indicated that wind stress divergence is linearly related to downwind SST gradient, and wind stress curl is linearly related to the crosswind component of the SST gradient. The authors stated that this coupling supports the hypothesis that surface winds vary in response to SST modification of the marine atmospheric boundary layer. Additional studies reported similar results in other locations [O'Neill et al. (2003); O'Neill et al. (2005)]. If the parameterization of stability effects is not accurate, the results of these studies would be contaminated by stability effects on surface roughness as well as on the actual winds. With accurate compensation for parameterized stability effects, scatterometer ENW and u_* would be related using C_D , as shown in Equation 1.3. Where MABL stability causes measured wind and u_* to differ, the scatterometer retrievals should correlate with u_* , and not with wind [Weissman et al. (1994)]. **Is it possible to investigate the relationship between wind stress, scatterometer ENWs, and buoy winds for specific atmospheric stability cases? Do scatterometer winds appropriately reflect ENW in all stability conditions? Can wind flow dynamics in regions of air-sea temperature differences be investigated using scatterometer retrievals?** In this dissertation, Chapter 4 utilizes *in situ* direct eddy-covariance stress measurements taken during the CLIMODE field campaign and colocated scatterometer data to address these questions. This type of study is important for validating the investigations of scatterometer wind response to MABL modification and could provide an accurate source of information on stability-related physical processes. Such dynamics are important for weather forecasting as well as wind resource assessment, and include bound-

ary layer flow, the sea breeze/land breeze regimes, and the formation of coherent structures such as roll vortices.

1.1.7 Questions to answer

Because there is a strong interest in using scatterometer retrievals in all areas of the ocean, and having discussed these specific potential causes of complications in scatterometer retrievals, the main research question becomes: **By focusing on these specific physical processes of atmospheric stability and surface currents separately and using the best scatterometer and *in situ* products available, can the effects on scatterometer-retrieved ENW be quantified?**

1.2 Objectives and overview of dissertation organization

To answer these questions, the first step is the validation of a new ultra-high resolution (UHR) QuikSCAT product in the primary region of interest, the Gulf of Maine [Plagge et al. (2009), provided as Chapter 2]. The two main benefits of these data over standard products are increased spatial resolution and coastal coverage. These benefits open up scatterometry for increased use in weather forecasting, ocean circulation modeling, and resource assessment. For these applications, scatterometer winds could be used to provide two main products: anemometer wind (useful for forecasting and resource assessment), and wind stress (for forecasting and circulation forcing). How well do scatterometer wind retrievals represent either of these products? What are the main controls on the validity of scatterometer winds applied in these ways?

Once the UHR product is shown to be valid in the Gulf of Maine, the next step is to use these data along with additional *in situ* and satellite measurements to attempt to isolate the affect of air-sea controls on scatterometer response. Accordingly, Chapter 3 focuses on surface current measurements at two buoys in the Gulf of Maine with three resolutions

of colocated scatterometer winds, utilizing the coastal and tidal currents of the region to minimize any contamination of dynamics due to water temperature fronts that are associated with larger western boundary currents. Chapter 4 then investigates the atmospheric issues, using the results of Chapter 3 to incorporate ocean surface velocity and thus focus on air-sea stability dynamics. Chapter 5 provides overall conclusions of this dissertation.

Bibliography

- Accadia, C., S. Zecchetto, A. Lavagnini, and A. Speranza, 2007: Comparison of 10-m wind forecasts from a regional area model and QuikSCAT Scatterometer wind observations over the Mediterranean Sea. *Monthly Weather Review*, **135** (5), 1945–1960.
- Bourassa, M., 2006: Satellite-based observations of surface turbulent stress during severe weather. *Atmosphere-Ocean Interactions*, W. Perrie, Ed., Wessex Institute of Technology, Advanced Fluid Mechanics Series Vol. 39, Vol. 2, 35–52.
- Chelton, D. B. and M. H. Freilich, 2005: Scatterometer-based assessment of 10-m wind analyses from the operational ECMWF and NCEP numerical weather prediction models. *Monthly Weather Review*, **133** (2), 409–429.
- Chelton, D. B., M. H. Freilich, J. M. Sienkiewicz, and J. M. Von Ahn, 2006: On the use of quikscat scatterometer measurements of surface winds for marine weather prediction. *Monthly Weather Review*, **134** (8), 2055–2071.
- Chelton, D. B., M. G. Schlax, M. H. Freilich, and R. F. Milliff, 2004: Satellite measurements reveal persistent small-scale features in ocean winds. *Science*, **303** (5660), 978–983.
- Chelton, D. B., et al., 2001: Observations of coupling between surface wind stress and sea surface temperature in the eastern tropical pacific. *Journal of Climate*, **14** (7), 1479–1498.
- Colton, M. C., W. J. Plant, W. C. Keller, and G. L. Geernaert, 1995: Tower-based measurements of normalized radar cross-section from Lake Ontario - evidence of wind stress dependence. *Journal of Geophysical Research-Oceans*, **100** (C5), 8791–8813.
- Davidson, K. L., P. J. Boyle, and P. S. Guest, 1992: Atmospheric boundary-layer properties affecting wind forecasting in coastal regions. *Journal of Applied Meteorology*, **31** (8), 983–994.

- Ebuchi, N., H. C. Graber, and M. J. Caruso, 2002: Evaluation of wind vectors observed by QuikSCAT/SeaWinds using ocean buoy data. *Journal of Atmospheric and Oceanic Technology*, **19** (12), 2049–2062.
- Freilich, M. and R. Dunbar, 1999: The accuracy of the NSCAT 1 vector winds: Comparisons with National Data Buoy Center buoys. *Journal of Geophysical Research-Oceans*, **104** (C5), 11 231–11 246.
- Hoffman, R. N. and S. M. Leidner, 2005: An introduction to the near-real-time QuikSCAT data. *Weather and Forecasting*, **20** (4), 476–493.
- Jones, I. S. F. and Y. Toba, 2001: *Wind Stress over the Ocean*. Cambridge University Press.
- Kara, A. B., E. J. Metzger, and M. A. Bourassa, 2007: Ocean current and wave effects on wind stress drag coefficient over the global ocean. *Geophysical Research Letters*, **34** (1), doi:10.1029/2006GL027849.
- Kara, A. B., A. J. Wallcraft, and M. A. Bourassa, 2008: Air-sea stability effects on the 10 m winds over the global ocean: Evaluations of air-sea flux algorithms. *Journal of Geophysical Research-Oceans*, **113** (C4), doi:10.1029/2007JC004324.
- Kelly, K., S. Dickinson, and G. Johnson, 2005: Comparisons of scatterometer and TAO winds reveal time-varying surface currents for the Tropical Pacific Ocean. *Journal of Atmospheric and Oceanic Technology*, **22** (6), 735–745.
- Kelly, K., S. Dickinson, M. McPhaden, and G. Johnson, 2001: Ocean currents evident in satellite wind data. *Geophysical Research Letters*, **28** (12), 2469–2472.
- Kudryavtsev, V., D. Akimov, J. Johannessen, and B. Chapron, 2005: On radar imaging of current features: 1. Model and comparison with observations. *Journal of Geophysical Research-Oceans*, **110** (C7), doi:10.1029/2004JC002505.
- Liu, W. T., K. B. Katsaros, and J. A. Businger, 1979: Bulk parameterizations of air-sea exchanges of heat and water vapor including molecular constraints at the interface. *J. Atmos. Sci.*, **36**, 1722–1735.

- Liu, W. T. and W. Tang, 1996: Equivalent neutral wind. JPL Publication 96-17, Jet Propulsion Laboratory.
- Nghiem, S. V., F. K. Li, and G. Neumann, 1997: The dependence of ocean backscatter at ku-band on oceanic and atmospheric parameters. *IEEE Transactions on Geoscience and Remote Sensing*, **35** (3), 581–600.
- O'Neill, L., D. Chelton, and S. Esbensen, 2003: Observations of SST-induced perturbations of the wind stress field over the Southern Ocean on seasonal timescales. *Journal of Climate*, **16** (14), 2340–2354.
- O'Neill, L., D. Chelton, and S. Esbensen, 2005: High-resolution satellite measurements of the atmospheric boundary layer response to SST variations along the Agulhas Return Current. *Journal of Climate*, **18** (14), 2706–2723.
- Phillips, O. M., 1977: *Dynamics of the Upper Ocean*. 2d ed., Cambridge University Press.
- Pickett, M. H., W. Q. Tang, L. K. Rosenfeld, and C. H. Wash, 2003: QuikSCAT satellite comparisons with nearshore buoy wind data off the US West Coast. *Journal of Atmospheric and Oceanic Technology*, **20** (12), 1869–1879.
- Plagge, A. M., D. C. Vandemark, and D. G. Long, 2009: Coastal Validation of Ultra-High Resolution Wind Vector Retrieval from QuikSCAT in the Gulf of Maine. *IEEE Geoscience and Remote Sensing Letters*, **6** (3), 413–417.
- Quilfen, Y., B. Chapron, and D. Vandemark, 2001: The ERS scatterometer wind measurement accuracy: Evidence of seasonal and regional biases. *Journal of Atmospheric and Oceanic Technology*, **18** (10), 1684–1697.
- Song, Q. T., P. Cornillon, and T. Hara, 2006: Surface wind response to oceanic fronts. *Journal of Geophysical Research-Oceans*, **111** (C12).
- Tang, W. Q., W. T. Liu, and B. W. Stiles, 2004: Evaluations of high-resolution ocean surface vector winds measured by QuikSCAT scatterometer in coastal regions. *IEEE Transactions on Geoscience and Remote Sensing*, **42** (8), 1762–1769.

- Verschell, M., M. Bourassa, D. Weissman, and J. O'Brien, 1999: Ocean model validation of the NASA scatterometer winds. *Journal of Geophysical Research-Oceans*, **104 (C5)**, 11 359–11 373.
- Weissman, D. and H. Graber, 1999: Satellite scatterometer studies of ocean surface stress and drag coefficients using a direct model. *Journal of Geophysical Research-Oceans*, **104 (C5)**, 11 329–11 335.
- Weissman, D., et al., 1997: Measurements of ocean surface stress using aircraft scatterometers. *Journal of Atmospheric and Oceanic Technology*, **14 (4)**, 835–848.
- Weissman, D. E., 1990: Dependence of the microwave radar cross-section on ocean surface variables - Comparison of measurements and theory using data from the Frontal Air-Sea Interaction Experiment. *Journal of Geophysical Research-Oceans*, **95 (C3)**, 3387–3398.
- Weissman, D. E., K. L. Davidson, R. A. Brown, C. A. Friehe, and F. Li, 1994: The relationship between the microwave radar cross-section and both wind-speed and stress - model function studies using Frontal Air-sea Interaction Experiment data. *Journal of Geophysical Research-Oceans*, **99 (C5)**, 10 087–10 108.
- Wu, J., 1991: Effects of atmospheric stability on ocean ripples - A comparison between optical and microwave measurements. *Journal of Geophysical Research-Oceans*, **96 (C4)**, 7265–7269.
- Zhang, F. W., W. M. Drennan, B. K. Haus, and H. C. Graber, 2009: On wind-wave-current interactions during the shoaling waves experiment. *Journal of Geophysical Research*, **114**.

CHAPTER 2

Coastal Validation of Ultra-High Resolution Wind Vector Retrieval from QuikSCAT in the Gulf of Maine

2.1 Prologue

The following is a paper written by the author and submitted for review and publication with IEEE's Geoscience and Remote Sensing Letters in 2008-2009, based entirely on work completed as part of the author's doctoral research, and presented in its published form as required by copyright. The co-authors are Dr. Douglas Vandemark, the author's PhD advisor, and Dr. David Long at Brigham Young University, who created the data under evaluation. The research and writing is the author's own, with limited additions and edits from the co-authors as well as several anonymous reviewers. It should additionally be mentioned that the "reselected" data discussed here was used extensively in further research, especially as detailed in Chapter 3 .

©2009 IEEE. Reprinted, with permission, from A. M. Plagge, D. C. Vandemark, and D.G. Long, Coastal Validation of Ultra-High Resolution Wind Vector Retrieval from QuikSCAT in the Gulf of Maine, IEEE Geoscience and Remote Sensing Letters, July 2009.

2.2 Abstract

An experimental 2.5 km ultra-high resolution (UHR) wind product provided by NASA's QuikSCAT scatterometer offers the potential for new access to coastal surface wind dynamics at the mesoscale level and below. To give future users the best indication of the value of these data, the UHR wind retrievals must be fully validated in near-shore areas. Comparison

with meteorological buoys and standard QuikSCAT products allows detailed investigation of UHR winds. Speed and direction residuals are calculated between all scatterometer products and collocated buoys. An ambiguity selection routine improves wind direction agreement between the UHR winds and the other products. Magnitude residuals follow the patterns of the standard QuikSCAT winds, with a 1-2 m/s positive bias in light winds (below 4 m/s) and high winds (above 16 m/s) and standard deviations consistently below 3 m/s. After application of a land contamination removal algorithm, the UHR product provides extended coverage near the coast. An example of a specific wind event illustrates the potential benefits of improved resolution measurements for examining ocean-atmosphere dynamics.

keywords: Wind, Meteorology, Remote Sensing

2.3 Introduction

Ocean vector winds from the Seawinds instrument have been widely used since the sensor's launch on the QuikSCAT satellite in 1999. This Ku-band scatterometer was designed to retrieve wind speed and direction at a 25 km resolution, through normalized radar backscatter measurements and a geophysical model function. A newer product provides wind vectors at a resolution of 12.5 km (Tang et al. (2004)). QuikSCAT covers 90% of the globe in 24 hours and the spatial and temporal coverage provided makes scatterometer-derived wind data valuable for a variety of users.

In many coastal areas, weather forecasting abilities are complicated by land-ocean and atmosphere-ocean coupling (Accadia et al. (2007), Davidson et al. (1992)). Coastal wind users need better tools to understand, model, and predict particular microscale meteorological features, such as the sea breeze and frontal and trough passages. Currently, satellite scatterometer wind data are used to improve oceanographic and weather models but it cannot resolve many nearshore dynamics occurring at length scales smaller than tens of kilometers. A higher resolution satellite wind product could provide an important tool to

meet these needs. One known source is synthetic aperture radar (SAR). However, while SAR systems provide an extremely high resolution (10 – 100 m) view of wind magnitude, coverage from even the two most accessible SAR instruments (Radarsat and Envisat) is infrequent at best, and data can be quite costly. Secondly, although it is possible to retrieve wind direction from SAR, this is complicated. It is for these reasons that a high-resolution scatterometer wind product could benefit many users in the coastal ocean community. This type of product may resolve processes closer to shore and in greater detail than current scatterometer retrievals, and yet provide vector winds at a better temporal resolution than SAR.

Such an enhanced wind product is currently being created at Brigham Young University (Long et al. (2003), Williams and Long (2007)). This product is a novel attempt to go beyond the native resolution of the sensor to provide 2.5 km resolution winds. However, because of the methods used to create the product, there is an expected increase in noise, and additional questions about the reliability of a product that so thoroughly pushes the spatial resolution limits of the sensor. Therefore, before these new wind data can be used to investigate near-shore dynamics they must be fully evaluated. This study presents such a test using a year of data (2006) in the Gulf of Maine.

The first section discusses the data and validation analysis methods, as well as an additional postprocessing step to improve direction estimation. Comprehensive comparison with buoy winds provide the basis for the data evaluations. Results are provided in detail, including nearshore vs. offshore comparisons, cross-swath trend analysis, directional accuracy, and spatial coverage. Finally an example showing the scientific value of the enhanced wind retrievals is provided.

2.4 Methods

2.4.1 Data

The 2.5 km ultra-high resolution (UHR) wind product is, like the standard QuikSCAT products, available twice daily in all weather, with an extensive time series provided by the QuikSCAT data record from 1999 to present. The data were produced using the AVE algorithm (Long et al. (2003)).

The dense network of meteorological buoys in the Gulf of Maine provides an ideal testbed for this study (see Fig. 3-1). Further information is obtained by comparing the UHR winds with standard QuikSCAT 25 km and 12.5 km Level 2B (L2B) swath retrievals (produced by the NASA Scatterometer Project and distributed by the NASA Physical Oceanography Distributed Active Archive Center at the Jet Propulsion Laboratory). Each type of scatterometer data is collocated with each buoy by finding all pixels within a 10 km radius of the buoy location and taking the average for both speed and direction. Buoy and scatterometer measurements occur within ± 30 minutes of one another. The collocation for 2006 produces 8,292 pairs for the UHR retrievals and 5,806 and 1,696 pairs for the L2B 12.5 km and 25 km winds respectively. Buoys closer than 100 km to shore are considered “nearshore”; farther are “offshore.”

An initial comparison of UHR wind magnitude with that provided by the buoys, as well as with winds from a regional mesoscale meteorological model (run jointly by University of New Hampshire and AER, Inc.), indicated that high UHR retrieved wind speeds seen along the coast were an artifact of land contamination. The data were regenerated using a land contamination removal algorithm (Owen et al. (2003), Owen and Long (2009)), and the new masked wind retrievals avoid most of the near-shore bias.

Figs. 2-2 and 2-3 show a sample swath of UHR and L2B 12.5 km wind magnitude with unit wind vectors overlaid. Additionally, the color of the overlaid circular buoy symbols indicates buoy wind speed, according to the same scale as the UHR magnitude image. In

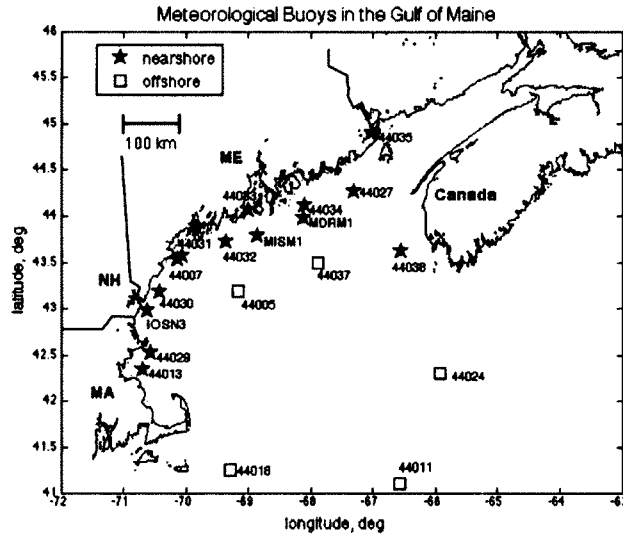


Figure 2-1: Buoy network in the Gulf of Maine. *Acknowledgments: NOAA's National Data Buoy Center and the Gulf of Maine Ocean Observing System*

this image from January 16, there is a strong northwest flow with wind speeds ranging from 8 m/s near the coast to 24 m/s farther offshore. As shown by the figures, the scatterometer wind retrievals for both products closely match the buoy wind data. Fine-scale structure seen in the UHR winds is not evident in the 12.5 km data: for instance, the locally high wind flow over Massachusetts Bay is more easily distinguished in Fig. 2-2 than in Fig. 2-3 (at 41.5 N, 70.5 W).

2.4.2 Statistical analysis

The present study follows recent research that has focused on individual buoy-satellite pass analysis and direct comparison of buoy wind magnitude with that from the different scatterometer products (Plagge et al. (2008a)). Statistical methods are used to analyze a year of scatterometer-buoy pairs, including mean and standard deviation calculations. Speed and direction residuals (scatterometer minus buoy) are organized according to buoy wind speed, buoy station, and cross-swath position (Tang et al. (2004)).

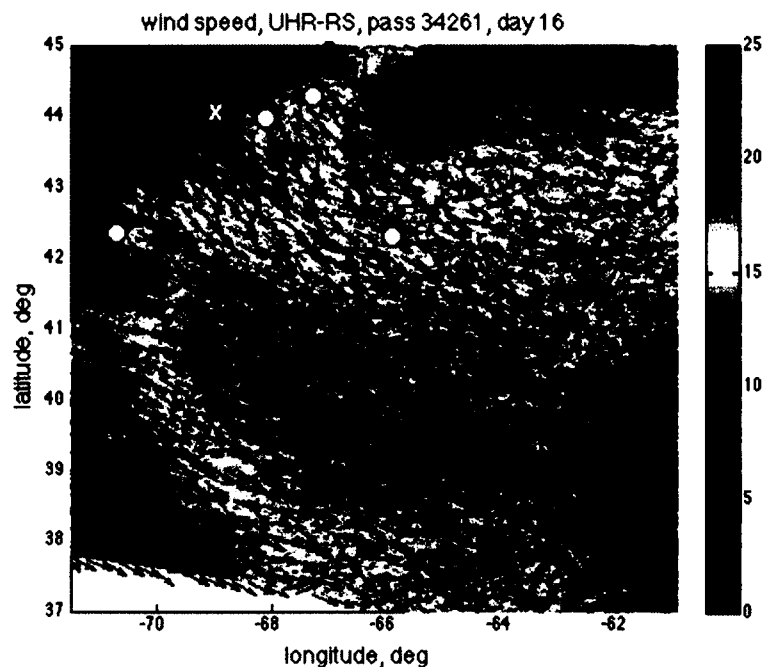


Figure 2-2: UHR and buoy wind magnitude for Jan 16, 2006; sub-sampled (every 4th) unit wind vectors shown in black; buoy speeds in circles (“x” indicates no data).

2.4.3 Ambiguity re-selection

Initial statistical analyses indicated instances where the UHR wind directions do not agree well with buoy winds or coincide with the direction from the other scatterometer products. Detailed examination of the original UHR data show significant differences between the UHR and L2B wind directions in certain passes (Plagge et al. (2008b)).

Because QuikSCAT obtains multiple “looks” at the ocean surface, wind direction can be determined as well as wind speed. There are several possible estimates of speed and direction for each measurement, referred to as “ambiguities.” Occasional errors in the selection of ambiguities are expected (Long et al. (2003)). It was hypothesized that in specific instances, the initial choice of ambiguity was flawed. A new algorithm selects one of the four UHR ambiguities with the minimum vector difference from the L2B 12.5 km product. This reselected speed and direction data is referred to as the UHR-RS product. Fig. 2-4 shows the improvement in direction for a subsection of a sample pass (October 18, 2006).

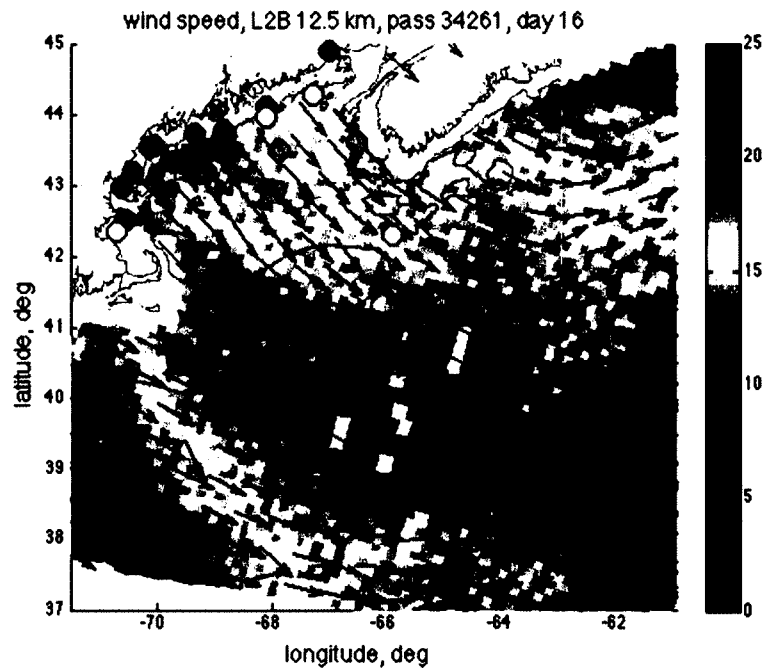


Figure 2-3: L2B 12.5 km and buoy wind magnitude for Jan 16, 2006; sub-sampled (every 10th) unit wind vectors shown in black buoy speeds in circles ("x" indicates no data).

Due to the fact that the new ambiguity choice is based on a minimum vector difference for each pixel, it sometimes occurs that an individual pixel's speed or direction appears to be farther from the "true" estimate. The residuals for the original UHR data throughout 2006 have a magnitude mean of -0.30 ± 2.26 m/s and a directional mean of 2.79 ± 50.77 degrees. The reselected data (UHR-RS) have a magnitude mean of -0.29 ± 2.33 m/s and a directional mean of 1.67 ± 51.17 . It should be stressed that 1) although the overall quality of the data has not changed a great deal, specific cases throughout the year were repaired using this post-processing step, and 2) the buoy comparison is not the only metric used to determine the value of the reselection. In a few cases, the algorithm mis-selects the ambiguity, but these instances are isolated and are often single pixels that could be repaired by filtering (not used here due to the desire to keep the highest possible resolution); the improvement in large (10 to 100s km) regions of direction retrievals outweighs the slight increase in noise.

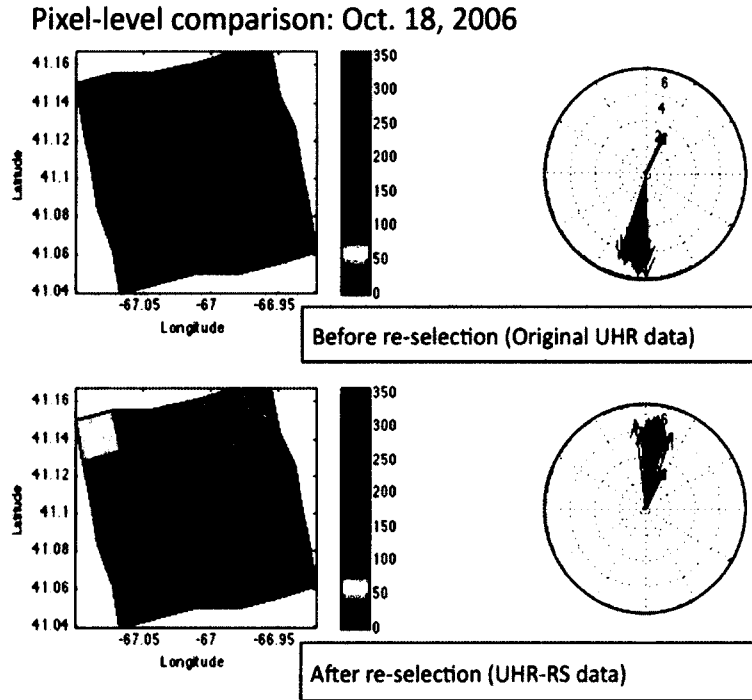


Figure 2-4: Pixel-level comparison of UHR speed and direction before and after re-selection routine. Pixel color indicates direction in degrees. Arrows on rose show wind vectors from the UHR pixels (blue) and a nearby buoy (bold black).

2.5 Results

2.5.1 Speed and direction

After implementation of the reselection process, the statistics for the full year are re-computed. Scatterometer-minus-buoy residuals are organized according to buoy wind magnitude and buoy station (see Figs. 2-5 and 2-6); statistics are summarized in Table 2.1.

Speed error increases slightly in both light wind and high wind conditions as expected (Tang et al. (2004), Pickett et al. (2003)), but mean error and standard deviation for UHR-RS wind magnitude matches those for the standard QuikSCAT products (Tang et al. (2004), Pickett et al. (2003), Chelton and Freilich (2005)). In all products, standard deviations are slightly greater for nearshore buoys; additionally, wind speeds above 15 m/s show a mean UHR-RS speed 2-3 m/s below that measured by the buoys. Standard deviation of wind direction is higher than most published values for even the standard products (especially at

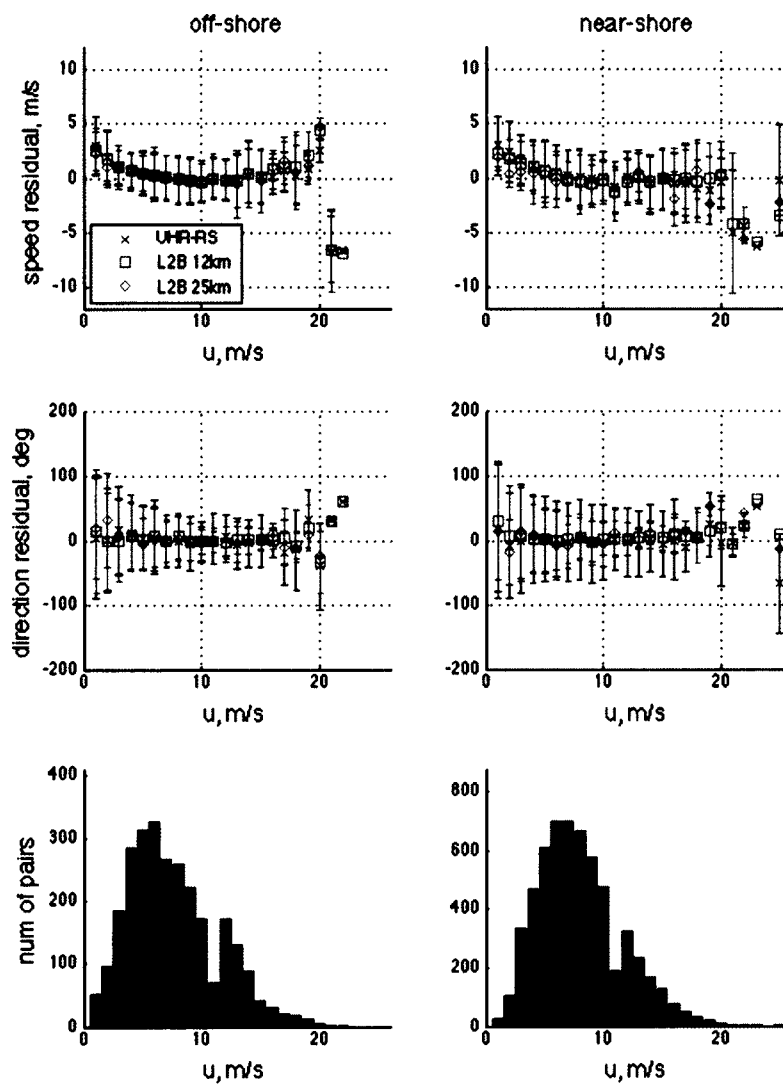


Figure 2-5: Summary of scatterometer-minus-buoy residuals for 2006, plotted according to buoy wind speed. Green indicates 25 km data, red 12.5 km, and blue UHR-RS.

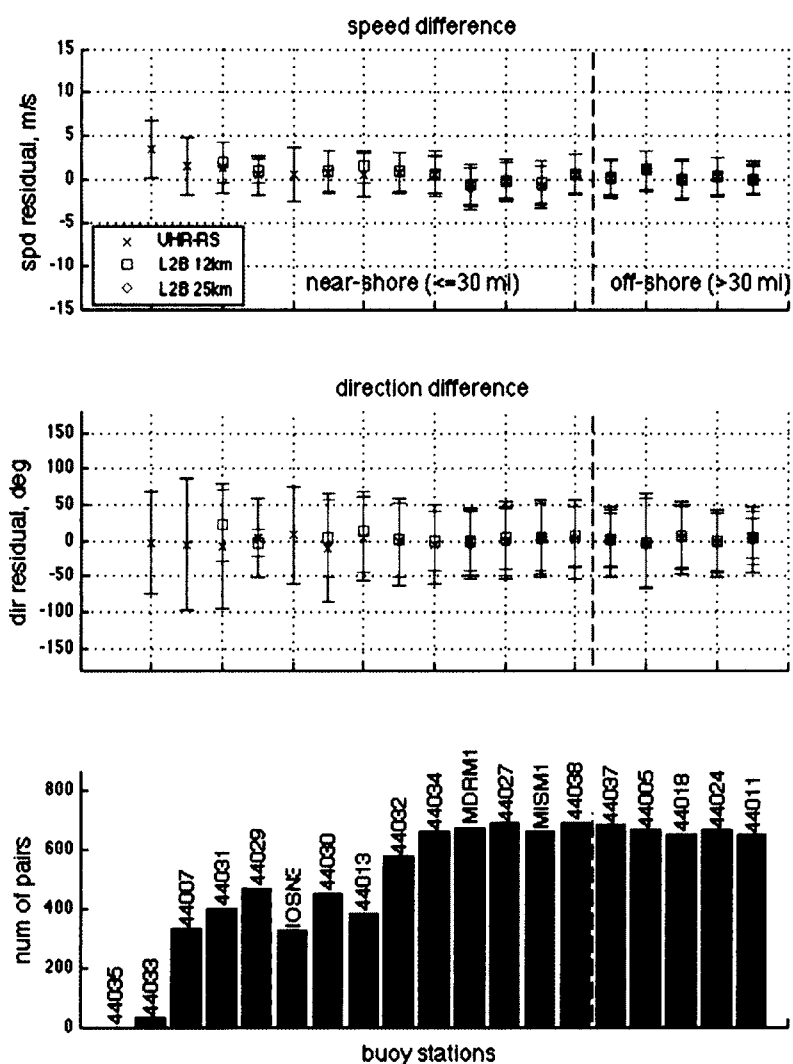


Figure 2-6: Summary of scatterometer-minus-buoy residuals for 2006, plotted according to buoy station (arranged according to distance from shore). Green indicates 25 km data, red 12.5 km, and blue UHR-RS.

			nearshore	offshore	all	farswath	nearswath	nadir
$ U $	UHR-RS	bias	-0.48	-0.09	-0.29	-0.22	0.09	0.32
		std	2.65	1.98	2.33	2.34	2.05	1.67
	12.5 km	bias	-0.62	0.07	-0.29	-0.17	0.09	0.23
		std	2.29	2.07	2.18	2.46	2.14	1.72
	25 km	bias	-0.54	0.33	-0.11	-0.11	0.12	0.19
		std	1.99	2.05	2.02	2.49	2.18	1.72
ϕ	UHR-RS	bias	0.17	3.29	1.67	-2.18	-1.59	-1.81
		std	55.82	46.09	51.17	52.37	47.09	55.05
	12.5 km	bias	8.45	4.31	6.47	-0.48	0.46	0.94
		std	33.56	35.21	34.35	51.96	39.41	41.60
	25 km	bias	6.52	2.26	4.44	-2.90	0.68	1.84
		std	33.30	32.30	32.81	52.24	40.88	35.78

Table 2.1: Data summary for 2006; $|U|$ indicates magnitude residuals, ϕ indicates directional residuals, “NS” and “OS” are nearshore and offshore respectively.

winds below 7 m/s) with the residuals showing an average standard deviation of 34 degrees for the 12.5 km and 33 degrees for the 25 km. The reasons for this are most likely related to 1) the absolute accuracy of the buoy measurements themselves, 2) the time difference, and 3) the fact that the study takes place in the coastal ocean, where the wave field is not always full developed and other sources of surface roughness can complicate the backscatter signal. Standard deviation for the UHR residuals vary from 50 degrees to 30 degrees in the 5 to 15 m/s range; on average they are 35% higher than the L2B residuals. Residuals for all three data types are worse in the nearshore region than in the offshore region, especially in higher winds.

When compared across the satellite swath, residuals generally show greater bias and a higher standard deviation in the nadir and far swath regions (Table 2.1). This is attributed to the viewing geometry of the satellite; QuikSCAT uses a conically scanning dual pencil beam antenna, with an inner and an outer beam. A single location on the ocean’s surface will generally be observed four times with multiple viewing geometries: twice by both beams, once as they look forward and once as they look aft. This variety of “looks” is what allows the determination of both speed and direction. The greatest diversity of azimuth and incidence angles, and therefore the best quality data, is found in the near swath, whereas

retrievals from the far swath (which has only two flavors because it is only sampled by the outer beam) and the nadir region (having only two azimuth angles despite two beams) are less accurate (Chelton and Freilich (2005)). However, in this study the effects are generally minimal, as can be seen in Table 2.1.

2.5.2 Near-shore coverage

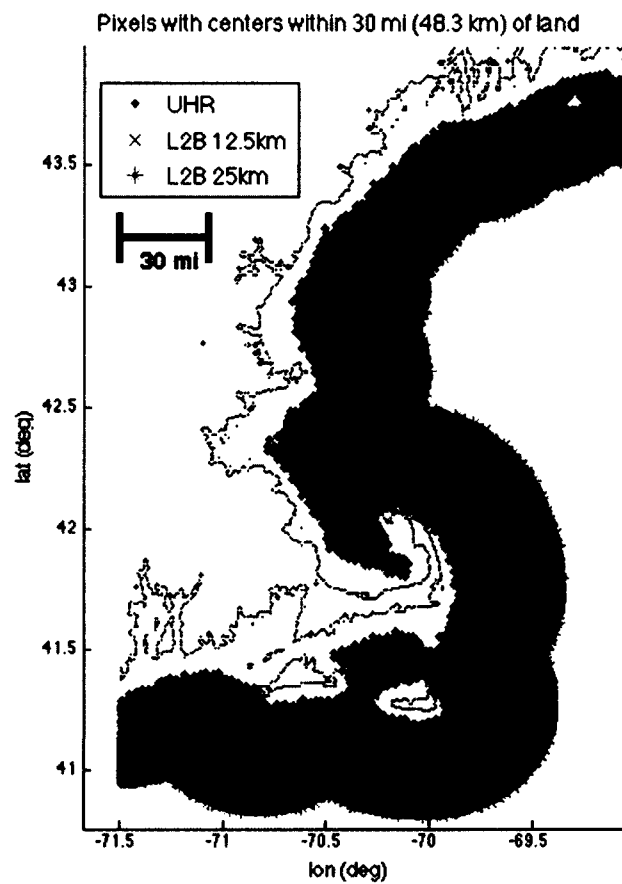


Figure 2-7: Cumulative pixel center locations in January 2006: 3 types of QuikSCAT data.

Overall, the UHR-RS data in the Gulf of Maine represent the best spatial range of scatterometer wind retrievals in the coastal area. The nearshore coverage shows a marked improvement over even the L2B 12.5 km data. Fig. 2-7 shows every pixel center for Jan-

uary 2006 within the 30 mile limit in the Massachusetts Bay region for the UHR-RS data in black, the L2b 12.5 km data in dark gray, and the L2B 25 km in light gray. In many regions, the UHR-RS data come 10 km closer to the coast than the L2B 12.5 km data and 25 km closer than the L2B 25 km data. A proxy for this can also be seen in the number of buoy collocation pairs for each data type, again for one month in 2006; the UHR product reaches within 10 km of the near-shore buoys 46% of a possible 980 matches, whereas the 12.5 km data only found a pair 23% of the time. The fact that this 30 mile limit coincides with the local National Weather Service forecast office's region of responsibility for nearshore maritime forecasting makes this increase in available information especially critical.

2.5.3 Illustration of one potential UHR-RS benefit

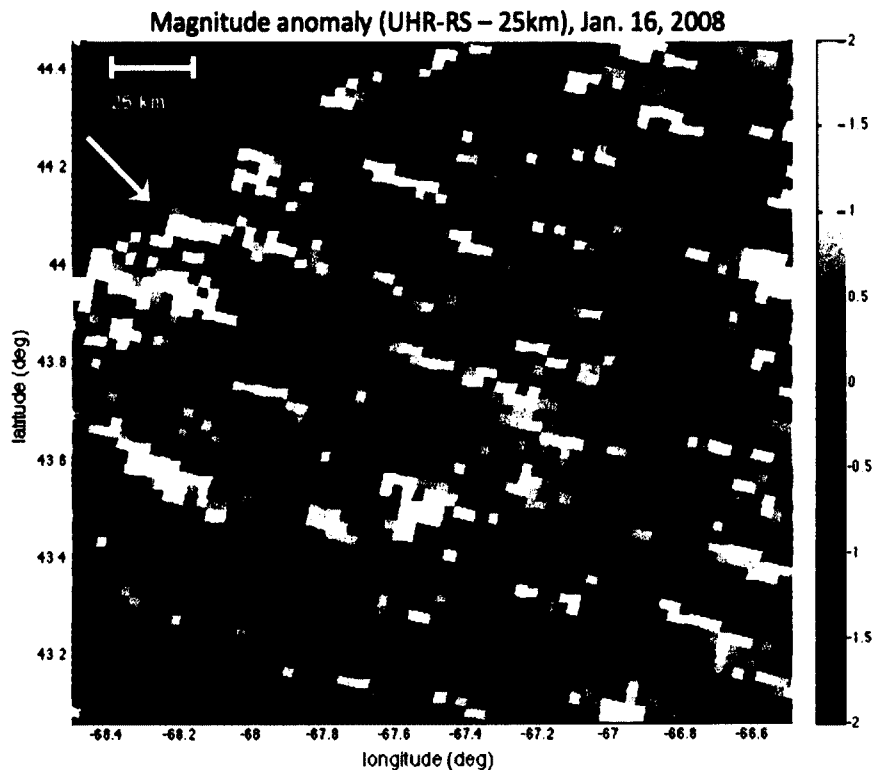


Figure 2-8: Evidence of roll vortices during northwest flow event, January 16, 2006. White arrow shows prevailing wind direction.

Besides the increase in near-shore coverage, another significant advantage to the UHR-

RS data is the improved identification of the type of marine atmospheric boundary layer processes that occur at lengthscales of 5 to 20 km. To this end, cold air offshore flow is an important wind regime that is being investigated in the Gulf of Maine using the UHR winds. For the purposes of this study, offshore flow is defined as moderately high wind (above 10 m/s) from the northwest, and occurs generally in mid-January and late February to early March. In several instances of this type of flow, the existence of roll vortices is indicated in the UHR magnitude retrievals but not seen in the L2B 12.5 km data. An example can be seen in Fig. 2-8, which shows the magnitude anomaly between the UHR-RS and 25 km L2B data for the wind event shown in Figs. 2-2 and 2-3. Horizontal streaking aligned with the prevailing wind direction suggests coherent structure in the MABL, in the form associated with roll vortices. The presence of these vortices is confirmed by MODIS True Color imagery. Additionally, the range of directions visible in the UHR wind vectors in Fig. 2-2 are potentially associated with boundary layer convection due to downdrafts at the surface. Identification of these dynamics can be important to scientists studying boundary layer processes (Davidson et al. (1992)) and ocean-atmosphere coupling (Pullen et al. (2006)); this outcome is therefore quite encouraging and a focus of future studies.

2.6 Conclusion

This work indicates the potential of the ultra-high resolution scatterometer winds in the coastal zone. UHR-RS wind retrievals are shown to be of similar quality to standard QuikSCAT products in the coastal region, although users should be aware that an ambiguity reselection process similar to the one described here is recommended for any project that incorporates wind direction. The one clear benefit of the UHR-RS data appears to be in the improved distance to the shore, providing scientists, forecasters, and other users with information previously unavailable. Additionally, increased resolution does have the capacity to allow improved access to dynamics associated with air-sea interaction, providing further benefit to the scientific community.

Bibliography

- Accadia, C., S. Zecchetto, A. Lavagnini, and A. Speranza, 2007: Comparison of 10-m wind forecasts from a regional area model and QuikSCAT Scatterometer wind observations over the Mediterranean Sea. *Monthly Weather Review*, **135** (5), 1945–1960, doi: 10.1175/MWR3370.1.
- Chelton, D. B. and M. H. Freilich, 2005: Scatterometer-based assessment of 10-m wind analyses from the operational ecmwf and ncep numerical weather prediction models. *Monthly Weather Review*, **133** (2), 409–429.
- Davidson, K. L., P. J. Boyle, and P. S. Guest, 1992: Atmospheric boundary-layer properties affecting wind forecasting in coastal regions. *Journal of Applied Meteorology*, **31** (8), 983–994.
- Long, D. G., J. B. Luke, and W. Plant, 2003: Ultra High Resolution Wind Retrieval for SeaWinds. *International Geoscience and Remote Sensing Symposium*, Toulouse, France, 1264–1266.
- Owen, M. P. and D. G. Long, 2009: Land contamination compensation for QuikSCAT near-coastal wind retrieval. *IEEE Transactions on Geoscience and Remote Sensing*, **47** (3), 839–850, to appear.
- Owen, M. P., K. M. Stuart, and D. G. Long, 2003: Ultra-High-Resolution Near-Coastal Wind Retrieval for QuikSCAT. *Coastal Ocean Remote Sensing*, R. Foulin, Ed., SPIE, Vol. 6680.
- Pickett, M. H., W. Q. Tang, L. K. Rosenfeld, and C. H. Wash, 2003: QuikSCAT satellite comparisons with nearshore buoy wind data off the US West Coast. *Journal of Atmospheric and Oceanic Technology*, **20** (12), 1869–1879.

- Plagge, A. M., D. C. Vandemark, and D. G. Long, 2008a: Evaluation of QuikSCAT ultra-high resolution wind retrieval in the Gulf of Maine. OS1893, Ocean Sciences Meeting, Orlando, FL.
- Plagge, A. M., D. C. Vandemark, and D. G. Long, 2008b: Validation and evaluation of QuikSCAT ultra-high resolution wind retrieval in the Gulf of Maine. *Proceedings of the International Geoscience and Remote Sensing Symposium*, Boston, MA.
- Pullen, J., J. D. Doyle, and R. P. Signell, 2006: Two-way air-sea coupling: A study of the Adriatic. *Monthly Weather Review*, **134** (5), 1465–1483.
- Tang, W. Q., W. T. Liu, and B. W. Stiles, 2004: Evaluations of high-resolution ocean surface vector winds measured by QuikSCAT scatterometer in coastal regions. *IEEE Transactions on Geoscience and Remote Sensing*, **42** (8), 1762–1769.
- Williams, B. L. and D. G. Long, 2007: Hurricane Wind Field Estimation from SeaWinds at Ultra High Resolution. *Proceedings of the International Geoscience and Remote Sensing Symposium*, Barcelona, Spain, 1075–1078.

CHAPTER 3

Examining the impact of surface currents on satellite scatterometer and altimeter ocean winds

3.1 Prologue

The following is a paper written by the author and submitted for review and potential publication in AMS's Journal of Atmospheric and Oceanic Technology in 2012, based entirely on work completed as part of the author's doctoral research. The co-authors are Dr. Douglas Vandemark and Dr. Bertrand Chapron, a member of the author's doctoral committee. All of the research and most of the writing is the author's own, with limited additions and edits from the co-authors. As explained in the prologue of Chapter 2, the UHR data used here (see Sec. 3.4) is the reselected UHR data described in that chapter.

3.2 Abstract

A five-year dataset collected over two surface current and meteorological moorings allows rigorous evaluation of questions surrounding wave/current interaction and the scatterometer. Results demonstrate that scatterometer winds represent winds relative to the moving sea surface, affirming previous observational efforts that inferred the phenomenon using climatological approaches over larger time and space scales in equatorial and Western boundary currents. Comparisons of wind residuals between Ku-band QuikSCAT and buoy measurements show near one-to-one correlation with ocean surface velocity for 5, 12.5, and 25 km resolution wind speed products, especially under conditions of moderate wind speed and near-neutral atmospheric stability. No measurable correlation is observed between wind direction residuals and current vectors, indicating a weak effect of surface currents on derived wind direction at the length scales observed by this scatterometer. Similar analyses

are applied to C-band ASCAT satellite wind measurements at the same sites as well as to satellite altimeter winds, and overall confirm the results seen with QuikSCAT; differences are likely the combined result of sampling, satellite wind algorithms, and geophysical wind-wave coupling in the presence of currents. On the whole, this study affirms that at length scales of 10 km and longer the scatterometer wind can be considered to be current-relative. Observed differences between earth-relative and current-relative wind of order 10-20% of the wind velocity are not uncommon in this and other ocean regions and this study more fully validates that microwave remote sensing winds appear to respond to wind stress even in the presence of larger scale currents.

3.3 Introduction

The ever-increasing number of surface current measurements across the world's oceans is leading to renewed appreciation for the role that surface currents play in atmosphere-ocean dynamics. These observations, from drifters, gliders, profilers, and satellites within the global ocean observing system, present a next challenge - the incorporation of a fluid air-sea boundary condition into atmosphere-ocean coupling, with impacts both upon wind stress at the sea surface and the resulting ocean circulation (Kara et al. (2007)) as well as atmospheric boundary layer modifications (Chelton et al. (2004), O'Neill et al. (2005), Chelton et al. (2006)). As part of these issues, there is increased recognition of the fundamental effect of surface currents on near-surface wind speeds derived using satellite microwave systems. Winds inferred using these sensors rely on changes in surface backscatter or emission tied to the geometrical roughness changes driven by surface wind waves. In the presence of currents, waves will grow with the effective wind, leading many to directly interpret satellite winds as a wind stress or a current-relative wind, rather than one that is relative to the fixed earth reference. While intuitive, supporting evidence for this premise remains limited (Dickinson et al. (2001), Quilfen et al. (2001), Chelton et al. (2004), Kelly et al. (2005)) in large part because the effect is typically small with respect to the mean wind and because measurement approaches to quantitatively isolate the effect require an exacting approach. This study presents an attempt to more fully demonstrate surface current impacts within

the context of satellite scatterometer ocean wind measurements.

Satellite scatterometry is the most widely applied approach for the global measurement of near-surface ocean wind speed and direction. The measurement principle involves radar detection of surface gravity and gravity-capillary wave changes that primarily reflect the winds observed near the air-sea interface (cf. Donelan and Pierson (1987)). The complexity across multiple geophysical problems involved in analytically relating radar backscatter to waves and then to wind stress is daunting and, to date, the method for inverting wind vector data from radar observations is an empirical model function developed to relate *in situ* wind measurements to radar backscatter. This approach is mature (e.g. Freilich and Dunbar (1999), Ebuchi et al. (2002), Tang et al. (2004), Bentamy et al. (2008)) and leads to global scatterometer wind products with accuracy of better than 1.2 m s^{-1} and 10 degrees. However, scatterometry still has several issues to resolve or constrain if long-term, uniform, and climate-relevant wind vector data are to be produced. First, the satellite sensor community operates several different scatterometers with varying probing wavelengths (L, C, and Ku-band) and viewing geometries; thus a separate empirical model function is required in each case along with subsequent cross-platform consistency evaluations. Another issue is due to the fact that the scatterometer wind is derived from ocean wind waves and not the earth-relative wind itself. This point has led many to assume the scatterometer is a more closely akin to a wind stress measurement system (e.g. Weissman and Graber (1999)). Yet, primarily because of a paucity of direct *in situ* wind stress observations, empirical scatterometer wind stress models or data products are either absent or unvalidated.

Using Monin-Obukhov similarity theory, the standard approximation relating the stress to the wind for the scatterometer is written in terms of a neutral atmospheric stability and current-relative wind vector at 10 m above the ocean (Liu and Tang (1996), Bourassa (2006)):

$$\mathbf{U}_{10N} = \mathbf{U}_s + \frac{\mathbf{u}_{*a}}{\kappa} \ln z/z_0 \quad (3.1)$$

Here, the parameter κ is von Karman's constant, \mathbf{u}_{*a} is the friction velocity, and the term

$\ln z/z_0$ refers to the approximately logarithmic increase in wind speed with height. This term depends not only on altitude above the surface (z , here 10 m) but on the properties of the surface (roughness length, z_0). The left-hand side of the equation can be derived in terms of measured scalars to yield a bulk U_{10N} ; this is the usual means of developing a scatterometer wind vector geophysical model function (GMF). The term U_s , the surface ocean current vector, is an additive term that assumes that currents dictate a fluid bottom boundary condition but do not impact, for example the roughness length z_0 .

Numerous past field and wave tank experiments (e.g. Plant (1977), Moore and Fung (1979), and Donelan and Pierson (1987)) have shown that radar backscatter is primarily induced by shorter gravity-capillary waves of order 1-20 cm. However, it is also known that different wave scales respond differently to changes in the terms on the left-hand side of Eq. 3.1 – terms imposed to parameterize atmosphere-ocean coupling attributed to all ocean and atmospheric boundary layer dynamics but specifically reflective of atmospheric stability, frontal gradients in either fluid, longer gravity waves in the range from seas to swell, and wave-current interactions. Do all scatterometer model functions (the right-hand side of Eq. 3.1) yield the same U_{10N} and, more to the point, do C-band and Ku-band systems yield the same results for various geophysical conditions at the air-sea interface? In this paper we attempt to observationally address the following questions: does the kinematic boundary condition hold for the pertinent wavelengths (i.e. do the applicable wind waves grow the same in and out of regions with a moving ocean)? Is this the same for Ku-band sensors as for C-band? At what length and time scales is this true? The answers to these questions are crucial for several reasons. First, because synthetic aperture radar (SAR) wave/current studies have shown differences at Ku- and C-band (Lyzenga (1998), Johannessen et al. (2005), Kudryavtsev et al. (2005), Marmorino et al. (2011)). Next, because surface currents become more important as scatterometer applications are expanded and refined. These applications include but are not limited to (1) climate records, (2) fine-scale evaluations of air-sea coupling over frontal adjustment zones (eddies, the ITCZ, and western boundary currents), (3) assimilation of scatterometer winds into surface current products in regions with persistent strong currents such as the equatorial Pacific, and (4) any use of

scatterometer winds in coastal regions with strong and highly dynamic currents.

The few observational studies addressing the effects of surface currents on scatterometer wind retrievals focus mostly in the equatorial region, where strong wave-current and air-sea interactions appear to complicate the relationship, and where only climatological or sub-surface ocean current estimates have been used. For these reasons, many of the questions above remain. In their 2005 paper, Kelly et al. show good agreement between zonal collocated wind differences and climatological zonal currents for Tropical Atmosphere Ocean (TAO) buoys and QuikSCAT (Kelly et al. (2005)). An earlier study by Quilfen et al. also shows a measurable but weak correlation between C-band scatterometer wind residuals and measured current at 10 meters depth on two TAO buoys (Quilfen et al. (2001)). However, both of these studies note that it is difficult to quantify the effect in part due to the lack of sufficient surface current measurements; additionally, the study of Kelly et al. (2005) was unable to find an expected relationship between meridional wind residuals and currents. As part of a comprehensive study of QuikSCAT wind vector accuracy at ocean buoys including TAO and various National Data Buoy Center (NDBC) buoys, Ebuchi et al. (2002) attempted to explain the differences between QuikSCAT and buoy winds by correlating the wind speed residuals with both sea surface temperature (SST) and air-sea temperature difference. They suggested that the very low correlations that resulted might be due to neglecting the effects of surface currents; but their attempt to remove the current effects by repeating the study using only NDBC buoys outside the strong currents of the equatorial region produced correlations that were just as low.

Accordingly, our approach is to gain a larger sampling of data and range of surface and wind conditions by using a coastal region with a large diurnal reversing current and an extensive *in situ* near-surface current measurement record. We investigate the effects of surface currents on collocated scatterometer retrievals at both Ku- and C-band, and with a data sample population large enough to permit filtering to ameliorate competing factors such as atmospheric stability and sea state. We include assessment of current impacts on satellite altimeter winds (cf. Vandemark et al. (1997)) for the same sites in order to infer if

a broader portion of the ocean wave spectrum responds in a manner similar to that for the waves controlling the scatterometer signal.

3.4 Data and Methods

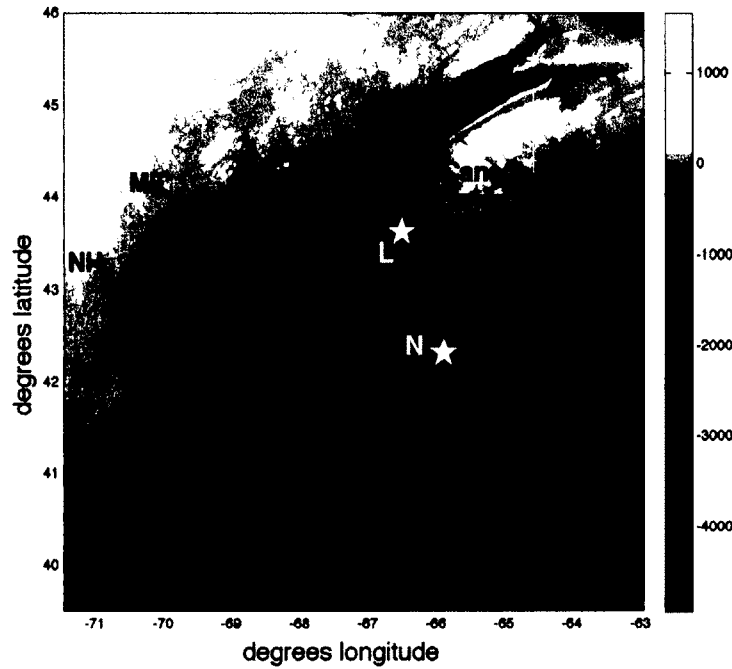


Figure 3-1: Map of the Gulf of Maine region in the northeast US and Canada including bathymetry and with the inset showing the study site. Star symbols indicate regional observing system buoys (black) with this study’s surface current and wind measurement time series nodes, buoys N and L, shown in white.

The study site is the eastern Gulf of Maine centered about buoys N and L as noted in Fig. 3-1 - a location selected for several reasons. First, the region is known for strong reversing semidiurnal (M2) tides (Bigelow (1927), Dupont et al. (2003)) that lead to a local daily variation in surface currents upwards of -0.3 to 0.3 m s^{-1} . The tides, combined with wind driven and bathymetrically controlled coastal currents, provide a large dynamic range in the mean flow bottom boundary condition for air-sea interaction and an average near-surface current velocity of about 40 cm s^{-1} (Fig. 3-2) at both buoys L and N. The second feature of the site is the long-term hourly record of both ocean currents and surface wind vector

measured at these two buoys during a period of twice-daily satellite scatterometer passes that extends from 2004-2011 for Buoy N and 2003-2008 for Buoy L. Moreover, QuikSCAT scatterometer wind vector measurements at multiple resolutions were recently validated in this region (Plagge et al. (2009)¹) and thus the mean agreement between QuikSCAT and *in situ* winds for this site is well established. A final observation regarding the site concerns the spatial length scales associated with the surface currents at the two buoys. Buoy N is moored within the NE Channel, a region of deep water exchange for the Gulf of Maine while buoy L is located N of Browns Bank and inflow from the coastal Scotian current (Smith et al. (2001)). In both cases, local bathymetry and the forcing lead to spatial variability in currents of $O(20\text{-}40\text{ km})$ (e.g. Manning et al. (2009)). This issue will be addressed later in the study.

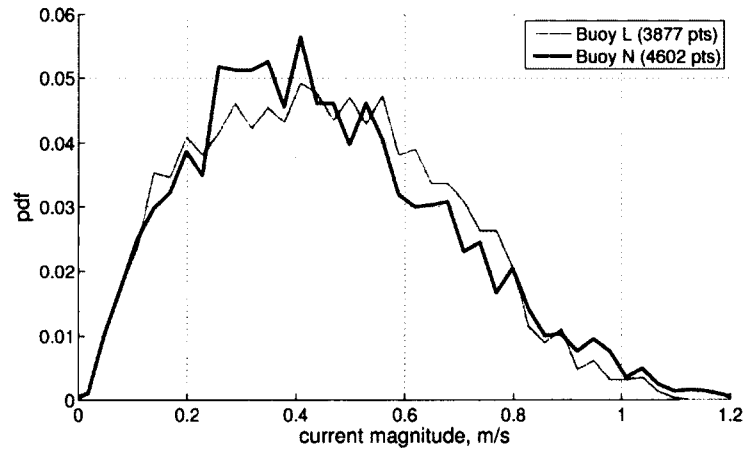


Figure 3-2: Histogram of observed surface current magnitude for both buoys within the collocated datasets.

Buoy near-surface currents are measured using an Aanderraa model RCM 9 current meter with an accuracy of 0.15 cm s^{-1} or 1% of the reading and operated at 2 m depth, close enough to the surface to minimize the effects of shear with depth. Winds are measured using RM Young or Vaisala Windsonic anemometers with an accuracy of 0.3 m s^{-1} with 8-minute averaged winds every hour and obtained via the National Data Buoy Center (Buoy N and L are NDBC stations 44024 and 44038 and are owned and operated by the Univ.

¹Presented here as Chapter 2

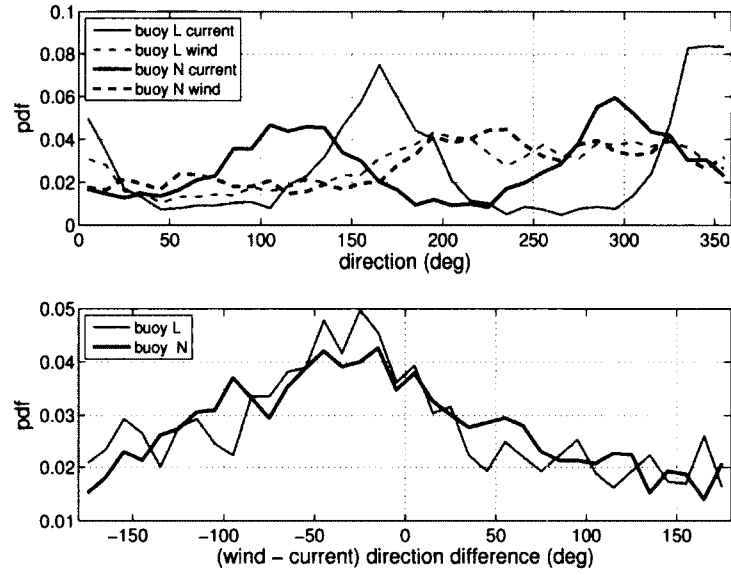


Figure 3-3: Histogram of observed wind and surface current direction for both buoys L and N (upper panel) and the directional difference between the wind and the current (lower). Both are provided using meteorological convention (direction from which the fluid arrives) and both are derived from the datasets used in Fig. 3-2.

of Maine). Ancillary buoy measurements also utilized in this study are air and sea surface temperature, relative humidity, atmospheric pressure and ocean significant wave height. To compare with scatterometer winds, the buoy wind measurements are adjusted to provide a 10-m neutral stability wind estimate using the COARE 3.0 bulk flux algorithm (Fairall et al. (2003), and further explained in Ch. 4). All wind data from this point forward are 10-m neutral winds. Fig. 3-3 provides the distribution of buoy-observed directions for the wind and surface current at both buoy locations within the total co-registered scatterometer/buoy database. The N-S (NW-SE) orientation of the M2 tidal ellipse for buoy L (N) is apparent in the surface current record, as distinguished by the twin peaks in both solid lines in Fig. 3-3a. The directional difference between the wind and current vector is also shown and it is clear that a fairly uniform distribution between wind and current vectors is observed. As expected, this site yields a data set with a wider range of wind-current conditions than found for equatorial regions with their more persistent winds and currents (Quilfen et al. (2001); Kelly et al. (2005)).

The primary scatterometer wind data for this study come from the QuikSCAT satellite Ku-band scatterometer and we evaluate data provided for three spatial resolutions: 25 km (L2B product from NASA-JPL’s Physical Oceanography Distributed Active Archive Center (PODAAC)), 12.5 km (L2B, PODAAC), and 3-5 km (provided by Dr. David Long of Brigham Young University). The latter are referred to as ultra-high resolution (UHR) data (Owen et al. (2003)). Because regional surface current structures are of a finite spatial scale, it was desirable to examine all three data products to assess the potential impact of footprint size in this current impacts investigation. Although UHR data are still considered experimental, they have previously been validated in the Gulf of Maine (Plagge et al. (2009)). To summarize the validation, UHR-buoy residuals are comparable with standard QuikSCAT products, with a slight increase in directional noise but additionally increased spatial enhancement of frontal features. The selected wind vector cell (WVC) solution for each cell is the first, most likely, choice given in each dataset as prescribed in the user handbook (Dunbar et al. (2006)).

The process for collocating *in situ* and QuikSCAT data both spatially and temporally is documented in previous work (Plagge et al. (2009)). Briefly, collocated wind observations between buoy and scatterometer must occur within thirty minutes (buoy-based current and wind measurements are effectively coincident). For every pass within the time frame of a given buoy/scatterometer match, all scatterometer wind vector cells within a 10 km radius of the buoy have been averaged to provide the average wind speed and direction for each resolution. This process provides a total of 4739 triplet matches (scatterometer, buoy wind, and current data) for the UHR, 3996 matches for the 12.5 km, and 2250 matches for the 25 km product.

As discussed in Ebuchi et al. (2002) it is important to consider and address data quality flagging and scatterometer wind vector ambiguity selection in any detailed analysis of wind residuals. Several pre-filtering steps are taken prior to analyses. For all scatterometer products, and before collocation, any wind vector cell estimate flagged as occurring during rain is rejected. Next, any triplet where any wind speed lies above 18 m s^{-1} or where

the current magnitude lies outside of three standard deviations of the mean are rejected to exclude infrequent extreme event data. Finally, cases where the scatterometer direction estimate lies beyond 45 deg. from the buoy are rejected as being cases of poor WVC ambiguity selection. After these latter quality control steps, 3627 UHR triplets, 3250 12.5 km triplets, and 1862 25 km triplets remain. Overall, the results of following analyses with and without such filtering are statistically similar excepting slightly improved linear correlation coefficients.

Comparison of QuikSCAT and buoy wind speeds from the resulting data set are shown in Fig. 3-4 for each resolution and buoy with the linear correlation coefficient and a linear least-square regression fit between the data shown in each panel. The level of agreement between satellite and *in situ* data is consistent with that obtained in the previously cited studies in terms of standard deviation and bias, although one does observe a systematic scatterometer wind overestimation above 12-15 m s⁻¹ in all three products and at both buoys, an observation also noted in previous work in the Gulf of Maine (Plagge et al. (2009)).

Our approach to a broader assessment of current impacts on satellite microwave sensor winds at this site entails performing similar matchup comparisons and analyses of C-band scatterometer and Ku-band satellite altimeter data, following on from earlier studies that worked with much smaller data sets (Quilfen et al. (2001), Vandemark et al. (1997)). The first additional matchup datasets contain measurements from the European Space Agency's Advanced Scatterometer (ASCAT). ASCAT operates at a C-band frequency, and standard data products are provided at 25 km and 12.5 km resolution since 1 Nov. 2007. Bentamy et al. (2008) indicates that ASCAT winds are comparable to QuikSCAT winds globally, and have similar root-mean-squared differences when compared with buoy data (1.72 m s⁻¹ and 18°). Since Sept. 2010, a newer type of ASCAT wind vector retrieval, cited as the coastal product, also provides 12.5 km resolution data but utilizes a significantly smaller data processing window than the 100 km window of the standard ASCAT products. All ASCAT/buoy matchup data for this study were supplied by A. Verhoff from the Royal Netherlands Meteorological Institute (KNMI). Due to the shorter ASCAT data record and

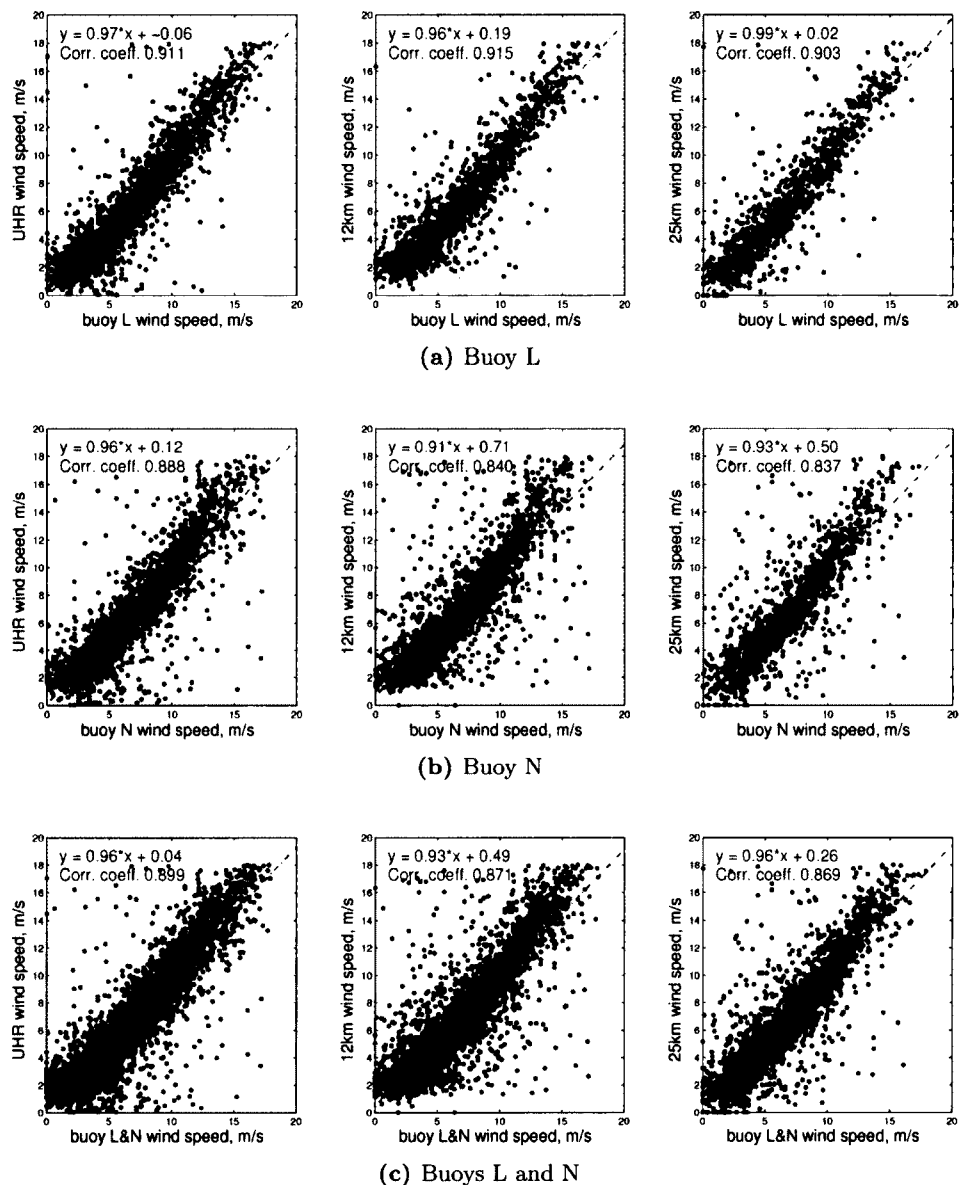


Figure 3-4: Wind speed measurement comparisons between the earth-relative buoy and collocated QuikSCAT observations at a) buoy L, b) buoy N, and c) data for both sites. Panels across each row represent the differing QuikSCAT wind products with highest resolution UHR data on the left, the 12.5 km product in the middle, and the 25 km on the right. A dashed line provides the result from a linear regression fit; this fit and the correlation coefficient are noted in the upper left of each panel.

swath coverage differences, there are fewer triplets for the ASCAT match-ups: 836 triplets for the 12.5 km product, 941 for the 25 km product, and 138 for the coastal product after quality control. For satellite ocean altimetry, we collocate wind speed estimates obtained using three separate Ku-band altimeters: Jason-1, Jason-2, and Envisat, using project Geophysical Data Records as extracted from the Radar Altimetry Database System (Scharroo (2008)). Note that the nominal spatial resolution for the altimeter is 6 km, inherently a finer spatial scale, and thus less error due to spatial smoothing should be obtained. Any measurements within a 15 km radius of buoy N were averaged, yielding 388 total collocated triplets over the period 2004-present. It should also be noted that due to differing satellite tracks, neither ASCAT nor the altimeters were able to provide collocations with buoy L.

3.5 Results

Analyses in this study are focused on isolating the current impact on scatterometer U_{10N} explicit in Eq. 3.1. First, we assume that wind speed residuals between a microwave satellite wind and the fixed earth reference mooring wind measurement relates to \mathbf{U}_s in this equation. In this study we will examine the residual against an effective surface velocity (u_p) where the relevant surface velocity is the vector component projected onto the buoy's wind direction (θ_{bwind}) and defined as

$$u_p = |\mathbf{U}_s| * \cos(\theta_s - \theta_{bwind}) \quad (3.2)$$

This approach differs somewhat from past field studies that separately address mostly zonal wind and current components within sites having well defined large scale currents (Quilfen et al. (2001), Kelly et al. (2005)) along these axes. By using u_p , all possible combinations of wind and current directions are enfolded in a single statistical assessment. The inclusion of all conditions should allow us to best capture large currents associated with local wind and circulation beyond just the tidal flow (Smith et al. (2003)), but may also lead to a higher level of non-current induced variability in the wind residual due to the range of other processes and conditions that can affect wind residual assessment in the coastal zone

(Freilich and Dunbar (1999), Plagge et al. (2009), Portabella and Stoffelen (2009)). Before proceeding, we also examined the requisite assumption that scatterometer wind direction estimates are unbiased with respect to the relative angle between the buoy's wind and surface current directions. This is the case for our datasets, with no angular difference sector exhibiting biases greater than 6 degrees. Therefore using speed or wind vector differences yield nearly equivalent results and the focus is solely on wind speed going forward.

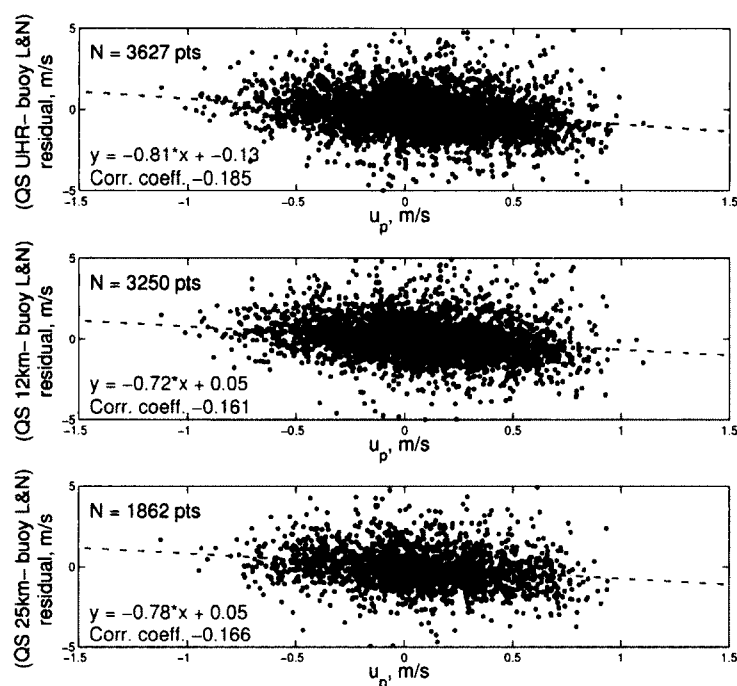


Figure 3-5: Wind speed differences (QuikSCAT - buoy) versus the projected surface current velocity u_p with results provided for each QuikSCAT wind product. Data represent all wind, wave, and current conditions within the datasets at buoys L and N. The sample population (N) is noted in each panel.

QuikSCAT wind residuals versus u_p for all data contained in the pre-filtered matchup data sets at both buoys (L and N) are presented in Fig. 3-5. A separate panel is shown for each of the three Ku-band scatterometer products. Positive (negative) u_p indicates that the projected current and wind are aligned in the same (opposite) direction. The data scatter about zero with an rms of nearly 2 m s^{-1} . Most importantly, there is a clear negative correlation evident in the data indicating the scatterometer wind exceeds the buoy in the event

of an opposing current. Noted linear regression fit parameters are similar for all three resolutions and show slopes of -0.8 to -0.9 highlighted with the grey dashed line in each panel. The linear correlation (R) coefficients are quite similar (-0.185 (UHR), -0.161 (12.5 km), and -0.166 (25 km)) and the 95% confidence interval for R lies above -0.12 for all three cases.

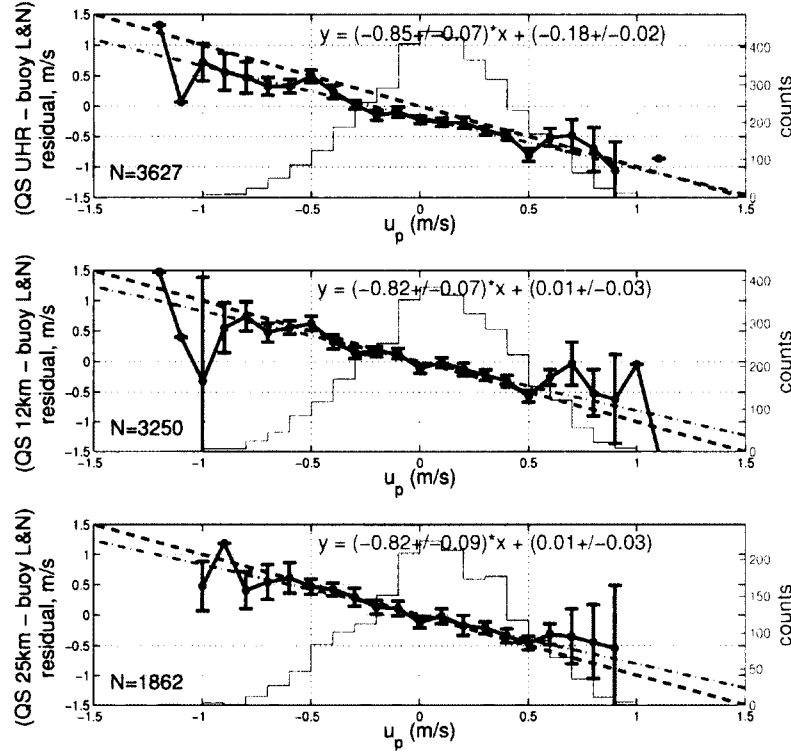


Figure 3-6: Bin-averaged wind speed differences (QuikSCAT - buoy) versus u_p (10 cm s⁻¹ bins) for the same datasets in Fig. 3-5. Error bars represent standard error within each bin. The black dashed curve represents a -1:1 line while the gray dot-dashed is the result from a weighted linear regression (see text). Sample population is noted on each panel.

Fig. 3-6 also presents the same data after bin-averaging versus u_p , with a change in the y axis to accentuate the 1:1 anticorrelation with currents that is expected if the scatterometer residuals are indeed current-relative. The black-dashed line shows this ideal slope of -1. A weighted linear least-squares model is applied to the binned data, using the inverse of each bin's standard error as the weights. Only bins containing at least 10 points contribute to the fit, to satisfy the central limit theorem. A histogram of samples in each bin is shown as a grey solid line. Fit coefficients and their uncertainty are provided on each

	Resolution	Slope	Slope SD	Y-Inter.	Y-Inter. SD	Corr.	N
Buoy L	UHR	-0.83	0.10	-0.23	0.03	-0.201	1615
	12 km	-0.87	0.10	-0.04	0.04	-0.195	1282
	25 km	-0.86	0.13	0.00	0.05	-0.195	847
Buoy N	UHR	-0.87	0.09	-0.15	0.03	-0.175	2015
	12 km	-0.84	0.09	+0.03	0.03	-0.143	1972
	25 km	-0.81	0.13	0.00	0.05	-0.146	1017
Buoys L and N	UHR	-0.85	0.07	-0.18	0.02	-0.185	3627
	12 km	-0.82	0.07	+0.01	0.03	-0.161	3250
	25 km	-0.92	0.10	+0.01	0.03	-0.166	1862

Table 3.1: Slopes, intercepts, and their uncertainties for the weighted least squares fit of wind speed residuals (m s^{-1}) versus u_p for different QuikSCAT resolutions and for different buoys.

panel. To within the confidence intervals given, these slope estimates agree with those from the unweighted slope values given in Fig. 3-5 for each QuikSCAT resolution. Again, each QuikSCAT product yields a similar result of a negative slope lying between -0.82 and -0.85. Also note that the significance level of the wind residual relationship versus u_p is evident from the error bars, extending out to a range of u_p of -0.6 to 0.6 m s^{-1} . While the figures show combined results for buoys L and N, those for the individual buoys were similar. All weighted fit parameters are provided in Table 3.1.

While these initial results show a clear correlation between speed residuals and u_p and a slope of nearly -1, the correlation coefficient values fall well below the levels of 0.4 to 0.6 cited in past field scatterometer studies (Kelly et al. (2001), Quilfen et al. (2001)). This evaluation includes all data collected without consideration for varied sea state and air-sea conditions. As noted in the introduction, detecting and reducing spurious correlation amongst factors (waves, atmospheric stability, currents, geophysical model function errors) controlling the scatterometer winds at the 1-2 m s^{-1} level is difficult. As one example, consider the possible case where stable atmospheric conditions systematically bias the scatterometer winds low and also regularly coincide with positive u_p in our region. This would negate or ameliorate the current impact depending on the covariance between these effects. To investigate whether current impacts can be more clearly resolved, we computed the aforementioned statistics after filtering by differing wind, wave, and atmospheric stability

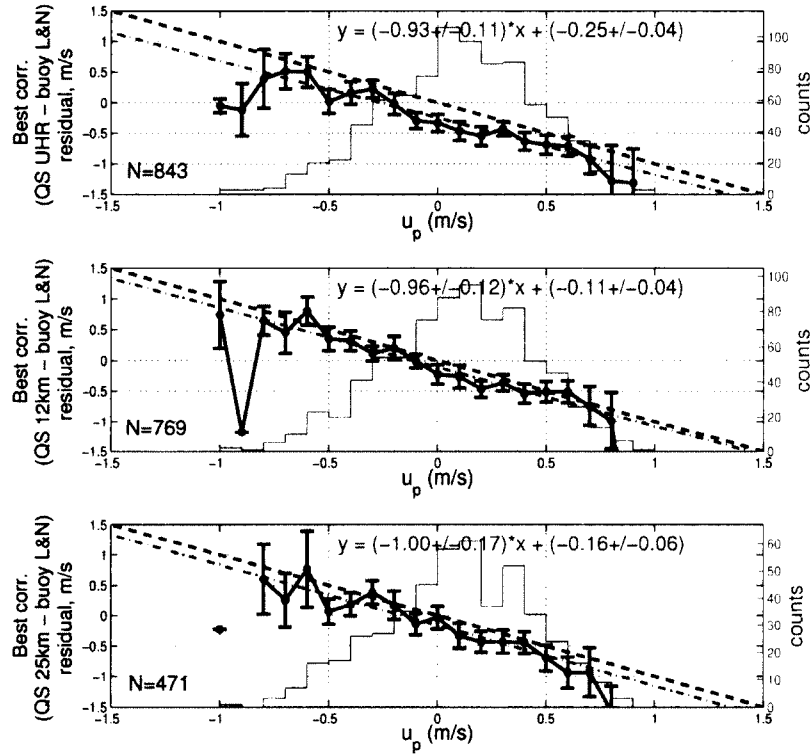


Figure 3-7: Binned wind speed residuals (QuikSCAT minus buoy) versus the effective surface current for the conditions chosen to show the best correlation: moderate wind speed and neutral atmospheric stability. This and all subsequent binned figures follow the methodology of Fig. 3-6).

regimes (cf. Ebuchi et al. (2002)). Results, including linear correlation coefficients, are given in Table 3.2. Slopes and correlations are not significantly different across the table for varied scatterometer resolutions.

In general, the best results are seen for moderate winds, low sea states (<1.6 m) and near neutral stability. This region does not experience a wide range of wave conditions and thus wave impacts are unlikely to be a large factor in the results of this study. But increased noise and/or bias in scatterometer-buoy wind comparisons at low winds (Plagge et al. (2009), Ebuchi et al. (2002), Kelly et al. (2005)) and for strongly stable or unstable boundary layer conditions do appear to lead to weaker correlations and lower or higher slopes. From numerous past studies addressing scatterometer and buoy intercomparisons, it is reasonable to assume that the best constraint on conditions for surface current impact

Regime/Rule	Res.	Slope	Slope SD	Y-Int.	Y-Int. SD	Corr.
<i>buoy wind speed</i> ≤ 5	UHR	-0.82	0.10	-0.14	0.03	-0.192
	12.5 km	-0.86	0.11	+0.06	0.04	-0.167
	25 km	-1.00	0.15	-0.01	0.05	-0.161
$5 < \text{buoy wind speed} \leq 10$	UHR	-0.95	0.09	-0.41	0.03	-0.206
	12.5 km	-0.98	0.09	-0.21	0.03	-0.213
	25 km	-1.01	0.13	-0.21	0.04	-0.204
<i>buoy wind speed</i> > 10	UHR	-1.05	0.18	+0.28	0.05	-0.193
	12.5 km	-0.94	0.22	+0.42	0.07	-0.112
	25 km	-1.07	0.25	+0.51	0.09	-0.173
<i>sig. wave height</i> ≤ 1	UHR	-0.96	0.12	-0.44	0.04	-0.198
	12.5 km	-0.94	0.11	-0.27	0.04	-0.238
	25 km	-1.01	0.14	-0.34	0.05	-0.223
$1 < \text{sig. wave height} \leq 1.6$	UHR	-1.17	0.14	-0.28	0.05	-0.262
	12.5 km	-1.24	0.12	-0.11	0.05	-0.295
	25 km	-1.28	0.17	-0.11	0.06	-0.268
<i>sig. wave height</i> > 1.6	UHR	-0.82	0.12	+0.17	0.04	-0.160
	12.5 km	-0.86	0.12	+0.35	0.04	-0.166
	25 km	-0.84	0.18	+0.41	0.06	-0.132
$-0.4 \leq z/L \leq 0.1$ (near-neutral)	UHR	-0.86	0.09	-0.06	0.03	-0.210
	12.5 km	-0.90	0.10	+0.11	0.04	-0.18
	25 km	-0.79	0.13	+0.07	0.05	-0.194
$z/L > 0.1$ (stable)	UHR	-1.00	0.10	-0.61	0.04	-0.196
	12.5 km	-0.95	0.10	-0.41	0.04	-0.168
	25 km	-0.94	0.15	-0.35	0.05	-0.149
$z/L < -0.4$ (unstable)	UHR	-0.70	0.22	+0.57	0.06	-0.131
	12.5 km	-0.72	0.23	+0.67	0.07	-0.098
	25 km	-0.55	0.35	+0.57	0.10	-0.127
Best: mod. wind, near-neut.	UHR	-0.93	0.11	-0.25	0.04	-0.250
	12.5 km	-0.96	0.12	0.11	0.04	-0.256
	25 km	-1.00	0.17	-0.16	0.06	-0.266
Worst: light wind, unstable	UHR	-0.52	0.28	+0.66	0.08	-0.122
	12.5 km	-0.55	0.29	+0.78	0.09	-0.071
	25 km	-0.31	0.46	+0.69	0.13	-0.116

Table 3.2: Statistics from the same weighted least squares fit of wind residuals versus currents as for Table 3.1 but after filtering for different air-sea interface conditions. Significant wave height and the Monin-Obukov stability length scale parameter (L) come from buoy observations; stability of boundary layer is based on definitions in Large and Pond (1982). Results are for combined buoy L and N datasets.

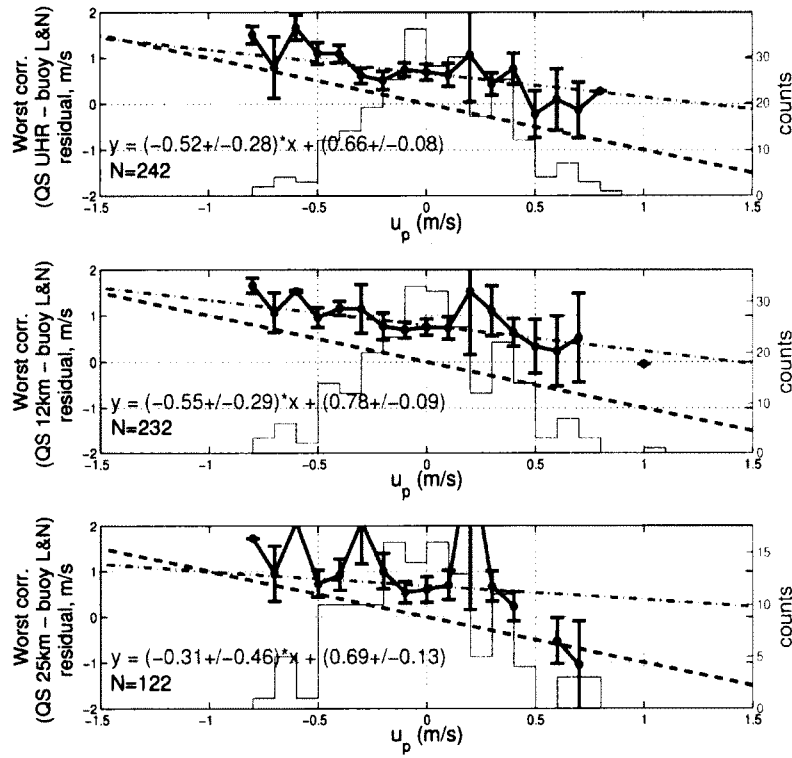


Figure 3-8: Binned wind speed residuals (QuikSCAT minus buoy) versus the effective surface current for conditions giving worst correlation: light wind and unstable boundary layer.

assessments are those of near-neutral atmospheric stability ($-0.4 \leq z/L \leq 0.1$) and moderate wind speeds of $5\text{--}10 \text{ m s}^{-1}$. Under those filtering conditions, we achieve correlations of -0.250 (UHR), -0.256 (12.5 km) and -0.266 (25 km) with the bin-averaged results shown in Fig. 3-7. By contrast, the conditions that yield the weakest correlation are those for light winds and unstable boundary layers ($z/L < -0.4$). In this case, the relationship is far from $-1:1$ for all resolutions (Fig. 3-8), and the correlations quite low: -0.122 (UHR), -0.071 (12.5 km), and -0.116 (25 km).

Results from a similar evaluation of C-band ASCAT satellite scatterometer data are shown in Figs. 3-9 and 3-10. The lower data sample size is apparent in comparison to QuikSCAT but the scatter of the data is somewhat reduced and, most importantly, a negative correlation versus u_p is also observed. However, it is also clear that there is a large

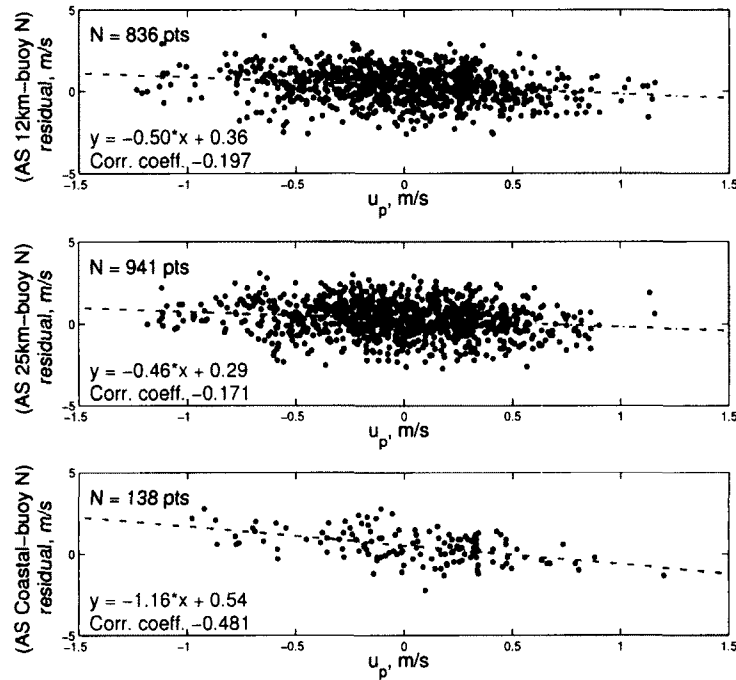


Figure 3-9: Wind speed differences (ASCAT - buoy) versus the projected surface current velocity u_p with results provided for each ASCAT wind product. Data represent all wind, wave, and current conditions within the dataset at buoy N, 2007-2011.

difference in the slopes observed for the 12 km and 25 km products (-0.53 and -0.51 for binned slopes), and that for the Coastal ASCAT product (-1.07 binned slope). Only the coastal products lies near that observed for the Ku-band QuikSCAT. The correlation coefficient for the coastal product of -0.48 is also elevated beyond that seen for any other dataset.

Altimeter-buoy wind residuals versus u_p are shown in Figs. 3-11 and 3-12. As previously mentioned, only observations at buoy N are used because the passage of altimeter tracks near to buoy L was much more limited. Recall that this dataset represents a compilation drawn from the combination of Ku-band sensors aboard the Jason-1, -2, and Envisat platforms. While again the sample population is much lower than for QuikSCAT, these data show remarkably similar results to that shown for QuikSCAT, for example in Fig. 3-6. The weighted least squares fit of Fig. 3-12 yields a slope of -0.97 ± 0.26 and the linear correlation coefficient of 0.204 is near that seen for the scatterometer. These altimeter results are for

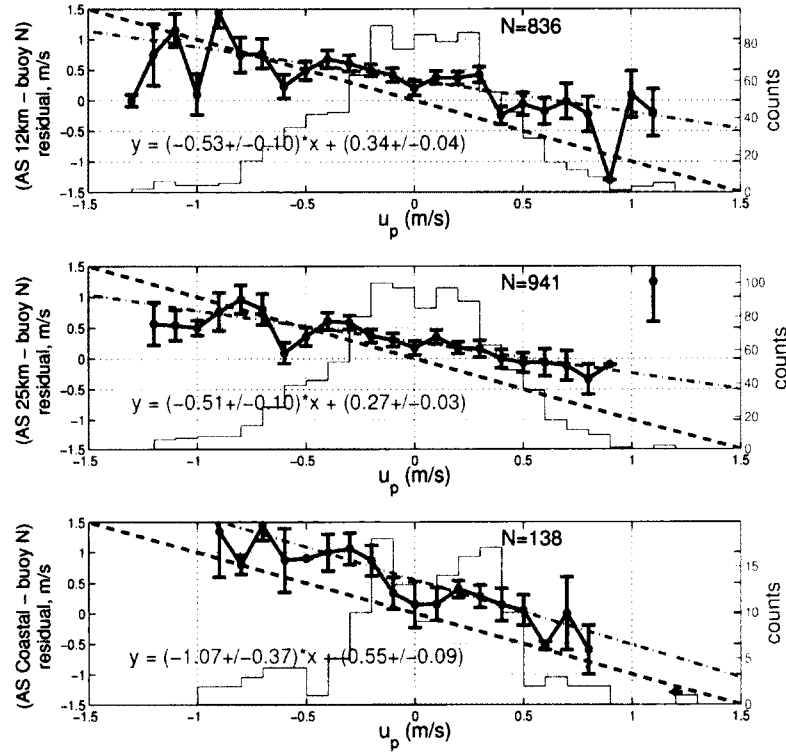


Figure 3-10: Wind speed differences (ASCAT minus buoy) binned according to u_p (see Fig 3-9 for correlations).

the full range of observed surface conditions without filtering for wind regimes or stability effects, due to the limited number of samples.

3.6 Discussion

The observational evidence to date concerning the treatment of scatterometer ocean wind as a current-relative velocity lies primarily within five studies (Quilfen et al. (2001), Cornillon and Park (2001), Dickinson et al. (2001), Kelly et al. (2001), Kelly et al. (2005)) with the former addressing the C-band ERS scatterometer and the remainder Ku-band NSCAT or QuikSCAT data. In most cases, these studies relate separate long-term averages of currents and of wind (or wind vector) residuals leading to convincing causal evidence such as Fig. 4 in Cornillon and Park (2001), Fig. 6 in Chelton et al. (2004), and Fig. 3 in Kelly

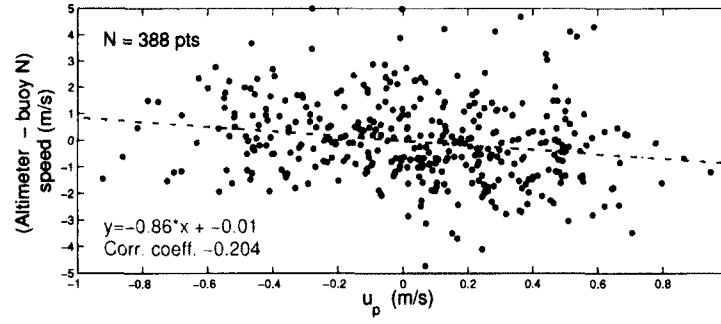


Figure 3-11: Wind speed differences (Altimeter - buoy) versus projected surface current velocity u_p . Data represent all wind, wave, and current conditions within the collocated dataset at buoy N, 2004-2011.

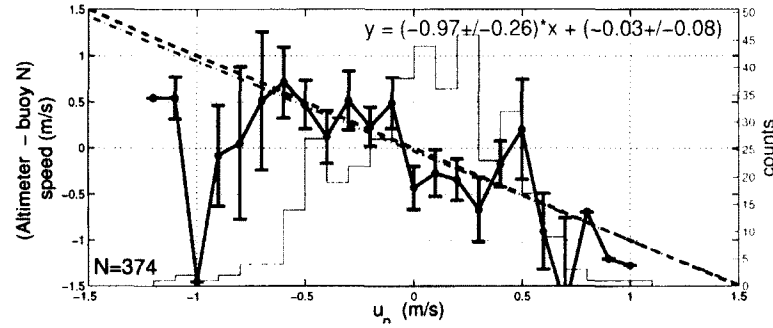


Figure 3-12: Residuals for altimeter minus buoy N wind speeds, binned according to u_p .

et al. (2001). However, only Dickinson et al. (2001) provides a quantitative estimate of the transfer function between observed zonal wind differences and the zonal current with their linear regression coefficient being 1.3 at Ku-band, suggesting enhanced wind perturbation beyond the 1:1 relationship with U_s of Eq. 3.1. Results from the C-band ERS scatterometer seen in Fig. 10 in Quilfen et al. (2001)) indicate a slope possibly exceeding 1.0 but actual linear regression coefficients are not provided. Given the low value of the linear correlation coefficient and varied noise sources contributing to mask current impacts in all of these studies, it is understandable that direct and formal quantification has been difficult. Results presented here for QuikSCAT provide a new and complementary quantification with detailed estimates of uncertainty as summarized in Fig. 3-7 and Table 3.2. The observed relationship between wind residuals and the effective current in the Gulf of Maine region clearly affirms that the scatterometer yields a current-relative wind. Moreover, the data lead us to conclude that for the Ku-band scatterometer there is no statistical justification to

deviate from a slope of 1.0 with the actual best-case isolation for currents yielding a slope of -0.96 ± 0.12 (for 12 km data). The large sample population and use of the daily variations in tidal flow contained in this study seem to allow isolation of the phenomenon, but we do note that much averaging is required as the circulation dynamics near our buoys L and N (Smith et al. (2003)) are much more active than within the persistent warm core rings of large-scale currents used in previous investigations, possibly leading to increased differences due to time-and-space lags. This is the likely reason for the observed linear correlation coefficients nearer to 0.2 as opposed to 0.4 to 0.6 cited earlier.

Another possible contribution to low correlations is boundary layer (BL) modification due to stability. For a two-layer BL model, the inner (surface) layer is logarithmic and corrected for stratification, humidity, and surface roughness (the neutral version of this is given as Eq. 3.1), and the outer is a stratification-dependent Ekman layer, associated with rotation of the wind with height and stability (Businger and Shaw (1984); Brown and Liu (1982)). At the surface, it is assumed that the stress direction is the same as the wind direction. But in certain circumstances, the direction of the wind at the height of the anemometer on the buoys (3 m) may have already been affected by stratification, (Businger and Shaw (1984), Fig. 2), causing it to be different from the direction derived at the surface from the scatterometer. This turning or rotation could impact the validity of u_p as defined, and add noise to the overall results. This would be especially true during stable conditions. However, given the methods for calibrating the scatterometer GMFs, using the basic surface layer model and the buoy wind direction without an additional turning angle is sufficient for a study containing the range of conditions present here (Foster (2012)).

Results from section 3.5 also serve to address the question of equal treatment of C-band and Ku-band scatterometer data as well as that from systems such as the microwave altimeter. It is understood that the ocean radar backscatter for each sensor is uniquely related to the transmit frequency, polarization and incidence angle and the interaction of the signal with the spectrum of waves on the sea surface. However, for these three systems and most passive and active microwave wind sensors, the fundamental issue of a changing

bottom kinematic boundary condition should lead to a current-relative wind for the cases of large scale currents. In this study we find this to be the case, where the C-band ASCAT coastal wind product data, the Ku-band altimeter winds, and QuikSCAT all yield statistically similar results over the same buoy sites. Knowing the altimeter reflects a broader integration of wave scales in its backscatter and wind estimates compared to the weighting of scatterometers towards 2-8 cm scale gravity-capillary wave roughness scales (cf. Mouche et al. (2007)), we infer that all wave scales shorter than roughly 10-20 m are, on average, adjusted to the local wind and surface current environment. One can then expect similar results for lower frequency radar (e.g. L-band) and for passive microwave systems such as SSM/I, AMSR-E and Windsat. Results also offer insight into the spatial scale of currents near buoys N and L in the Gulf of Maine and, in turn, why the upper panel ASCAT data of Figs. 3-9 and 3-10 differ from ASCAT coastal product findings. Similar current-relative regression statistics are observed for all three QuikSCAT data products spanning down from 25 to 12 to the nominally 5 km UHR. This is not the case for the ASCAT data where the relationship between currents and the wind residuals is largely lost for the 25 and 12 km data. This apparent difference between ASCAT and QuikSCAT is known to be a consequence of the data processing window rather than physics. Once we incorporated the newer coastal product into the study, it became clear that the shallow slopes obtained using data produced under the standard spatial Hamming window (of order 50 km at the 3 dB points) used to filter ASCAT 25 and 12 km data resulted in a satellite wind footprint smearing. This is consistent with the expectation that spatial averaging beyond 25 km would exceed the typical zonal length scale of currents in the Northeast channel near buoy B as well as northward at buoy L (Chen et al. (2011)). Future studies using ASCAT data in any buoy-satellite wind comparisons should closely consider these spatial windowing issues.

To further discuss the issues related to spatial variability of current interactions in scatterometry, a case study was developed to explore the effect across the marginal shelf region containing the two buoys. For this purpose, hindcast model surface wind data were differenced with scatterometer swath data to examine possible differences in wind field spatial structures in comparison to expected ocean currents. The weather model data come from

regional multi-resolution (3km, 9km, and 27km) weather research and forecasting (WRF) model output (Skamarock and Klemp (2008)) produced routinely at UNH. Our chosen products were the 3-hourly 9km domain 10-m wind vectors (u and v) and surface air temperature fields. The WRF model version was 2.1.2 and the Yonsei University scheme was used to parameterize the planetary boundary layer (Hong et al. (2006)). No ocean currents were used in the bottom boundary condition for WRF model runs and only climatological SST data were used. For diagnosing wind residuals, hourly hindcast oceanic surface current vectors were used from the Gulf of Maine Finite Volume Community Ocean Model (FVCOM) circulation model developed by Dr. Chen and colleagues the University of Massachusetts. Because it uses an unstructured grid, FVCOM's fields have no fixed resolution, but this output had spacing below 5 km at all nodes in our region of interest. For these data as well as the 12.5 km QuikSCAT retrievals, linear interpolation was used to resample all data to 9 km for comparison with the atmospheric model.

Fig. 3-13 presents one case of wind, current, and wind residual estimates from a 2-degree-by-2-degree area of the Gulf of Maine that includes Buoy L and N and represents a region of strong M2 tidal flow. Note that Fig. 3-1 provides a full regional map and the location of this region of interest. This specific case occurred near to 00UTC 27 Dec. 2008 and is chosen to illustrate one extreme case of current impacts upon scatterometer winds. Here the ocean model (2258UTC 26 Dec. 2008, see panel a) indicates flood tide conditions with the currents greater than 50 cm s^{-1} generally directed to the NNW and with enhanced flow near to Nova Scotia (43.3N) and also in the center near Brown's Bank (closed bathymetric contour near 42.5N, 66.2W). QuikSCAT winds (2312UTC, Dec. 26 2008, see panel c) are from the NNW nearly in opposition to the tidal flow. This December case was also chosen for uniformity in the sea surface temperature fields (not shown) to limit non-current impacts due to marine boundary layer and SST front features. Fig. 3-13b WRF-predicted winds (00UTC Dec. 27 2008) indicate a much smoother spatial field than for QuikSCAT but similar NNW direction. The average WRF wind speed within this ROI was 2.41 m s^{-1} below QuikScat, a number significantly in excess of the mean current (0.4 m s^{-1}). We therefore create the wind residual between QuikSCAT and WRF to take into account the

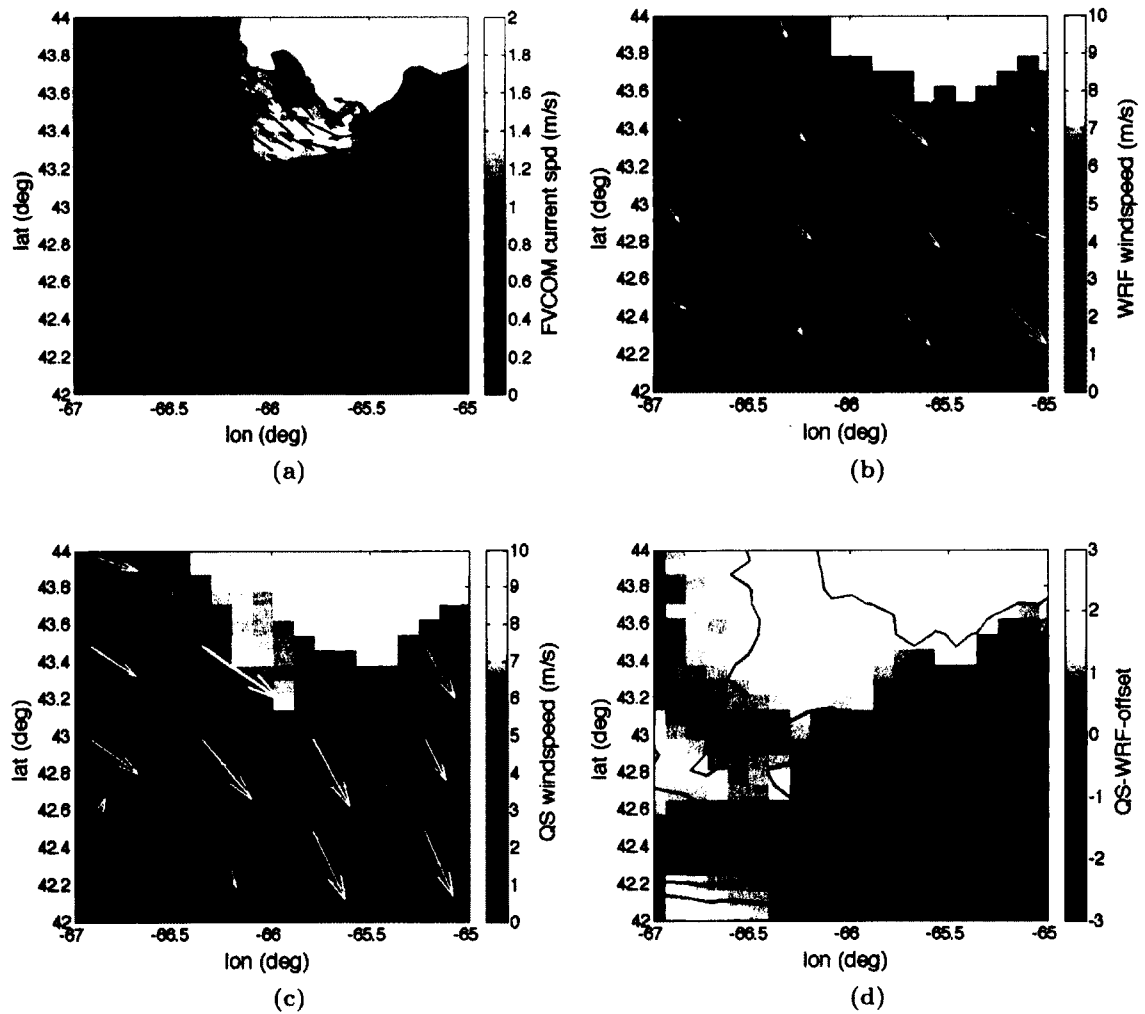


Figure 3-13: Spatial view of surface current effects on a QuikSCAT pass from 23:01 UTC Dec. 26, 2008, for the region southwest of Nova Scotia, depicted as a black box in Fig. 3-1. (a) FVCOM surface current magnitude (grayscale) and vectors (black arrows) from a run at 22:58 UTC Dec. 26, 2008. (b) WRF wind speed from a model run at 00:00 UTC Dec. 27, 2008 with white arrows showing subsampled WRF wind vectors. (c) 12km QuikSCAT wind speed; here white arrows show subsampled QuikSCAT wind vectors. (d) Windspeed residual (scatterometer minus model), including an offset determined by the mean wind speed difference and the mean current speed within the ROI.

mean wind speed offset and the mean current offset, and arrive at the wind difference map of Fig. 3-13d. Note that the WRF data are for 00UTC and the scatterometer data are taken one hour before, yet it is the spatial variation of the residuals (seen in panel d) that is most important here along with its relationship to the ocean currents given in Fig. 3-13a. The wind residual map indicates a clear enhancement of the scatterometer winds in Fig. 3-13d near to the coast of Nova Scotia and then periodic enhancement towards the SSW across to Georges Bank in the very SW corner of the image. These features are qualitatively similar to the dynamics of the FVCOM currents in Fig. 3-13a. While illustrative, we found it difficult to use this WRF-FVCOM-QuikSCAT approach to rigorously examine current effects in this region because of the combined issues of time and space variability of the tidal currents, temporal differences between model and satellite products, and model inaccuracies. The work performed in large scale and persistent currents (Chelton et al. (2004), Kelly et al. (2005), Park et al. (2006)) have shown better results in that respect.

3.7 Conclusions

This study has used *in situ* mooring data and measurements of the tidally dominated currents in the Gulf of Maine to show that satellite winds derived from Ku-band scatterometry, C-band scatterometry, and Ku-band altimetry all provide a current-relative, rather than earth-relative, wind speed. We are able to quantify this conclusion by finding slopes between buoy and satellite wind residuals and the wind-projected currents that lie at -0.96 ± 0.12 , -1.07 ± 0.37 , and -0.97 ± 0.26 , for best-case 12 km QuikSCAT, coastal ASCAT, and a complement of altimeters respectively. While the expectation and demonstration of ocean current effects upon scatterometer winds is not new, this study significantly advances quantitative certainty in the current-relative wind assumption made within Eq. 3.1, and in its application to winds derived both from satellite sensors that primarily respond to short-scale Bragg waves and those responding to a broader spectrum such as the altimeter and radiometer.

On the whole, this study affirms that for surface currents with length scales of 10 km and longer, microwave remote sensing winds can be considered to be current-relative; a result that is consistent *in situ* and satellite scatterometer comparisons in large equatorial currents (Dickinson et al. (2001), Quilfen et al. (2001)). The difference between earth-relative and current-relative wind can be quite pronounced across this coastal site where current magnitudes of 10-20% of the wind velocity are quite common, and the impact on the pseudostress would be even higher. In fact, the region's reversing M2 tide must be driving a measurable semi-diurnal difference in the wind stress over a fairly large portion of the eastern Gulf of Maine for those cases when the synoptic winds near alignment with the tidal ellipse. Typical twice-daily sampling by scatterometry is unlikely to fully capture this feature, but predictive regional atmosphere-ocean modeling should consider this impact (cf. Kara et al. (2007)). As discussed elsewhere (Chelton et al. (2004), Park et al. (2006)), the present results also predict that wind stress curl fields computed from scatterometer data in this region will, at times, show spatial structure that is closely related to the tidal flow and its interactions with bathymetry in the Gulf of Maine. Based on the similar findings of current impacts for the altimeter and scatterometer, it is expected that when the spatial scale of the currents and thus the kinematic boundary condition is large enough, even the 50 km footprint of scanning microwave radiometers will provide current-relative winds; this has significant implications for developing accurate long-term climate records that merge satellite wind speed and wind vector data.

3.8 Acknowledgments

This study was made possible by the long-term field measurements openly provided by the Univ. of Maine buoy group and our thanks go to Dr. Neal Pettigrew and his team, as well as NOAA Integrated Ocean Observing System funding. The authors also acknowledge the invaluable support and assistance of Dr. David Long at BYU, Dr. Rich Signell at USGS, Dr. Ernesto Rodriguez at JPL, Dr. Anton Verhoef with KNMI, Dr. C. Chen at the Univ. Massachusetts, Dartmouth, and Dr. Hui Feng at UNH. Funding for the authors come

from the NASA Graduate Student Research Program Grant NNX09AU69G, and NASA's Ocean Vector Wind Science Team Grant NNX10A085G.

3.9 Appendix

The preceeding has been taken in its entirety from the draft submitted to AMS in January 2012. The following describes additional details that did not become part of the submitted paper in order to present a more complete picture of the work supporting the investigation.

3.9.1 Directional Impacts

In addition to the aforementioned studies that focus on the differences in retrieved wind magnitude when the winds blow directly along/against the current, recent work by Zhang et al. (2009) has shown that winds blowing across a strong surface current field can refract the energy-containing waves away from the mean wind direction, shifting the direction of the stress vector in comparison to the wind vector. Earlier papers by Rieder and colleagues [Rieder et al. (1994); Rieder and Smith (1998)] also confirm the impacts of waves on stress vector direction. From these studies, it might be expected that in the presence of currents, a sensor that responds to stress – like a scatterometer – would measure a different wind direction than that seen by an anemometer, but as was mentioned in Section 3.5, no statistically significant relationship was found between directional residuals and current. This was further confirmed for this dataset using several different statistical analyses. Provided here is a binned plot (Fig. 3-14) showing that there is no evident coupling between surface current and directional residual; the linear correlation coefficient values fall below the level of significance. This was the case for QuikSCAT as well as for ASCAT collocations. While these wind-stress-current directional dynamics are no doubt present, it may be that the resolution of existing scatterometry products is not sufficient to reveal them.

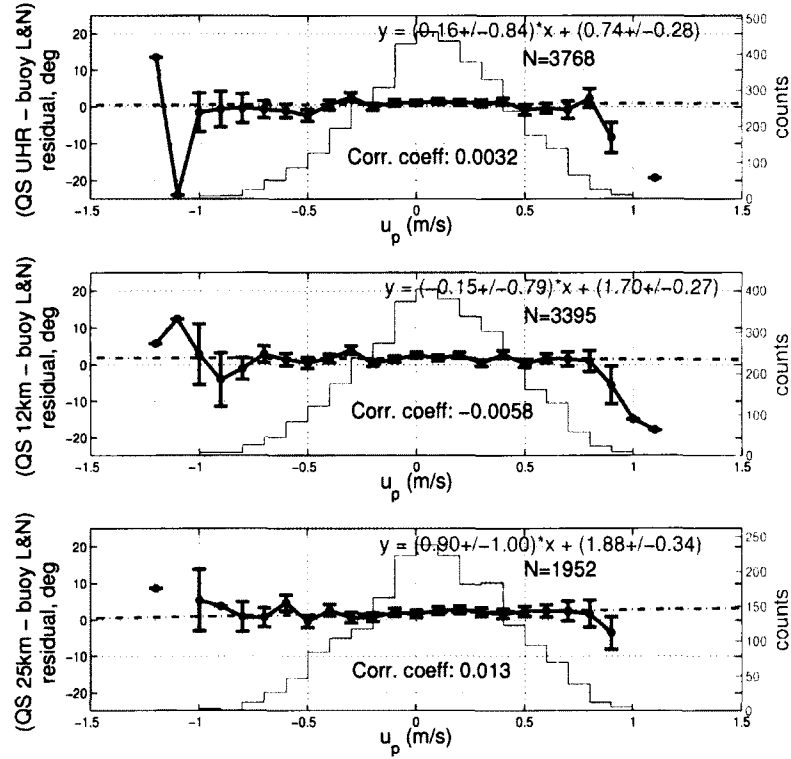


Figure 3-14: Bin-averaged wind speed differences (QuikSCAT - buoy) versus u_p (10 cm s⁻¹ bins) for the same datasets used in Figs. 3-5 and 3-6. Error bars represent standard error within each bin. The gray dot-dashed line is the result from a weighted linear regression (see text). Sample populations and correlation coefficients are noted on each panel.

3.9.2 Spatial Case Study Challenges

Although it has already been mentioned in the discussion of Fig. 3-13, it is worth reiterating the difficulty of finding a case to demonstrate the nature of QuikSCAT-current dynamics in a spatial sense. There were many limitations, two of which related purely to timing. Because of the failure of QuikSCAT in late 2009 and the fact that the WRF model runs did not begin until March 2008, there was a limited overlap in data records within our specific data compilation. Secondly, because QuikSCAT passed over the Gulf of Maine approximately every 12 hours, and the WRF analysis was performed every three hours, the number of satellite passes and model runs within half an hour of each other were very slim. Even extending the window to passes/runs within one and a half hours of each other only provided a total of 45 cases within 2008, for instance. Another restriction was also somewhat based on time: it was necessary to only choose instances when the tidal current flow

was maximum or near maximum, and only areas where that flow was sufficient to expect a discernible impact on the QuikSCAT fields. Additionally, the best areas of the Gulf of Maine in terms of strong consistent currents were in the Bay of Fundy, over Georges Bank, and within the Northeast Channel, so I narrowed my search to these areas. Furthermore, because of the importance of the relative directions of current and wind, instances were also limited to times of relatively steady and homogeneous wind flow, to ensure that the timing differences between ocean model and scatterometer/WRF wind fields did not cause unexpected mis-matches of direction. The other major complication dealt with temperature fields, both of air and of sea. The oceanography of the Gulf of Maine is such that moderately strong sea surface temperature (SST) fronts are not uncommon. The presence of these SST fronts means that local stability can be quite variable, and as changes in stability affect scatterometer retrievals in complicated ways (see Ch. 4), it was desirable to avoid areas/times of strong air-sea temperature differences. Because of the importance of these dynamics, temperature fields were examined not only from WRF (air) and FVCOM (ocean), but also from SST products from satellite, including 8-day averages from MODIS and blended products available from Remote Sensing Systems.

All of these qualifications (along with previously mentioned built-in error due to regrid-ding, interpolation, and accuracies of the models themselves) meant that over the full time period of WRF and QuikSCAT data availability, there were only ten cases that met stated requirements and were worth investigating by eye. Of these cases, three appeared to show patterns representing surface currents in the QuikSCAT fields that were not present in the WRF winds, but only one (the case shown in Fig. 3-13) appeared to confirm expectations in a meaningful manner. It seems logical that if it was this hard to find an illustration, it is likely that the effects are not first-order for the time/area considered, despite the strong currents in several of the regions examined. Given the degree to which air-sea temperature seems to correlate with differences between the scatterometer and model winds, this work also confirms the importance of a full investigation of stability effects on scatterometer retrievals (see Ch. 4).

Bibliography

- Bentamy, A., D. Croize-Fillon, and C. Perigaud, 2008: Characterization of ASCAT measurements based on buoy and QuikSCAT wind vector observations. *Ocean Sci.*, **4**, 265–274.
- Bigelow, H. B., 1927: *Physical oceanography of the Gulf of Maine*. U.S. Govt. Print. Off., 526 pp.
- Bourassa, M. A., 2006: Satellite-based observations of surface turbulent stress during severe weather. *Atmosphere-Ocean Interactions*, W. Perrie, Ed., Wessex Institute of Technology, Advanced Fluid Mechanics Series Vol. 39, Vol. 2, 35–52.
- Brown, R. A. and W. T. Liu, 1982: An operational-large scale marine planetary boundary layer model. *J. Appl. Meteorol.*, **21** (3), 261–269.
- Businger, J. A. and W. J. Shaw, 1984: The response of the marine boundary layer to mesoscale variations in sea-surface temperature. *Dynam. Atmos. Oceans*, **8**, 267–281.
- Chelton, D. B., M. H. Freilich, J. M. Sienkiewicz, and J. M. Von Ahn, 2006: On the use of QuikSCAT scatterometer measurements of surface winds for marine weather prediction. *Mon. Wea. Rev.*, **134** (8), 2055–2071.
- Chelton, D. B., M. G. Schlax, M. H. Freilich, and R. F. Milliff, 2004: Satellite measurements reveal persistent small-scale features in ocean winds. *Science*, **303** (5660), 978–983.
- Chen, C., et al., 2011: Tidal dynamics in the Gulf of Maine and New England Shelf: An application of FVCOM. *J. Geophys. Res.*, **116** (C12010).
- Cornillon, P. and K.-A. Park, 2001: Warm core ring velocities inferred from NSCAT. *Geophys. Res. Lett.*, **28**, 575–578.
- Dickinson, S., K. A. Kelly, M. Caruso, and M. J. McPhaden, 2001: Comparisons between the TAO buoy and NASA scatterometer wind vectors. *J. Atmos. Oceanic Technol.*, **18**, 799–806.

- Donelan, M. A. and W. J. Pierson, 1987: Radar scattering and equilibrium ranges in wind-generated waves with application to scatterometry. *J. Geophys. Res.*, **92 (C5)**, 4971–5029.
- Dunbar, R., et al., 2006: QuikSCAT Science Data Product User Manual, Version 3.0. JPL Document D-18053 - Rev A, Jet Propulsion Laboratory, Pasadena, CA.
- Dupont, F., C. G. Hannah, and D. Greenberg, 2003: Modelling the sea level in the Upper Bay of Fundy. *Atmos.-Ocean*, **43 (1)**, 33–47.
- Ebuchi, N., H. C. Graber, and M. J. Caruso, 2002: Evaluation of wind vectors observed by QuikSCAT/SeaWinds using ocean buoy data. *J. Atmos. Oceanic Technol.*, **19 (12)**, 2049–2062.
- Fairall, C. W., E. F. Bradley, J. E. Hare, A. A. Grachev, and J. B. Edson, 2003: Bulk parameterization of air-sea fluxes: Updates and verification for the COARE algorithm. *J. Climate*, **16**, 571–591.
- Foster, R., 2012: personal communication, Apr. 5.
- Freilich, M. H. and R. S. Dunbar, 1999: The accuracy of the NSCAT 1 vector winds: Comparisons with National Data Buoy Center buoys. *J. Geophys. Res.*, **104 (C5)**, 11 231–11 246.
- Hong, S.-Y., Y. Noh, and J. Dudhia, 2006: A new vertical diffusion package with an explicit treatment of entrainment processes. *Mon. Wea. Rev.*, **134**, 2318–2341.
- Johannessen, J. A., V. Kudryavtsev, D. Akimov, T. Eldevik, N. Winther, and B. Chapron, 2005: On radar imaging of current features: 2. Mesoscale eddy and current front detection. *J. Geophys. Res.*, **110 (C7)**.
- Kara, A. B., E. J. Metzger, and M. A. Bourassa, 2007: Ocean current and wave effects on wind stress drag coefficient over the global ocean. *Geophys. Res. Lett.*, **34 (1)**.
- Kelly, K. A., S. Dickinson, and G. C. Johnson, 2005: Comparisons of scatterometer and

- TAO winds reveal time-varying surface currents for the Tropical Pacific Ocean. *J. Atmos. Oceanic Technol.*, **22** (6), 735–745.
- Kelly, K. A., S. Dickinson, M. J. McPhaden, and G. C. Johnson, 2001: Ocean currents evident in satellite wind data. *Geophys. Res. Lett.*, **28** (12), 2469–2472.
- Kudryavtsev, V., D. Akimov, J. Johannessen, and B. Chapron, 2005: On radar imaging of current features: 1. Model and comparison with observations. *J. Geophys. Res.*, **110** (C7).
- Large, W. G. and S. Pond, 1982: Sensible and latent-heat flux measurements over the ocean. *J. Phys. Oceanogr.*, **12** (5), 464–482.
- Liu, W. T. and W. Tang, 1996: Equivalent neutral wind. Tech. Rep. 96-17, Jet Propulsion Laboratory, Pasadena, CA.
- Lyzenga, D. R., 1998: Effects of intermediate-scale waves on radar signatures of ocean fronts and internal waves. *J. Geophys. Res.*, **103** (C9), 18,759–18,768.
- Manning, J. P., D. J. McGillicuddy Jr., N. R. Pettigrew, J. H. Churchill, and L. S. Incze, 2009: Drifter observations of the Gulf of Maine Coastal Current. *Cont. Shelf Res.*, **29**, 835–845.
- Marmorino, G. O., B. Holt, M. J. Molemaker, P. M. DiGiacomo, and M. A. Sletten, 2011: Airborne synthetic aperture radar observations of spiral eddy slick patterns in the Southern California Bight. *J. Geophys. Res.*, **115**.
- Moore, R. K. and A. K. Fung, 1979: Radar determination of winds at sea. *Proc. IEEE*, **67** (11), 1504–1521.
- Mouche, A. A., B. Chapron, and N. Reul, 2007: A simplified asymptotic theory for ocean surface electromagnetic wave scattering. *Wave Random Complex*, **17** (3), 321–341.
- O’Neill, L. W., D. B. Chelton, and S. K. Esbensen, 2005: High-resolution satellite measurements of the atmospheric boundary layer response to SST variations along the Agulhas Return Current. *J. Clim.*, **18** (14), 2706–2723.

- Owen, M. P., K. M. Stuart, and D. G. Long, 2003: Ultra-High-Resolution Near-Coastal Wind Retrieval for QuikSCAT. *Coastal Ocean Remote Sensing*, R. Foulin, Ed., SPIE, Vol. 6680.
- Park, K. A., P. Cornillon, and D. L. Codiga, 2006: Modification of surface winds near ocean fronts: Effects of Gulf Stream rings on scatterometer (QuikSCAT, NSCAT) wind observations. *J. Geophys. Res.*, **111** (C3).
- Plagge, A. M., D. C. Vandemark, and D. G. Long, 2009: Coastal validation of ultra-high resolution wind vector retrieval from QuikSCAT in the Gulf of Maine. *IEEE Geosci. Remote Sens. Lett.*, **6** (3), 413–417.
- Plant, W. J., 1977: Studies of backscattered sea return with a CW dual-frequency, X-band radar. *IEEE J. Oceanic Eng.*, **2**, 28–36.
- Portabella, M. and A. Stoffelen, 2009: On scatterometer ocean stress. *J. Atmos. Oceanic Technol.*, **26** (2), 368–382.
- Quilfen, Y., B. Chapron, and D. Vandemark, 2001: The ERS scatterometer wind measurement accuracy: Evidence of seasonal and regional biases. *J. Atmos. Oceanic Technol.*, **18** (10), 1684–1697.
- Rieder, K. and J. Smith, 1998: Removing wave effects from the wind stress vector. *J. Geophys. Res.*, **103** (C1), 1363–1374.
- Rieder, K., J. Smith, and R. Weller, 1994: Observed directional characteristics of the wind, wind stress, and surface-waves on the open-ocean. *J. Geophys. Res.*, **99** (C11), 22 589–22 596.
- Scharroo, R., 2008: *RADS version 3.1 User Manual and Format Specification*. Delft University of Technology.
- Skamarock, W. C. and J. B. Klemp, 2008: A time-split nonhydrostatic atmospheric model for weather research and forecasting applications. *J. Comput. Phys.*, **227** (7), 3465–3485.

- Smith, P. C., C. N. Flagg, R. Limeburner, C. Fuentes-Yaco, C. Hannah, R. C. Beardsley, and J. D. Irish, 2003: Scotian Shelf crossovers during winter/spring 1999. *J. Geophys. Res.*, **108** (C11).
- Smith, P. C., R. W. Houghton, R. G. Fairbanks, and D. G. Mountain, 2001: Interannual variability of boundary fluxes and water mass properties in the Gulf of Maine and on Georges Bank: 1993-1997. *Deep-Sea Res. II*, **48**, 37–70.
- Tang, W. Q., W. T. Liu, and B. W. Stiles, 2004: Evaluations of high-resolution ocean surface vector winds measured by QuikSCAT scatterometer in coastal regions. *IEEE Trans. Geosci. Remote Sens.*, **42** (8), 1762–1769.
- Vandemark, D., J. B. Edson, and B. Chapron, 1997: Altimeter estimation of sea surface wind stress for light to moderate winds. *J. Atmos. Oceanic Technol.*, **14** (3), 716–722.
- Weissman, D. and H. Graber, 1999: Satellite scatterometer studies of ocean surface stress and drag coefficients using a direct model. *J. Geophys. Res.*, **104** (C5), 11 329–11 335.
- Zhang, F. W., W. M. Drennan, B. K. Haus, and H. C. Graber, 2009: On wind-wave-current interactions during the shoaling waves experiment. *Journal of Geophysical Research*, **114**.

CHAPTER 4

On the interpretation of scatterometer winds near sea surface temperature fronts

4.1 Prologue

The following is a paper intended for future submission to a peer-reviewed journal and for presentation at the 2012 NASA Ocean Vector Winds Science Team Meeting. The co-authors are Dr. James Edson of the University of Connecticut, and Dr. Douglas Vandemark. The dissertation author is the lead investigator and performed most of the writing and research for this chapter, although the work contained herein is an on-going collaboration between all three authors.

4.2 Abstract

Recently, much attention has been given to the interpretation of ocean surface wind fields across sea surface temperature fronts as determined using satellite scatterometer wind estimates. Although scatterometer products are generally assumed to represent well-calibrated equivalent neutral-stability winds, the wind waves controlling the scatterometer measurements may be responsive to a variety of forcing terms in regions of strong temperature fronts including wave-current interactions and atmospheric stability conditions that are not adequately captured by the scatterometer's geophysical model function. This leaves open the possibility that the scatterometer winds employed in ocean temperature front analyses are not in fact equivalent neutral winds and that subsequent analysis may be open to varied interpretation. To help address this potential ambiguity, this study employs a set of valuable new field observations including direct covariance momentum flux measurements from a mooring located in the Gulf Stream along with collocated scatterometer winds from

QuikSCAT. Comparison between scatterometer wind retrievals and the *in situ* wind and wind stress across a wide range of atmospheric stability conditions is performed using a long-term CLIMODE dataset spanning more than 15 months across 2005-2007. Results show that, in the mean, the Ku-band QuikSCAT model function provides accurate equivalent neutral wind estimates, particularly for the case of neutral through strongly unstable conditions. This work is also able to convincingly support the finding of large-scale wind adjustments across ocean surface temperature fronts; this effect appears to dominate over any surface layer stability adjustment in the wind by nearly an order of magnitude. This time-domain study furnishes wind stress observations at a fixed location that may serve to better integrate surface layer and larger-scale upper boundary interpretation of scatterometer data that have, to date, been primarily evaluated from a spatial perspective.

4.3 Introduction

Vector winds from satellite scatterometers have become indispensable for applications from weather forecasting to climate research, and are valued by scientists and researchers across many fields. As these data become more ubiquitous, the uses to which they are put become more varied, and scientific communities possibly unfamiliar with the history of the sensors are faced with the option of accepting scatterometer winds as “truth” or dismissing them – and the conclusions of studies based on their use – due to uncertainties in their validity. In one specific instance, there is an apparent disconnect within the air-sea interaction community, between researchers working at small-scale or submesoscale and those with a focus on larger scale dynamics, ranging from mesoscale to synoptic patterns. The latter group has embraced scatterometry for many years (e.g. Torres et al. (2003); Chelton et al. (2004); Park et al. (2006); Kara et al. (2008); Small et al. (2008); Zhang et al. (2009); O’Neill et al. (2010b)), but despite the general confidence in the accuracy of scatterometer winds (Ebuchi et al. (2002); Tang et al. (2004); Plagge et al. (2009), presented here as Chapter 2), there is a clear lack of observational evidence needed to rigorously confirm the universal appropriateness of these data in areas of complicated air-sea dynamics– in other words, in the areas of interest to many submesoscale researchers. This lack of evidence

could lead to a lack of confidence in (or the questioning of) results that would otherwise be useful to many groups throughout the air-sea community.

As a specific example, several investigators have recently published work describing observed coupling between winds and sea surface temperature (SST) fronts (Chelton et al. (2001), O'Neill et al. (2003), O'Neill et al. (2005), O'Neill et al. (2010a), Chelton and Xie (2010)). This work, in general, states that scatterometer-derived wind speed perturbations are related linearly to and correlated positively with mesoscale SST perturbations globally; the results appear to be both robust and consistent (with some regional variability). However, regions of substantial SST gradients (e.g. western boundary currents, warm and cold core rings) very often also exhibit changing currents, atmospheric temperatures, and long waves. This is material because scatterometer products themselves are not directly measured wind speeds and directions, but rather constructions based on model functions developed to relate radar backscatter with equivalent neutral wind through the mechanism of surface roughness. A potential issue to consider when applying ocean scatterometry to the study of surface winds in regions of SST gradients is the fact that thermodynamic effects may act to alter both the surface waves and atmospheric stability, possibly changing surface stresses and neutral winds while not affecting winds at a certain height above the surface (see Chapter 1). These dynamics could considerably complicate the results seen in studies such as those listed above. Without observations to show detailed responses of actual winds, neutral winds, stresses, and scatterometer retrievals in various stability regimes, it is impossible to address potential concerns about the validity of these types of wind-SST coupling investigations.

4.3.1 Marine Atmospheric Boundary Layer Dynamics and Monin-Obukhov Similarity Theory

Ocean surface roughness is determined by the wave field, which in turn is determined in large part by the exchange of momentum between the atmosphere and ocean imparted by the surface wind stress. The surface stress is often broken into two components: the tan-

gential or viscous stress that impart momentum directly to ocean currents and the normal stress that is supported by the wave field through form drag. The normal stress supported by the wind waves of $O(0.1-10 \text{ m})$ is responsible for most of the momentum flux once the sea become fully rough for wind speeds above 7.5 m/s (Donelan (1990)). The viscous stress supports most of the momentum exchange at wind speeds below 2 m/s . Between these two extremes lies a regime known as transitionally rough (Banner and Peirson (1998)) where surface waves support a substantial fraction of the stress. This relationship between wind speed, wind stress and surface roughness gives the underlying geophysical basis for using scatterometers to estimate the wind.

The layer of the atmosphere above the surface of the ocean is referred to as the marine atmospheric boundary layer (MABL). This layer can be described as the portion of the atmosphere affected by friction with the sea surface, leading to the turbulent exchange of momentum heat and mass. The region of the MABL where fluxes differ by no more than 10% is called the surface layer, or sometimes the constant flux layer, and is generally the lowest 10% of the MABL. The surface layer indicates that region of the atmosphere where the flow is governed by the generation of turbulence by wind shear, and enhanced (suppressed) by buoyancy (stratification). The lowest part of the surface layer where wave-induced fluctuation can impact momentum, heat and mass exchange is known as the wave boundary layer (WBL).

The turbulent flow statistics within most of the surface layer (i.e., outside of the WBL) can be investigated using a set of scaling arguments known as Monin-Obukhov (MO) similarity (or together, MOS). In MO similarity, the turbulence statistics are made dimensionless using length, temperature, humidity and velocity scales based on the (constant) surface fluxes. For example, the velocity scale is defined using the surface stress,

$$\tau = \rho_a \overline{w'u'} = -\rho_a u_*^2 \quad (4.1)$$

where ρ_a is the density of air; w' and u' represent the turbulent fluctuations of vertical wind and streamwise horizontal wind respectively, with the overbar denoting a time average; and u_* is the MO scaling parameter known as friction velocity. The measurement of near sur-

face stress through the velocity correlation shown above is known as the eddy correlation or direct covariance method.

The magnitude of the friction velocity is similar to turbulent velocity fluctuations in the surface layer. MOS then predicts that these dimensionless quantities are universal functions of z/L , where z is the height above the ocean surface, and L is the MO length,

$$L = -\frac{\Theta_v}{\kappa g} \frac{u_*^3}{\overline{w'\theta'_v}} \quad (4.2)$$

where Θ_v is the mean virtual potential temperature, κ is the von Karman's constant, g is the local gravitational acceleration, and $\overline{w'\theta'_v}$ represents the buoyancy flux. The MO length represents the height at which the generation of turbulence by shear is equal to the generation of turbulence due to buoyancy.

MOS theory has been validated in numerous field experiments in the marine surface layer (e.g., Edson and Fairall (1998); Edson et al. (2004)). These validation studies provide MOS predictions that the dimensionless shear should be a universal function of z/L :

$$\phi_m(z/L) = \frac{\kappa z}{u_*} \left[\frac{\partial U}{\partial z} \right] \quad (4.3)$$

where U is the mean streamwise wind and the subscript “m” refers to momentum. This function can be integrated to account for stability in the semi-logarithmic profile

$$U(z) = U(z_0) + \frac{u_*}{\kappa} (\ln(z/z_0) - \psi_m(z/L)) \quad (4.4)$$

where z_0 is the aerodynamic roughness length and ψ_m is related to the integral of ϕ_m via

$$\psi_m(z/L) = \int [1 - \phi_m(z/L)] \frac{d(z/L)}{z/L} \quad (4.5)$$

and where, during neutral conditions, $z/L = 0$, $\phi_m = 1$, and $\psi_m = 0$.

MOS functions such as Eq. 4.3 have proven extremely useful in the marine surface layer. For example, it is often difficult to directly measure the stress from platforms at sea due to motion contamination and flow distortion. Instead, air-sea investigators rely on MOS relationships such as Eq. 4.3 to estimate fluxes. One commonly used approach in numerical modeling is to combine Eqs. 4.1 and 4.3 to provide the flux-profile relationship

$$\tau = \phi_m(z/L) = \rho_a \frac{u_* \kappa z}{\phi_m(z/L)} \left[\frac{\partial U}{\partial z} \right] \quad (4.6)$$

Here, the term in front of the velocity gradient is known as the eddy viscosity, and flux

estimation using this approach is known as the gradient method. However, the gradient approach is also difficult to implement in the field because it requires measurements at multiple levels and remains very sensitive to flow distortion.

Instead, it is more common to use what is called the bulk method, an even simpler approach that relies on standard atmospheric and oceanic variables (velocities, temperatures, etc) and transfer coefficients. For instance, the bulk method relates the air-sea velocity difference to the surface stress using

$$\tau = \rho_a C_D U_r^2 \quad (4.7)$$

where C_D is the transfer coefficient for momentum, known as the drag coefficient, and U_r is the wind speed relative to the water surface. The drag coefficient can be parameterized as a function of atmospheric stability and surface roughness (represented by roughness length z_0) by combining Eqs. 4.1, 4.4, and 4.7 to obtain

$$C_D(z/z_0, z/L) = \frac{-\overline{uw}}{U_r^2} = \left(\frac{\kappa}{\ln(z/z_0) - \psi_m(z/L)} \right)^2 \quad (4.8)$$

This is the approach taken in the Coupled Ocean Atmosphere Response Experiment (COARE) algorithm (Fairall et al. (1996); Fairall et al. (2003)) used in this paper.

These equations (MOS in general) are not valid throughout the entire surface layer. Their application requires that the fluxes be constant with height, that conditions be both reasonably stationary and horizontally homogeneous, and that the kinetic energy that drives the fluxes be generated only by mechanical production and buoyancy and dissipated only by stratification. Therefore, MOS becomes invalid very close to the air-sea interface in the region of the WBL, where some of the momentum flux is influenced by wave-induced fluctuations. Although generally the WBL is confined to a within a few meters of the sea surface, during times of low wind and swell it can be higher. Additionally, as MOS validity requires stationary and homogeneous conditions, in a situation such as a frontal passage or at a location within a kilometer of an SST front, the equations presented above may not hold.

In addition, potential MABL dynamics in the region of an SST front include flow due to baroclinic adjustment. In a type of flow equivalent to the sea breeze often present in coastal

regions in the summertime, a gravity current is created as the cold dense air on the cool side of the SST front begins to flow to the warm side. Once this sea breeze situation develops, the turning of the wind with height (known as the thermal wind relationship) would tend to drive a geostrophic wind parallel to the SST front aloft. Generally, standard sea breeze conditions wouldn't allow full adjustment; however, the longer time scales associated with conditions near persistent SST fronts such as the Gulf Stream might allow for significant adjustment in this manner (Businger and Shaw (1984)).

4.3.2 Overview of Scatterometry

As mentioned above, the basic principles of scatterometry rely on the relationship between wind, wind stress, and surface roughness. Scatterometer vector winds are created by relating radar backscatter to ocean surface wind conditions using a geophysical model function (GMF). Each GMF is specific for each sensor, and takes into account frequency of radar, angles of azimuth and incidence, and polarization, inverting backscatter to provide estimates of wind speed and direction, and each has been tested and tailored using *in situ* measurements from buoys, aircraft, and ships. Through decades of study using tower-based [Colton et al. (1995)], airborne [Weissman (1990), Weissman et al. (1997)] and previous spaceborne [Freilich and Dunbar (1999), Verschell et al. (1999), Weissman and Graber (1999)] sensors, it was determined that the gravity-capillary waves on the surface of the ocean to which the radar backscatter responds are controlled by – are in equilibrium with – the wind stress at the ocean surface, τ [e.g., Liu and Tang (1996)]. Because *in situ* stress measurements are extremely rare, it was necessary to choose a parameter that could be observed using existing measurement techniques and then related uniquely to backscatter. Therefore, scatterometer GMFs have been developed to provide equivalent neutral winds (ENW). This concept is an extension of Eq. 4.4 in the previous section (Sec. 4.3.1). Using this equation, and recognizing under neutral conditions, $\psi_u = 0$, the ENW equation for neutral wind relative to the ocean surface (U_{rN}) becomes

$$U_{rN} = \frac{u_*}{\kappa} (\ln(z/z_0)) \quad (4.9)$$

As a reminder, this ENW can be in turn related back to stress τ through a drag coeffi-

cient, in this case a neutral drag coefficient:

$$\tau = \rho_a C_{DN} U_{rN}^2 = \rho_a U_{rN}^2 \frac{\kappa}{\ln(z/z_0)} \quad (4.10)$$

It can therefore be noted that surface stress – and consequently ENW relative to the sea surface – is a function of the surface roughness only, which is how scatterometer measurements of surface roughness can be used to estimate the ENW. Scatterometer GMFs have been calibrated to provide ENW at 10 m (U_{10N}) by utilizing bulk methods as described in Sec. 4.3.1 to relate neutral versions of *in situ* measured winds to scatterometer measurements. Studies such as Ebuchi et al. (2002) have validated ENW from scatterometer using meteorological buoy arrays such as those from the National Data Buoy Center.

Given these relationships and previous discussion, it is clear that both radar backscatter and the surface roughness to which it responds are directly related to the existing wave field at the ocean’s surface, not to the wind field itself. Although the winds are the primary forcing on the wave surface at the length scales to which the radar responds, any additional atmospheric or oceanic processes present will also contribute to surface roughness. This indicates that all types of turbulent dynamics are relevant to the discussion of scatterometer retrievals in the presence of strong thermodynamic signals: anything that affects either the surface roughness or the flux-profile (as represented here by C_{DN}) can therefore be expected to affect the “equivalent neutral wind” derived from the scatterometer. A number of studies since the 1980s present this dilemma; one example is Weissman et al. (1994), which investigates the relationship between the microwave radar cross section and both wind speed and stress using data from the Frontal Air-Sea Interactions Experiment (FASINEX), including airborne Ku-band scatterometer radar cross section measurements of the ocean surface along with coincident near-surface wind and wind stress from two ships (the R/Vs Endeavor and Oceanus), with the goal to investigate the effects of SST gradients and thermal stratification changes. Their results indicate that drag coefficient is strongly dependent on both wave state and atmospheric stratification, and that momentum transfer at a specic wind speed will depend on the sea state (and wave age) as well as on the wind speed [Weissman et al. (1994)]. Therefore, they state, radar backscatter is more closely related to surface stress than to neutral stability winds; thus scatterometer model functions

should be designed with respect to u^* and then individual calculations of U10N should be performed afterwards with considerations of existing sea state conditions [Weissman et al. (1994)]. Because scatterometer model functions have not been structured this way, the implication is that scatterometer winds near SST fronts are likely to be incorrect.

4.3.3 Scatterometry and SST Fronts

For the past decade, studies have been published using scatterometer products to investigate wind field adjustment near SST fronts [Chelton et al. (2001) through O'Neill et al. (2010a)]. One of the most recent of these, O'Neill et al. (2010a), gives an overview of the general observations from previous studies, provides a more recent investigation of various global regions (the Gulf Stream, the Kuroshio, the Agulhas Return Current, and the South Atlantic Current) with an improved methodology. One main outcome is the observation that wind speed perturbations are linearly related to and positively correlated with mesoscale SST perturbations over all four of the regions examined [O'Neill et al. (2010a)]. The aforementioned study uses 75 months of monthly-averaged spatially high-pass filtered fields of QuikSCAT wind speeds and AMSR-E SST and the equation

$$V' = \alpha_v T' \quad (4.11)$$

to describe the coupling (denoted by α_v and retrieved using a least squares fit) between bin-averaged wind speed perturbation (V') and mesoscale SST perturbations (T'). The authors provide α_v s for each of these regions, which range from 0.27 m/s per degC over the Gulf Stream to 0.49 m/s per degC over the Agulhas [O'Neill et al. (2010a)]. Their study also utilizes the vector nature of QuikSCAT winds to examine wind curl response to crosswind SST gradients and wind divergence response to downwind SST gradients, but the evaluation of these results is beyond the scope of this note. For a more detailed summary of some of these earlier papers, see Ch. 1.

Previous studies have focused on basin-size spatial scale and monthly time scales. Throughout these studies, atmospheric stability is discussed only in terms of how it is modified by ocean temperatures, without a discussion of how different air masses might

interplay, presumably because the methodology focuses on longer timescales where this assumption is valid. Furthermore, scatterometer winds are taken as true equivalent neutral winds. Although the work is persuasive, it cannot by itself prove that the wind dynamics apparent in the scatterometer data are those that would be measured locally, as the authors' lack of air temperature measurements cannot describe the actual stability and therefore they cannot confirm that the scatterometer winds are showing physically apparent wind adjustment rather than changes due to MOS or concerns raised in Weissman et al. (1994).

4.3.4 Hypotheses and Approach

By building upon the existing groundwork of air-sea and scatterometer studies, this study attempts to address the following hypotheses through a unique dataset. First, the data available here will be used to evaluate whether *in situ* winds corrected to neutral using MOS agree well with scatterometer winds, indicating that the scatterometer retrievals can be treated as equivalent neutral winds. Second, differences evident in both *in situ* and scatterometer winds during different air-sea stability conditions will be evaluated to determine the presence of (1) surface layer adjustment (SLA), often called “bottom-up effects,” described by changes in the definition of neutral due to MO correction, and (2) actual changes in wind across a front or between different air-sea regimes. This latter adjustment is referred to generally as boundary layer adjustment (BLA) due to “top-down effects,” and more specifically may indicate changes due to density-driven flow caused by changes in pressure and temperature. The presence of both types of adjustment dynamics in both types of wind measurements will likely be clear during cases of cold air advection (positive perturbations expected), but may be less clear during cases of warm air advection (negative perturbations expected) due to more complicated dynamics. Additionally (and as mentioned in Sec. 4.3.2), although it is accepted that scatterometers respond to wind stress, the lack of direct stress measurements has limited direct observation of this relationship. The present dataset is used to assess if scatterometer retrievals respond in the same way as *in situ* stress. Can direct stress measurements show the same dynamics for different stability regimes as wind speeds, giving further credence to the interpretation of scatterometer

response as stress?

The dataset for this study focuses on a detailed time-series at a point, with *in situ* measurements of stresses and fluxes and various oceanic and atmospheric parameters, collocated with scatterometer retrievals. The location of the mooring is an area of occasionally changing SST (due to meanders of the north wall of the Gulf Stream), and the long time series provides varying air temperature as well. Therefore, the scatterometer’s response to changes in stability can be directly addressed, using parameters such as z/L and air-sea temperature difference, and scatterometer ENW can be compared directly with *in situ* measured wind, neutral wind, and stress. A data record this complete has not hitherto been available for investigating scatterometer response to stability, and is extremely valuable for confirming the theories of many decades with actual observations.

This paper uses this valuable dataset to analyze the above hypotheses over the course of five additional sections. Section 4.4 describes the data and methods used for this investigation. In Section 4.5, results using these data are presented. Section 4.6 provides further context and discussion of these results, and Section 4.7 summarizes and reveals some impacts of our conclusions.

4.4 Data and Methods

The *in situ* data to be discussed here is from a mooring deployed from Nov. 2005 through Nov. 2007 at a location in the north wall of the Gulf Stream off the coast of the eastern U.S. (see Fig. 4-1), during the Clivar Mode Water Dynamic Experiment (CLIMODE).

4.4.1 Overview of CLIMODE and *In Situ* Data

The CLivar MDe Water Dynamic Experiment (CLIMODE) was designed to investigate the formation and subsequent evolution of subtropical mode water in the North Atlantic (Marshall et al. (2009)). Investigations have shown that a significant fraction of this mode

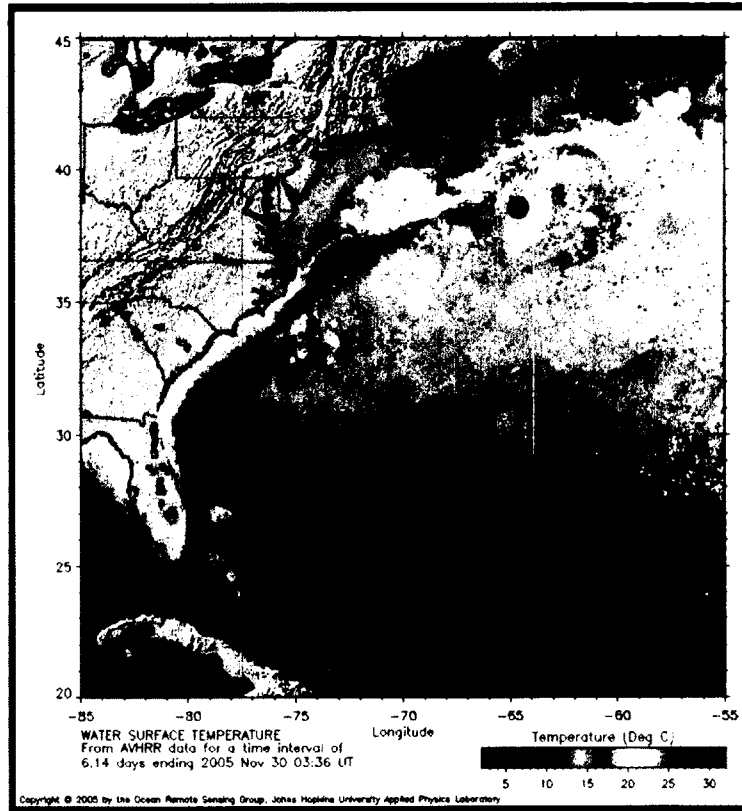


Figure 4-1: Map of the eastern coast of the US, showing SST from the AVHRR sensor. Buoy location indicated by circle. Acknowledgements to the Ocean Remote Sensing Group of Johns Hopkins University Applied Physics Laboratory.

water is formed due to air-sea interaction (see review of Hanawa and Talley (2001)). The formation is generally confined to winter and early spring (i.e., January to April) when the approximately 18°C mode water (EDW) outcrops in the vicinity of the North wall of the Gulf Stream. Of particular importance in this process is the advection of cold, dry air from the wintertime continent move over these outcropping regions in cold-air outbreaks (CAO). This advection of cold-dry air over the Gulf Stream drives extremely high surface latent and sensible heat fluxes due to large air-sea temperature and humidity difference and strong winds associated with the Noreasters driving the advection. This then drives intense convective activity and strong vertical exchange of both moisture and heat (see Fig. 4-2). Clouds are a key element in this process, producing large vertical motions and transporting moisture vertically. However, observations combined with the numerical simulation by Skillingstad and Edson (2009) show that the clouds also force relatively dry air from the middle atmosphere downward to the ocean surface. The result is surprisingly dry air

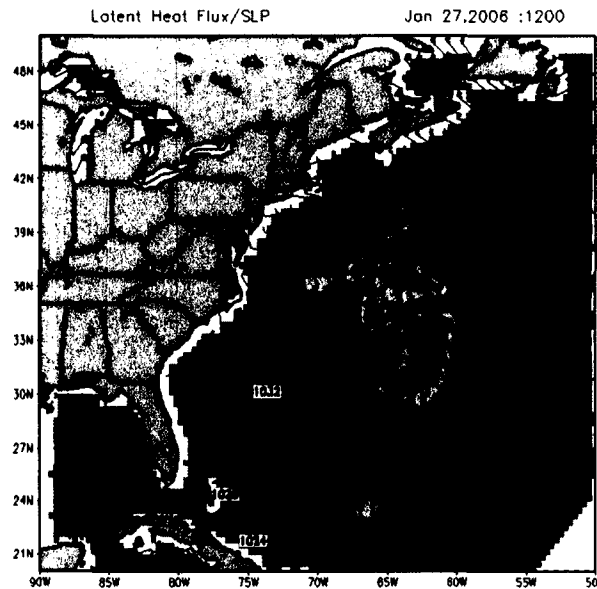


Figure 4-2: Surface pressure, winds and latent heat flux at 12 UTC on 27 January 2006 showing a cyclone to the north of Newfoundland drawing cold, dry air over the Gulf Stream. From Marshall et al. (2009).

offshore, often to distances over 1000 km (Marshall et al. (2009)).

These extreme conditions provide an unprecedented opportunity to improve our ability to measure and model the exchange of momentum, heat and mass over the open ocean. Therefore, an objective of the CLIMODE program was to collect high-quality mean meteorological and oceanic data in combination with direct estimates of the surface fluxes. To accomplish this, CLIMODE investigators deployed two highly instrumented platforms to provide surface fluxes and profiles of upper ocean and atmospheric boundary layer structure: a moored 3-m discus buoy and a drifting Air-Sea Interaction Spar (ASIS). This investigation relies on the data collected during the 15-month deployment of the discus buoy (pictured in Fig. 4-3).

A detailed description of the buoy deployment and measurement are provided by Bigorre et al. (2012). Briefly, the buoy supported two separate Air-Sea Interaction Meteorological Systems (ASIMET, Hosom et al. (1995)) systems to provide redundant measurement of

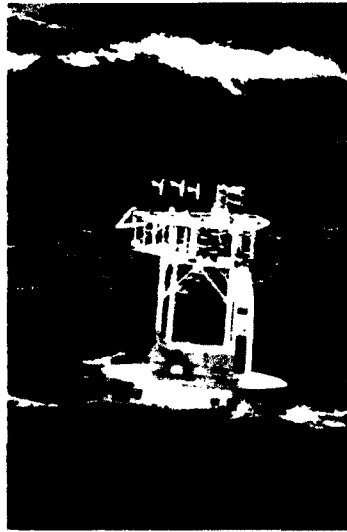


Figure 4-3: The 2.8 m discus mooring deployed from November 2005 to November 2006. It was replaced by an identical discus buoy that broke free of its mooring in February 2007.

wind speed and direction, air temperature, humidity, barometric pressure, rainfall accumulation, downwelling longwave and shortwave radiation, and sea surface temperature. Fluxes of momentum and buoyancy were computed using a low-power version of a Direct Covariance Flux System (DCFS) described by Edson et al. (1998). The DCFS was comprised of a 3-axis ultrasonic anemometer/thermometer for velocity and “sonic” temperature, a strapped-down inertial sensing system for platform motion (providing 3-axis accelerations and angular rates), and a compass for heading. The sonic temperature closely approximates the virtual temperature (Larsen et al. (1993)) and its correlation with the vertical velocity provides estimates of the buoyancy flux. The DCFS data is then used to compute the momentum and buoyancy fluxes using the direct covariance (or eddy correlation) method after correcting for platform motion (see Edson et al. (1998); Miller et al. (2008)).

These *in situ* measurements provide an unparalleled time series to compare with QuikSCAT data. As previously noted, access to direct covariance fluxes and direct stresses is very unusual, and furnish an additional descriptor of dynamics. To complete the *in situ* dataset, neutral buoy winds were computed using the COARE algorithm mentioned in Sec. 4.3.1; this algorithm was also used to compute parameters such as MO length L . Furthermore,

due to the results of Ch. 3 and the presence of a surface current meter on the buoy, all buoy winds compared with QuikSCAT winds are corrected to current-relative.

4.4.2 Scatterometer Data

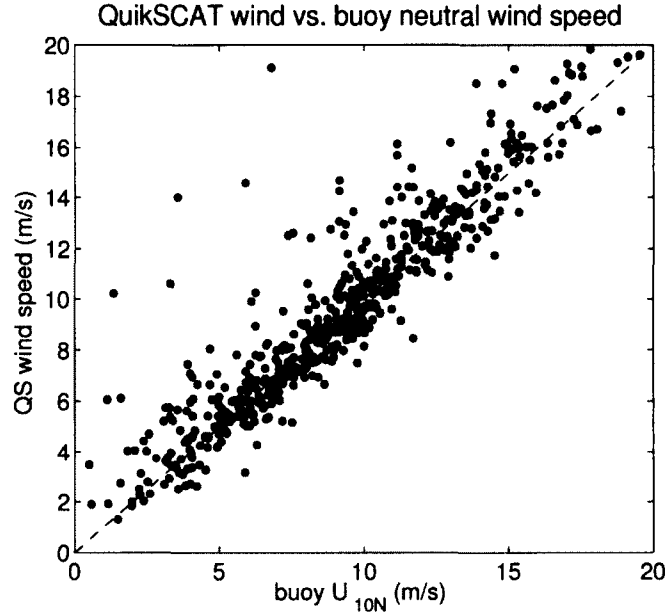


Figure 4-4: Scatterplot showing collocated QuikSCAT wind speeds vs. buoy neutral winds for entire dataset ($N = 586$).

The scatterometer data considered here are from the QuikSCAT sensor, specifically the 12.5 km resolution L2B QuikSCAT product from NASA-JPL’s Physical Oceanography Distributed Active Archive. The process for collocating *in situ* and QuikSCAT data both spatially and temporally is documented in previous work (see Plagge et al. (2009), presented here as Chapter 2). Briefly, for a successful collocation pairing, wind observations between buoy and scatterometer must occur within thirty minutes of each other, and for every satellite pass within the time frame of a match, all scatterometer wind vector cells (WVCs) within a 10 km radius of the buoy have been averaged to provide the average wind speed and direction. Any WVC that has been flagged by JPL’s algorithm as rain contaminated is discarded. With the exception of a few outliers, there is general agreement between QuikSCAT wind speed and *in situ* wind speed, as can be seen in Fig. 4-4.

4.5 Results

Given these datasets, it is possible to investigate differences in scatterometer winds and buoy winds in the region of a strong SST front. Precise measurements allow exploration of submesoscale dynamics through a very broad range of z/L , and larger, mesoscale dynamics through air and sea temperature differences. The investigation of the latter is also aided by the long data collection window, allowing monthly temporal averages over varying conditions.

4.5.1 Surface Layer Adjustment

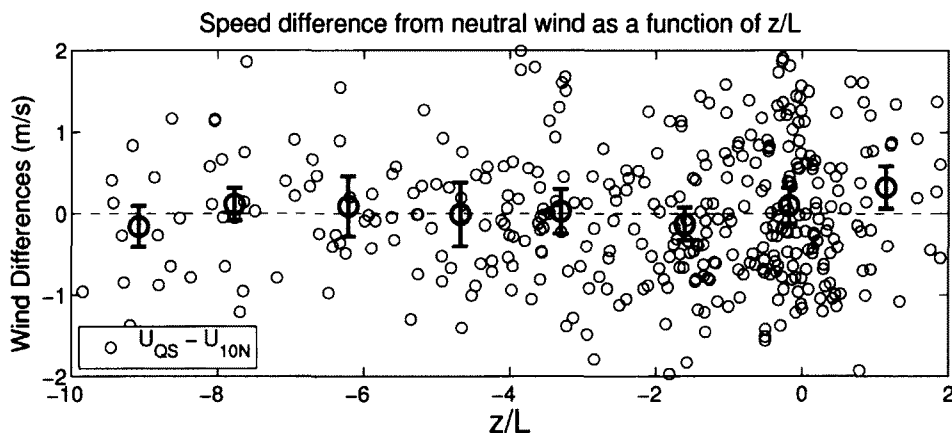


Figure 4-5: Plot of neutral wind speed difference (QuikSCAT wind speed minus buoy neutral wind speed) vs. z/L . Larger, bold circles indicate the average for each z/L bin; errorbars indicate standard error (SE, or standard deviation divided by the square root of the number of points in each bin)

The first analysis undertaken is to investigate whether the scatterometer winds obey MO similarity in the mean, and are therefore in agreement with an equivalent neutral wind estimate. This question is assessed in Fig. 4-5, which shows the difference between the QuikSCAT wind speeds and buoy ENW, with the differences binned with respect to z/L and the average plotted as a larger circle with errorbars. The binned averages of this difference are closely gathered around zero, indicating that in the mean, there is little difference

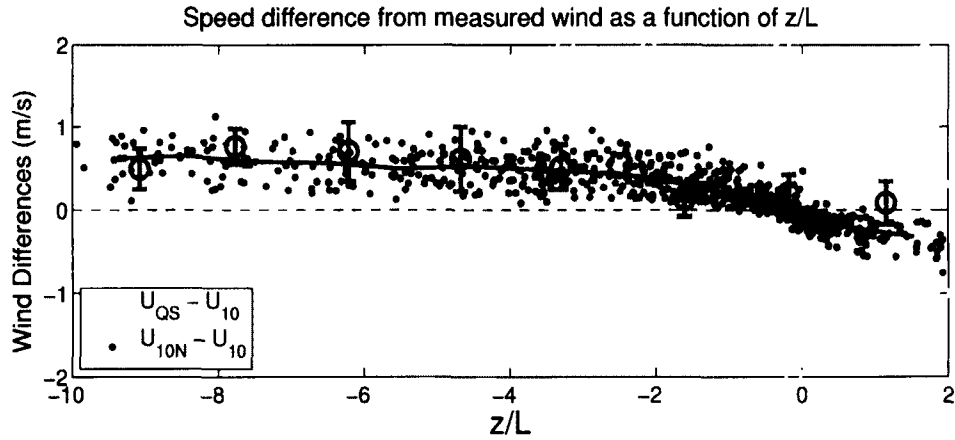


Figure 4-6: Plot of speed difference from measured wind vs. z/L . Black dots indicate buoy neutral winds minus buoy measured winds; gray circles indicate scatterometer wind minus buoy measured wind. Binned averages for black dots are connected with the black line, and binned averages for the gray circles are indicated by larger, bold gray circles with errorbars indicating SE.

between buoy winds corrected to neutral using MOS and those measured by the scatterometer; in other words, for the z/L conditions present in this study, QuikSCAT winds can be considered equivalent neutral winds. This is also evident in Fig. 4-6, which shows the two types of neutral wind data both differenced from the measured buoy wind speed; the shifted scatterometer winds are shown in gray circles, and the shifted buoy winds are shown as black dots. The black line connects the simple bin-averaged values of the black dots, and as such plots the MOS function that was used to correct measured wind to neutral wind. The heavy gray circles with the errorbars show the bin-averaged difference between QuikSCAT winds and measured buoy winds. It is clear that these heavy gray circles closely follow the black line, indicating the same result: that in the mean, QuikSCAT winds obey MOS and equal neutral winds. Also note that Figs. 4-5 and 4-6 show the magnitude of surface layer adjustment of winds to be less than 1 m/s.

Although Figs. 4-5 and 4-6 clearly show that the QuikSCAT winds match the buoy neutral winds in the mean, there is also significant scatter in the measurements themselves (also seen in Fig. 4-4). This indicates that the relationship between scatterometer and *in situ* winds is not merely a function of z/L , but also a function of other processes affecting the sea surface (as explained in Section 4.3.1) and the fact that the z/L measurements are

taken from the buoy and not from the scatterometer, meaning that there are at least some timing and spatial uncertainties. But besides these potential causes, it is likely that some of the scatter is due to dynamics occurring at a longer length scale than those encapsulated by MOS or accounted for by surface layer adjustment. These mesoscale dynamics would cause individual measurements to differ from the mean wind, and would represent adjustments to the larger boundary layer.

4.5.2 Boundary Layer Adjustment

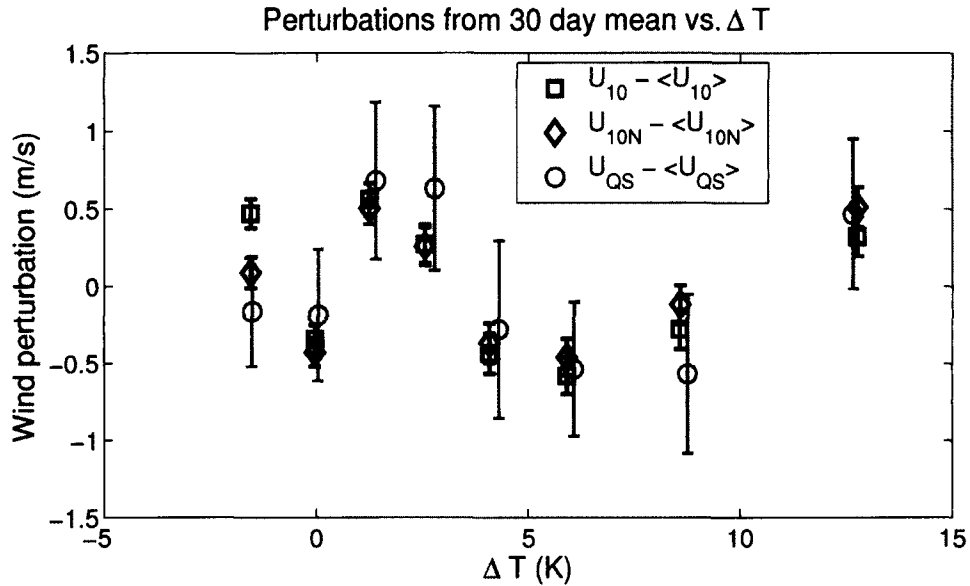


Figure 4-7: Wind speed perturbations (means calculated for each 30-day period) binned according to ΔT ; black squares show measured buoy speed perturbations, black diamonds show buoy neutral wind perturbations, and gray circles show scatterometer wind perturbations; for each case, errorbars show SE.

To examine additional effects due to changes in boundary layer dynamics in the region of an SST front, we look at the relationship between wind speed perturbations and local adjustments due to differences in air and ocean temperatures. For both buoy measured and neutral winds and for the scatterometer wind, the mean wind speed is calculated for each 30-day period within the field campaign. The appropriate monthly mean is subtracted from each data point in the collocated set, and the same process is repeated for in situ direct-covariance stress as well ($\tau - \langle \tau \rangle$). However, unlike the studies described in Sec. 4.3.3

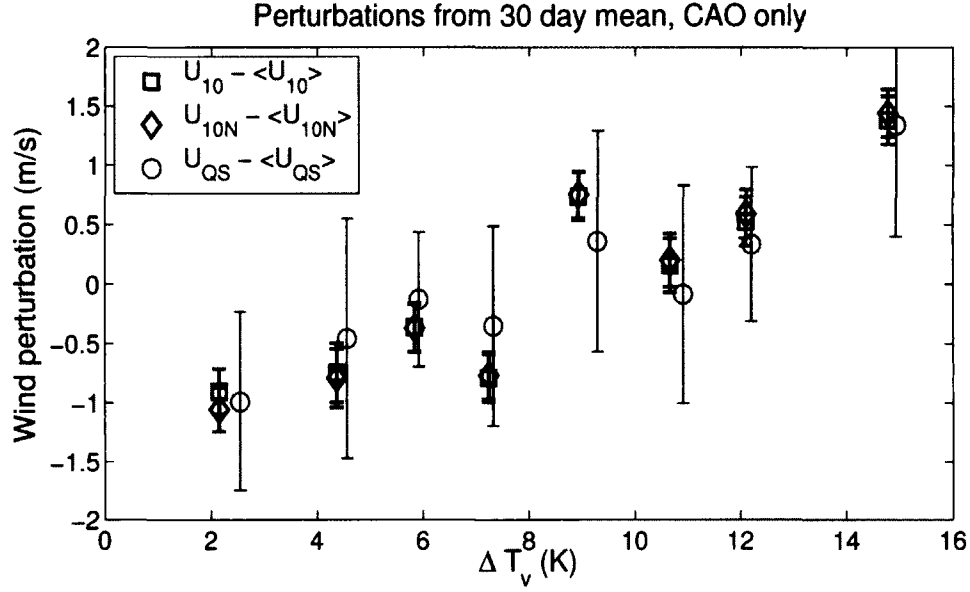


Figure 4-8: Wind speed perturbations binned according to ΔT for instances of unstable atmosphere and cold air advection only; plot uses same methodology as in Fig. 4-7

that utilized SST perturbations, this work makes use of the actual *in situ* difference between atmospheric and sea surface temperature ($\Delta T = T_{sea} - T_{air}$) to provide a more accurate interpretation of local stability. Although this is an additional difference from previous studies, it provides the best estimate of whether the local surface layer is stable or unstable during the time the measurements were taken.

Fig. 4-7 shows the perturbations of wind speed plotted against ΔT for the entire dataset. However, due to differences in advection as well the fact that the buoy moves into and out of the north wall of the Gulf Stream, it is very difficult to make sense of this plot; when the buoy is located very near the front, local stability is complicated by the advection of another air mass. In these cases, ΔT doesn't capture the full situation.

For this reason, when considering boundary layer effects, it is logical to limit the cases examined to explore distinct local stability and advection dynamics. Specifically, due to the location of the buoy, instances where the buoy wind direction is from the Northwest are likely to be cases of cold air advecting over warmer water, referred to here as cold air outbreaks (CAOs). To identify these cases, buoy wind directions are limited to between 300

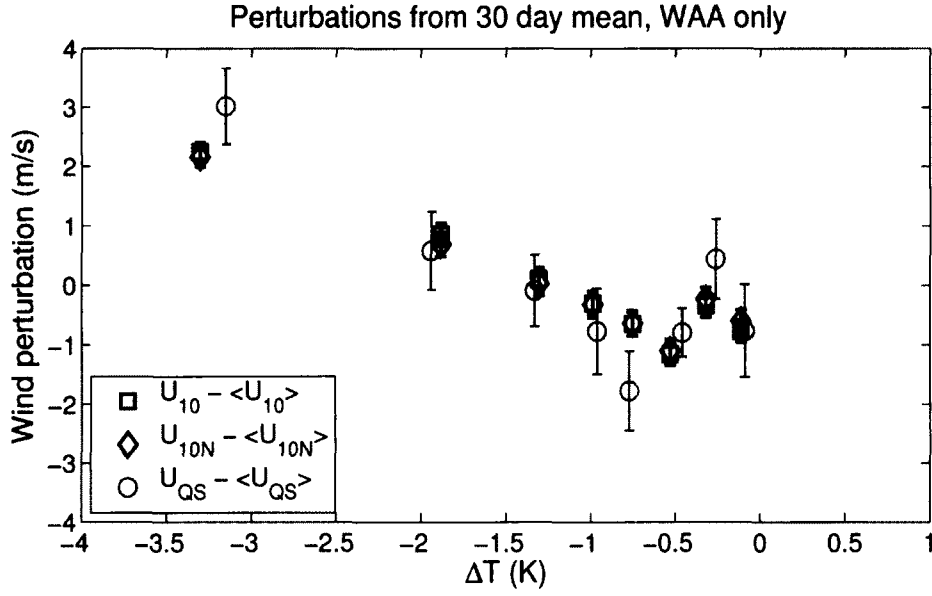


Figure 4-9: Wind speed perturbations binned according to ΔT for instances of stable atmosphere and warm air advection only; plot uses same methodology as in Fig. 4-7

degrees and 30 degrees (where direction is noted in the meteorological convention of wind from the designated compass measurement). Further limiting cases to those of unstable conditions using actual ΔT measurement (where $\Delta T \geq 0$) makes results even easier to interpret. Wind perturbations for unstable CAO dynamics are shown in Fig. 4-8.

The same approach was taken to isolate baroclinic coupling during times of stable atmosphere and warm air advection (WAA). In this case, wind directions were limited to greater than 145 degrees and less than 275 degrees, and temperature differences $\Delta T \leq 0$. Results are shown in Fig. 4-9. The number of instances of each type of stability regime can be seen in Fig. 4-10; there are fewer cases of stable WAA. Due to the nature of the study location, it was impossible to give a full accounting of all possible dynamics; for instance, there were fewer than 15 cases of stable CAO, making that situation impossible to analyze. Given these limitations, unstable CAO and stable WAA provide the best overview possible with this dataset, indicating boundary layer adjustment of winds.

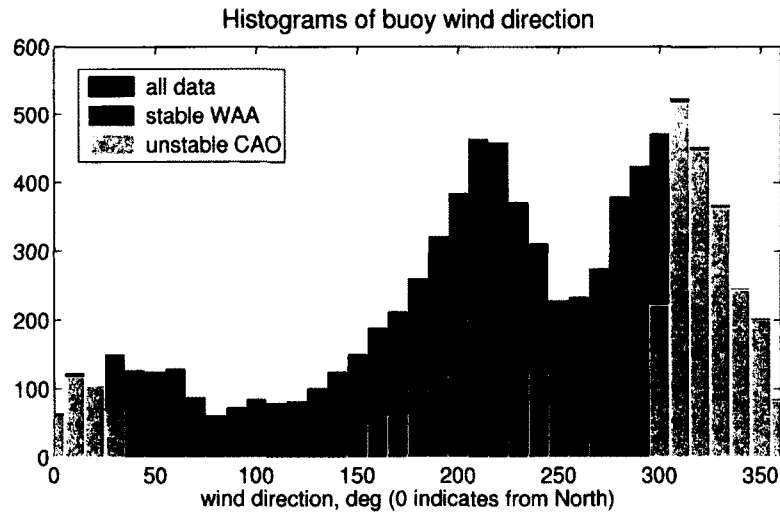


Figure 4-10: Histograms showing distribution of buoy wind direction, for all data and for limited “stable WAA” and “unstable CAO” cases.

4.5.3 Stress Perturbations

Stress perturbation versus temperature difference filtered for CAO and WAA follows same pattern as above figures, indicating that scatterometer is likely following stress as theory predicts (see Figs. 4-11 and 4-12). Because the stresses plotted here have been measured using a direct covariance system, and as such constitute a independent measurement compared with buoy anemometer-measured wind, this is an imporant addition to these results.

4.6 Discussion

The combination of these results show the presence of both surface layer adjustment and boundary layer adjustment. Further discussion illuminates the relative roles played by each.

4.6.1 Importance of SLA in Causing Wind Changes Across SST Fronts

As shown in Sec. 4.5.1, for all z/L conditions present in this study, QuikSCAT winds follow MOS and can be considered equivalent neutral winds. Although this should be well-established doctrine given the prevalence of work utilizing equivalent neutral winds from

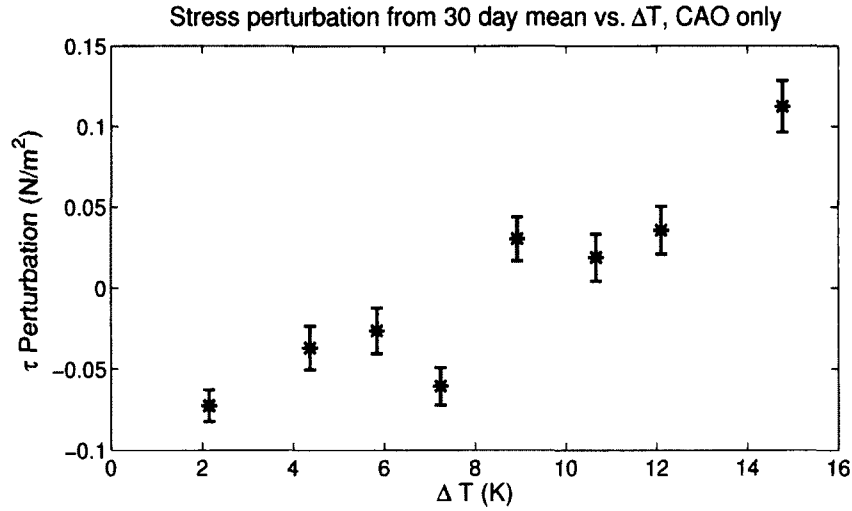


Figure 4-11: Buoy direct-covariance wind stress perturbations binned according to ΔT for instances of unstable atmosphere and cold air advection only; plot uses same methodology as in Fig. 4-7

scatterometer, studies that show this concretely with observations are extremely hard to find. Even Ebuchi et al. (2002), considered one of the hallmark buoy-scatterometer validation papers, could not show conclusively that in a varied stability environment the scatterometer winds were ENW. Furthermore, even some recent papers claim that scatterometer winds should not necessarily be considered neutral. For instance, Portabella and Stoffelen (2009) concluded, using data from the ERS scatterometer, buoy winds, and two varieties of ECMWF model winds, that ERS winds were statistically as close to real winds as they were to equivalent neutral winds. Apparently, any difference due to stability effects was masked by the larger uncertainty in the surface layer models used [Portabella and Stoffelen (2009)]. Our study provided more detailed *in situ* measurements and improved MOS functions and was able to show the opposite.

To further confirm this, Fig.4-13 shows the same result as Fig. 4-6, but in a slightly different way. In this case, it presents the ratios of scatterometer wind speed and buoy neutral wind speed to measured buoy wind speed. It is easy to see that these heavy gray circles representing the bin-averaged U_{QS}/U_{10} closely follow the black line (bin-averaged U_{10N}/U_{10}), indicating again that in the mean, QuikSCAT winds obey MOS and equal neutral winds. Furthermore, Fig. 4-13 makes it clear that even for this very large range of z/L ,

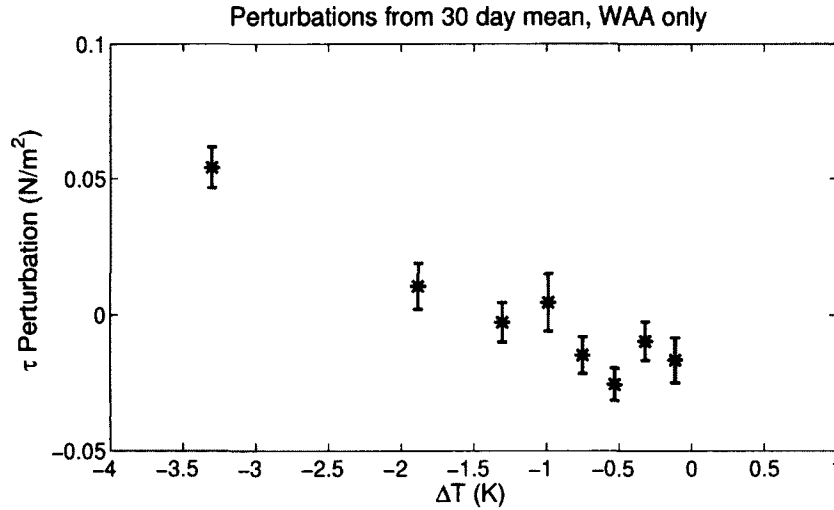


Figure 4-12: Buoy direct-covariance wind stress perturbations binned according to ΔT for instances of stable atmosphere and warm air advection only; plot uses same methodology as in Fig. 4-7

the surface layer adjustment can only ever account for less than 10% of the mean difference between neutral wind and measured wind; this can be seen in the fact that the mean ratios of U_{10N}/U_{10} and U_{QS}/U_{10} are less than 1.1 and even appear to asymptote, indicating that with an even greater range of stability, the same results could be expected.

The fact that SLA plays a relatively small role in the change of winds across an SST front can be seen in a mesoscale context as well. Remembering Fig. 4-8 and theory presented thus far, it is possible to draw the conclusion that if the data were to show only change to neutral due to SLA, the slope of $U_{10} - \langle U_{10} \rangle$ would be zero; in other words, there would be no change in measured wind due to a change in temperature conditions. On the contrary, in Fig. 4-8, all three wind perturbations showed similar slopes, providing proof of an actual change in wind as well as the fact that both versions of neutral wind have been corrected appropriately using MOS to show this change.

Fig. 4-14 shows the unstable CAO buoy data from Fig. 4-8, but in this iteration, the mean measured wind is removed from both the measured winds and the buoy neutral winds, providing a perturbation from U_{10} for both. The black squares are the same in both plots, but here the gray “x” shapes indicate $U_{10N} - \langle U_{10} \rangle$, and as such show the difference

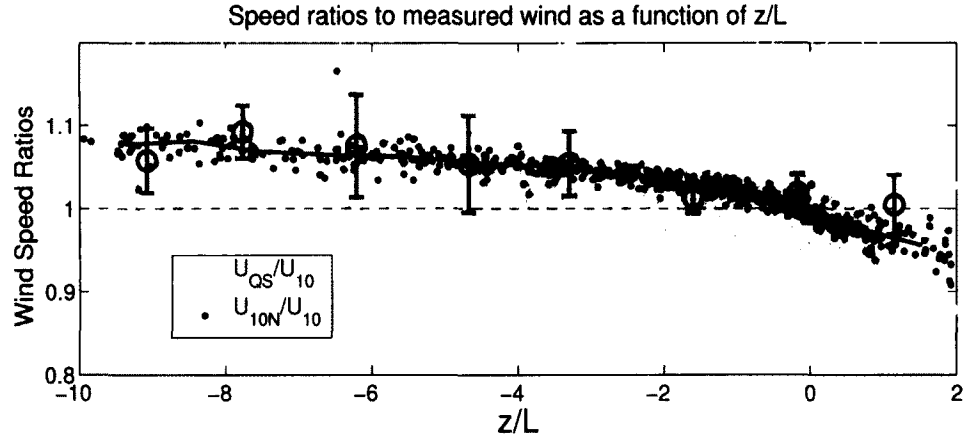


Figure 4-13: Plot of speed ratios to measured wind vs. z/L . Buoy neutral-to-measured wind ratios (U_{10N}/U_{10}) are shown as black dots with the bin-averaged values joined by a black line as in Fig. 4-6. The ratios of scatterometer-to-measured-buoy wind are shown in gray circles (U_{QS}/U_{10}), with bin-averaged values indicated by larger heavy gray circles with SE errorbars.

due to SLA on the buoy winds. This difference is not great, and in fact the slope only changes from 0.18 (measured wind perturbation) to 0.21 (wind perturbation of measured mean from neutral). This indicates that for both submesoscale and for mesoscale dynamics, the percentage of wind change due to surface layer adjustment is quite small, and accounts for only 10-15% of observed change.

4.6.2 Boundary Layer Adjustment Shown with ΔT and with SST Perturbation

As Fig. 4-8 and Fig. 4-9 show, for both CAO and WAA all three wind speed perturbations indicate a linear relationship with stability, with very similar slopes across the three products. During unstable conditions ($\Delta T > 0$), wind speed perturbations show increasing wind speeds. For these cases (CAO), dynamics are very clear and show that MOS is valid, as expected. Although the dynamics would be expected to be more complicated for times of stable atmosphere ($\Delta T < 0$), there is in fact an obvious decrease in wind speed compared with the respective mean for all three types of wind measurements. This is surprising, as the locality of the study is not ideal for the examination of stable atmosphere: the buoy was often very close to the edge of the front which could pose problems of limited fetch and

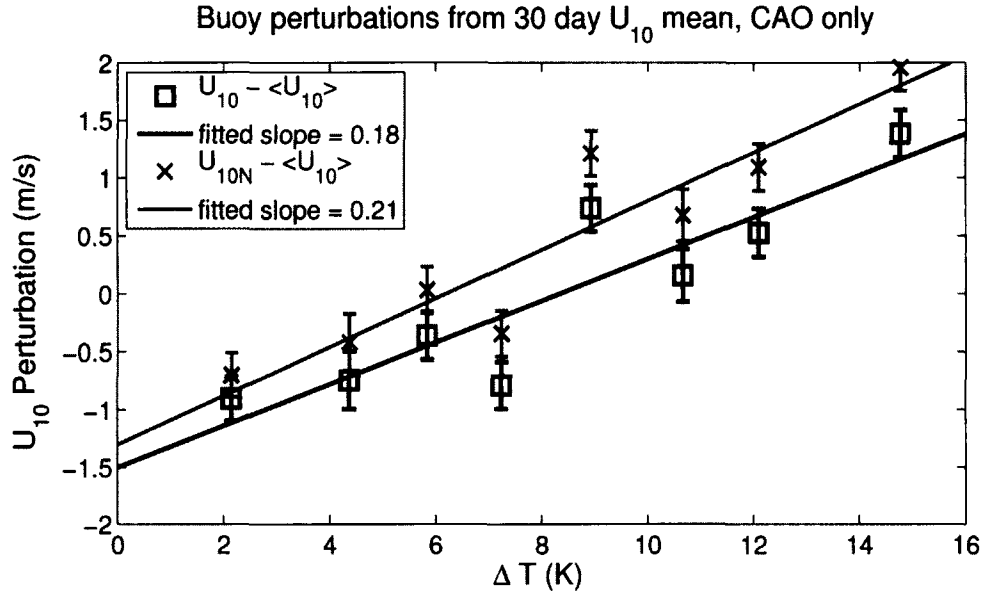


Figure 4-14: Buoy wind speed perturbations from U_{10} binned according to ΔT for instances of unstable atmosphere and cold air advection only; slopes indicated were determined using linear least squares fit and errorbars show SE.

incomplete adjustment. Also, these WAA cases would also include many of the dynamics associated with the breakdown of MOS, including vertical stratification and low level jets [Edson et al. (2007)]. However, despite these complications, the results indicate that the scatterometer still manages to provide a valid ENW and that the linear coupling of wind speed perturbation is still visible for scatterometer as well as buoy winds.

Given these statements, it is then possible to relate this work to the conclusions of previous papers. The present study tends to validate their results, despite differences in methodology. The method used by O'Neill et al. (2010a) functions because, by averaging all cases in a given region with a relatively constant sea surface temperature (such as the SST fronts associated with western boundary currents), and thereby collecting many data points, they are able to assume that on average, over warm (cold) water, conditions will be unstable (stable). In a sense, they are using a regional, monthly time-scale proxy to retrieve the results seen here. The present dataset and its actual stability measurements is able to show that their proxy does in fact work. Beyond this, the present results can be reconfigured to show wind perturbation as a function of SST perturbation instead of ΔT .

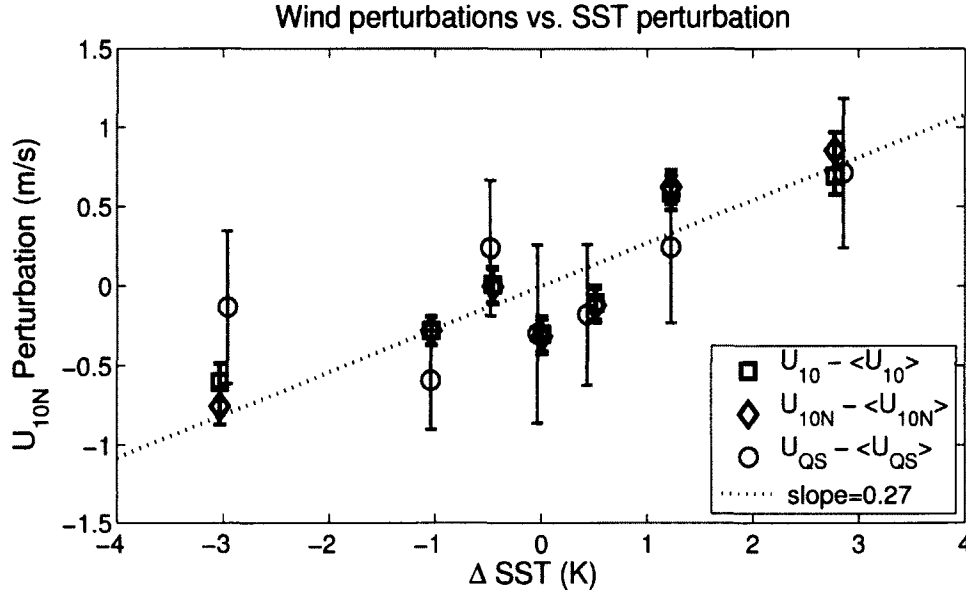


Figure 4-15: Wind speed perturbations binned according to ΔT_{sea} , methodology as in Fig. 4-7. Slope of 0.27 corresponds to the coupling coefficient given for the Gulf Stream in O'Neill et al. (2010a).

Here, like the previously discussed wind perturbations, SST perturbation (ΔT_{sea}) is not a spatial perturbation but a temporal one: for each 30 day period, a mean SST is calculated and then subtracted from the individual SST measurements recorded by the buoy. Fig. 4-15 shows a remarkable agreement between wind speed perturbations as a function of ΔT_{sea} and the coupling coefficient derived in O'Neill et al. (2010a) for the Gulf Stream ($\alpha_v = 0.27$).

4.6.3 Validation of Baroclinic Effects

Based on these outcomes, it can be confirmed that coupling between winds and SST seen in scatterometer studies is supported by our observations. But what would be causing these dynamics? If the above boundary layer adjustments are due to baroclinic adjustment, the velocity perturbations should ultimately be driven by pressure perturbations due to horizontal temperature gradients. When air pressure perturbations (calculated as before, with by subtracting the 30-day mean from individual *in situ* measurements) are compared with wind perturbations, the relationship is essentially opposite that seen between wind and SST perturbations (Fig. 4-16). This response is what would be expected if a pressure gra-

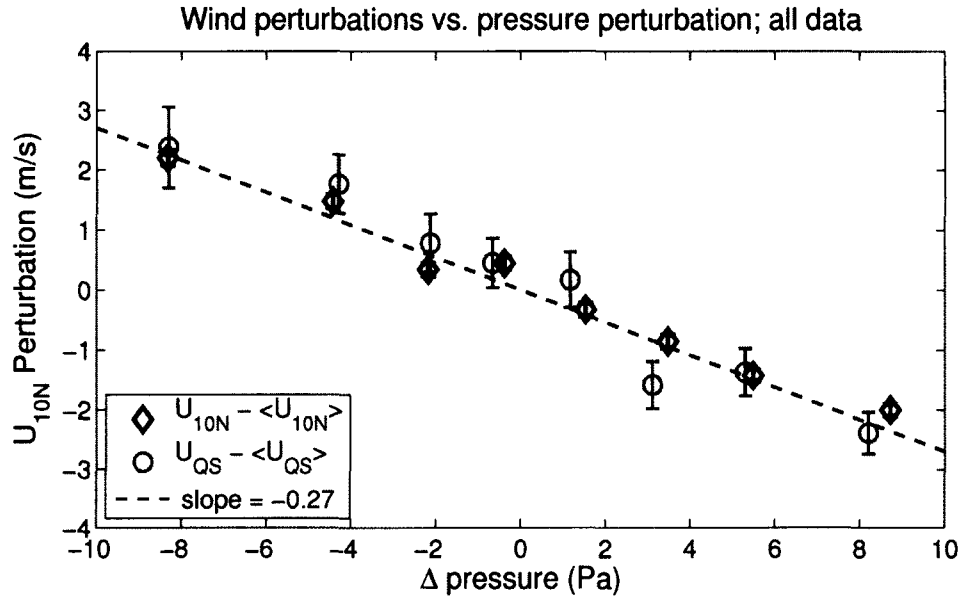


Figure 4-16: Wind speed perturbations binned according to ΔP_{air} , methodology as in Fig. 4-7. Slope of -0.27 corresponds to the opposite of the coupling coefficient given for the Gulf Stream in O'Neill et al. (2010a).

dient force (PGF) due to temperature differences was creating a sea-breeze-like effect: low pressure/high SST perturbations would be associated with higher velocity perturbations, as can be seen by comparing Figs. 4-15 and 4-16. Therefore, all of these results support the fact that the velocity perturbations seen in both scatterometer and buoy winds near SST fronts are driven by baroclinic adjustment. It should be mentioned that although wind differences correlated with pressure perturbations could also be due to synoptic weather patterns, the fact that wind coupling is also present with SST confirms that the effects seen here are most likely driven by baroclinic adjustment due to density-controlled flow.

4.6.4 Additional Effects of SST on Scatterometry

Because viscosity affects the production of capillary waves, and viscosity depends on water temperature, viscosity might be expected to contribute some amount to surface roughness changes on either side of an SST front. In the early days of scatterometry, some studies explored the relationship between seawater viscosity and radar backscatter during the process of creating GMFs [Liu (1984), Donelan and Pierson (1987), etc], but it is sel-

dom mentioned in more recent work. One of the few to discuss it at all, Park et al. (2006), notes that for a fixed wind speed, "viscosity increases (decreases) associated with SST decreases (increases) act to dampen capillary waves more (less) strongly and can contribute to weaker (stronger) scatterometer wind" but then proceeds to state that viscosity is generally thought to be less important than MABL influences on scatterometer retrievals [Park et al. (2006)]. Given the range of SST in this investigation (75% of the data lie between 20 and 35 degrees C, and only a few points lie below 10 degrees C), that statement is correct: change in viscosity due to this temperature range would be less than 27%, and would have minimal impact on the scatterometer retrievals. Even at high latitudes, Bentamy et al. (to be published) infer viscosity-related changes of less than 0.5 m s^{-1} between ASCAT and QuikSCAT. This indicates that only at SSTs lower than 5-7 degrees C does the response of surface roughness to SST-induced changes in viscosity substantially affect backscatter at the ocean wavelengths to which ASCAT and QuikSCAT respond.

4.7 Conclusions

This work uses a unique and important dataset to confirm commonly accepted theory using actual observation, and shows that scatterometer-retrieved winds can in fact provide a valuable resource in areas of strong SST gradients. Specific conclusions include:

- **The observations in this study confirm that scatterometer winds do appear to represent equivalent neutral winds:** *In situ* winds corrected to neutral using MOS reasonably match scatterometer winds, indicating that the scatterometer is indeed providing equivalent neutral winds. This is actually a very important result, providing comprehensive and concrete observations to support the implications of previous studies.
- **Differences evident in both scatterometer and in situ winds across SST fronts are a combination of both surface layer adjustment ("bottom-up" effects) and boundary layer adjustment ("top-down" effects):** This is true for both cases of stable and unstable atmospheric dynamics, but our findings also

show that SLA is an order of magnitude less than BLA, contributing less than 15% of observed change in wind.

- **Coupling between wind and SST observed via scatterometer as interpreted under ENW adjustment is consistent with our results:** At the location of this study and within this dataset, coupling is a reasonable interpretation of results that show buoy and scatterometer wind perturbations linearly related to both SST perturbations and ΔT .
- **Furthermore, the results seen here indicate that these wind perturbations are primarily driven by baroclinic adjustment:** Given the clear and opposite nature of the relationships between wind and SST perturbations and wind and pressure perturbations, the role played by a pressure gradient force and sea-breeze-like circulation is evident.
- **The response of *in situ* stress measurements echoes that of wind measurements from scatterometer:** Although the goal of this paper was not to fully support theory that the scatterometer is responding directly to wind stress, these results help to bolster that claim. Further work using this dataset may help to corroborate the interpretation of scatterometer retrievals as surface stress and eventually provide a validation of a scatterometer-derived stress product.

Bibliography

- Banner, M. L. and W. L. Peirson, 1998: Tangential stress beneath wind-driven air-water interfaces. *J. Fluid Mech.*, **364**, 115–145.
- Bentamy, A., S. A. Grodsky, J. A. Carton, D. Croizé-Fillon, and B. Chapron, to be published: Matching ASCAT and QuikSCAT winds. *J. Geophys. Res.*
- Bigorre, S., R. A. Weller, J. B. Edson, and J. D. Ware, 2012: A surface mooring for air-sea interaction research in the Gulf Stream, Part 2: Analysis of the observations and their accuracies. *J. Atmos. Oceanic Tech.*, submitted.
- Businger, J. A. and W. J. Shaw, 1984: The response of the marine boundary layer to mesoscale variations in sea-surface temperature. *Dynam. Atmos. Oceans*, **8**, 267–281.
- Chelton, D. and S.-P. Xie, 2010: Coupled ocean-atmosphere interaction at oceanic mesoscales. *Oceanography*, **23** (4), 52–69.
- Chelton, D. B., M. G. Schlax, M. H. Freilich, and R. F. Milliff, 2004: Satellite measurements reveal persistent small-scale features in ocean winds. *Science*, **303** (5660), 978–983.
- Chelton, D. B., et al., 2001: Observations of coupling between surface wind stress and sea surface temperature in the eastern tropical pacific. *J. Climate*, **14** (7), 1479–1498.
- Colton, M. C., W. J. Plant, W. C. Keller, and G. L. Geernaert, 1995: Tower-based measurements of normalized radar cross-section from Lake Ontario - evidence of wind stress dependence. *J. Geophys. Res.*, **100** (C5), 8791–8813.
- Donelan, M. and W. Pierson, 1987: Radar scattering and equilibrium ranges in wind-generated waves with application to scatterometry. *J. Geophys. Res.*, **92** (C5), 4971–5029.

- Donelan, M. A., 1990: *The Sea: Ocean Engineering Science*, chap. Air-sea interaction, 239–292. Wiley.
- Ebuchi, N., H. C. Graber, and M. J. Caruso, 2002: Evaluation of wind vectors observed by QuikSCAT/SeaWinds using ocean buoy data. *J. Atmos. Oceanic Technol.*, **19** (12), 2049–2062.
- Edson, J. and C. Fairall, 1998: Similarity relationships in the marine atmospheric surface layer for terms in the TKE and scalar variance budgets. *J. Atmos. Sci.*, **55**, 2311–2328.
- Edson, J., A. Hinton, K. Prada, J. Hare, and C. Fairall, 1998: Direct covariance flux estimates from mobile platforms at sea. *J. Atmos. Oceanic Tech.*, **15**, 547–562.
- Edson, J., et al., 2007: The coupled boundary layers and air-sea transfer experiment in low winds. *Bull. Amer. Met. Soc.*, **88** (3), 341–356.
- Edson, J. B., C. J. Zappa, J. A. Ware, W. R. McGillis, and J. E. Hare, 2004: Scalar flux profile relationships over the open ocean. *J. of Geophys. Res.*, **109**.
- Fairall, C. W., E. F. Bradley, J. E. Hare, A. A. Grachev, and J. B. Edson, 2003: Bulk parameterization of air-sea fluxes: Updates and verification for the COARE algorithm. *J. Climate*, **16**, 571–591.
- Fairall, C. W., E. F. Bradley, D. P. Rogers, J. B. Edson, and G. S. Young, 1996: Bulk parameterization of air-sea fluxes for Tropical Ocean-Global Atmosphere Coupled-Ocean Atmosphere Response Experiment. *J. of Geophys. Res.*, **101** (C2), 3747–3764.
- Freilich, M. and R. Dunbar, 1999: The accuracy of the NSCAT 1 vector winds: Comparisons with National Data Buoy Center buoys. *J. of Geophys. Res.*, **104** (C5), 11 231–11 246.
- Hanawa, H. and L. Talley, 2001: Mode waters. *Ocean Circulation and Climate*, J. Siedler, J. Church, and J. Gould, Eds., Academic Press, 373–386.
- Hosom, D. S., R. A. Weller, R. E. Payne, and K. E. Prada, 1995: The IMET (improved meteorology) ship and buoy systems. *J. Atmos. Ocean. Tech.*, **12** (3), 527–540.

- Kara, A. B., A. J. Wallcraft, and M. A. Bourassa, 2008: Air-sea stability effects on the 10 m winds over the global ocean: Evaluations of air-sea flux algorithms. *J. Geophys. Res.*, **113** (C4).
- Larsen, S. E., J. B. Edson, C. W. Fairall, and P. G. Mestayer, 1993: Measurement of temperature spectra by a sonic anemometer. *J. Atmos. Oceanic Technol.*, **10**, 345–354.
- Liu, W., 1984: The effects of the variations in sea-surface temperature and atmospheric stability in the estimation of average wind-speed by SEASAT-SASS. *J. Phys. Oceanogr.*, **14** (2), 392–402.
- Liu, W. T. and W. Tang, 1996: Equivalent neutral wind. JPL Publication 96-17, Jet Propulsion Laboratory.
- Marshall, J., et al., 2009: Observing the cycle of convection and restratification over the Gulf Stream system and the subtropical gyre of the North Atlantic Ocean: preliminary results from the CLIMODE field campaign. *Bull. Amer. Met. Soc.*, **90**, 1337–1350.
- Miller, S., C. Friehe, T. Hristov, and J. Edson, 2008: Platform motion effects on measurements of turbulence and air-sea exchange over the open ocean. *J. Atmos. Oceanic Technol.*, **25**, 1683–1694.
- O'Neill, L., D. Chelton, and S. Esbensen, 2003: Observations of SST-induced perturbations of the wind stress field over the Southern Ocean on seasonal timescales. *J. Climate*, **16** (14), 2340–2354.
- O'Neill, L., D. Chelton, and S. Esbensen, 2005: High-resolution satellite measurements of the atmospheric boundary layer response to SST variations along the Agulhas Return Current. *J. Climate*, **18** (14), 2706–2723.
- O'Neill, L. W., D. B. Chelton, and S. K. Esbensen, 2010a: The Effects of SST-Induced Surface Wind Speed and Direction Gradients on Midlatitude Surface Vorticity and Divergence. *J. Climate*, **23** (2), 255–281.

- O'Neill, L. W., S. K. Esbensen, N. Thum, R. M. Samelson, and D. B. Chelton, 2010b: Dynamical Analysis of the Boundary Layer and Surface Wind Responses to Mesoscale SST Perturbations. *J. Climate*, **23** (3), 559–581.
- Park, K., P. Cornillon, and D. Codiga, 2006: Modification of surface winds near ocean fronts: Effects of Gulf Stream rings on scatterometer (QuikSCAT, NSCAT) wind observations. *J. Geophys. Res.*, **111** (C3).
- Plagge, A. M., D. C. Vandemark, and D. G. Long, 2009: Coastal Validation of Ultra-High Resolution Wind Vector Retrieval from QuikSCAT in the Gulf of Maine. *IEEE Geosci. Remote Sens. Lett.*, **6** (3), 413–417.
- Portabella, M. and A. Stoffelen, 2009: On Scatterometer Ocean Stress. *J. Atmos. Oceanic Technol.*, **26** (2), 368–382.
- Skyllingstad, E. D. and J. B. Edson, 2009: Large-eddy simulation of moist convection during a cold air outbreak over the gulf stream. *J. Atmos. Sci.*, **66**, 1274–1293.
- Small, R. J., et al., 2008: Air-sea interaction over ocean fronts and eddies. *Dyn. Atmos. Oceans*, **45** (3-4, Sp. Iss. SI), 274–319.
- Tang, W. Q., W. T. Liu, and B. W. Stiles, 2004: Evaluations of high-resolution ocean surface vector winds measured by QuikSCAT scatterometer in coastal regions. *IEEE Trans. Geosci. Rem. Sens.*, **42** (8), 1762–1769.
- Torres, R., E. D. Barton, P. Miller, and E. Fanjul, 2003: Spatial patterns of wind and sea surface temperature in the Galician upwelling region. *J. Geophys. Res.*, **108** (C4).
- Verschell, M., M. Bourassa, D. Weissman, and J. O'Brien, 1999: Ocean model validation of the NASA scatterometer winds. *J. Geophys. Res.*, **104** (C5), 11 359–11 373.
- Weissman, D. and H. Graber, 1999: Satellite scatterometer studies of ocean surface stress and drag coefficients using a direct model. *J. Geophys. Res.*, **104** (C5), 11 329–11 335.
- Weissman, D., et al., 1997: Measurements of ocean surface stress using aircraft scatterometers. *J. Atmos. Oceanic Technol.*, **14** (4), 835–848.

- Weissman, D. E., 1990: Dependence of the microwave radar cross-section on ocean surface variables - Comparison of measurements and theory using data from the Frontal Air-Sea Interaction Experiment. *J. Geophys. Res.*, **95 (C3)**, 3387–3398.
- Weissman, D. E., K. L. Davidson, R. A. Brown, C. A. Friehe, and F. Li, 1994: The relationship between the microwave radar cross-section and both wind-speed and stress - model function studies using Frontal Air-sea Interaction Experiment data. *J. Geophys. Res.*, **99 (C5)**, 10 087–10 108.
- Zhang, F. W., W. M. Drennan, B. K. Haus, and H. C. Graber, 2009: On wind-wave-current interactions during the shoaling waves experiment. *J. Geophys. Res.*, **114**.

CHAPTER 5

Overall Conclusions

5.1 Summary

Ocean surface vector winds can be derived using satellite radars whose signal return magnitude (backscatter) depends on the roughness of the sea surface; because this roughness is primarily a function of wind speed and direction, radar backscatter can therefore be inverted through a model function to provide an estimate of vector wind. This process is called ocean wind scatterometry, and provides wind products commonly used in many applications. However, the roughness of the sea surface is not only a product of wind speed and direction, and can be influenced by additional atmosphere and ocean processes. This dissertation combines varied satellite scatterometer products from multiple sensors, collocated *in situ* measurements including wind, wind stress, surface currents, and air and water temperatures, and model simulations to evaluate long-standing assumptions that are often relied upon to interpret scatterometer vector winds in areas of complex air-sea dynamics. The observations that make up these datasets, including multi-year time series at numerous buoy locations and a set of direct eddy covariance flux and wind stress measurements at a mooring near the Gulf Stream, allow new approaches to older questions, as well as original investigations pertinent to adding to the general understanding of scatterometer data interpretation and application.

The work comprising this dissertation indicates that:

1. Ultra high resolution scatterometer winds from the SeaWinds sensor are valid even in coastal areas, providing a potential new tool for researchers interested in spatial wind field dynamics at scales of 5-20 km.
2. Satellite scatterometer wind retrievals, in contrast to *in situ* winds from buoy moor-

ings, appear to yield a measurement of wind flow relative to the motion of the ocean surface for Ku-band measurements as well as certain C-band products.

3. Wind products derived using scatterometry can appropriately be compared with winds that have been corrected for stability effects, and as such can be used to investigate changes in near-surface wind flow in the presence of sea surface temperature fronts.
4. Given the datasets used here, geophysical differences between scatterometer winds and anemometer winds are greater than differences between winds from sensors operating at different frequencies. However, artificial differences are created when satellite data are created using different processing methods, and the importance of cross-platform-calibration especially in areas of complex air-sea interaction cannot be ignored.

These conclusions and the methods employed should prove useful to the scientific community, as they provide much needed new support – even in areas of complex air-sea dynamics – for the use of theories that have been in place for decades.

5.2 Future work and implications

The work described has made several key steps to better verify the application scatterometer data as equivalent neutral 10 m winds in regions of complex air-sea coupling. Information gained from the study will be useful to many areas of society, from scientists, modelers and weather forecasters to Coast Guard emergency responders, boaters, and wind farm developers. Some of the possible impacts are discussed below.

5.2.1 Support for further scatterometer missions

As the 2007 National Research Council’s Decadal Survey of Earth Science and Applications from Space states, the satellite ocean vector wind measurements provided by

QuikSCAT have been invaluable to scientists and operational users alike [National Research Council (2007)]. The failure of the satellite since that time has left a gap that is only partially filled by the European scatterometer ASCAT and the Indian Space Research Organization's OSCAT¹. This is why much thought and effort has been focused on developing the next generation scatterometer: the NASA/NOAA extended ocean vector wind mission (XOVWM). This new mission is intended to go beyond QuikSCAT's objectives to deliver such additional benefits as higher spatial resolution and better coverage in coastal regions. These advantages are crucial to improved predictions of hurricanes and storm surges, better coastal circulation modeling for hazard prediction, and more accurate estimates of ocean upwelling in regions that are important to fisheries management: all applications integral to NASA's mission. Although the status of the XOVWM is now unclear, the results of this dissertation are clearly applicable for future extensions of scatterometry, in the US and within the international satellite community.

5.2.2 Ocean Modeling: wind work and curl of wind stress

Wind stress is the fundamental forcing term driving ocean currents, and of great concern to oceanographers attempting to model global ocean circulation. Hughes and Wilson (2008) indicate that accounting for ocean currents in scatterometer-ENW-derived wind stress can result in a decrease of 20-35% compared with non-current-corrected wind calculations. A change in wind work of this magnitude would result in a reduction of power from ocean currents by about 0.19 TW [Hughes and Wilson (2008)]. In addition to wind work, changes in global stress estimates from scatterometer would affect the curl of wind stress, another variable used by ocean modelers [Chelton et al. (2004)]. Given that this dissertation supports the current-relative nature of scatterometer retrievals, these issues can more accurately be resolved. By including a current "correction" in their study, Hughes and Wilson (2008) are accounting for something that is already built into the data. This dissertation provides ev-

¹ISRO's OSCAT is a Ku-band pencil scatterometer aboard Oceansat-2, an ocean-observing satellite launched in 2009. It was designed to be very similar to QuikSCAT's SeaWinds sensor, and cross-calibration has been reasonable. However, the satellite's lower orbit means that repeat times at a given location are not as frequent as they were for QuikSCAT.

idence that stress calculated from scatterometry can be considered current-relative at least at the scales of 20 km and larger that are typically of interest in prediction of circulation dynamics.

5.2.3 Offshore wind resource for power generation

Currently, offshore wind resource mapping is done by companies such as AWS Truewind, who use proprietary numerical models to produce maps of wind speed and expected power generation capability. Scatterometry is generally not utilized, as standard products do not reach close enough to the coast [Bailey (2009)]. Previous studies have used synthetic aperture radar data and numerical weather prediction models for wind field assessments [Beaucage et al. (2007); Ben Ticha (2007)]. In future work, it would be possible to create a UHR climatology corrected for stability and currents that would overlap with existing resource maps, allowing external validation of modeled wind resources. Further scientific support could be provided in the form of a regional study of New England sea breeze patterns. The sea breeze is primarily a summer phenomenon, and therefore its impacts on the resource predictions for this time of peak power consumption are of concern to AWS Truewind and several state agencies and wind farm developers [Bailey (2009)].

A related application for the corrected UHR winds would be to examine the extent to which scatterometer sampling of offshore wind speeds realistically represents wind speed distributions, a crucial assumption for resource assessment [Barthelmie and Pryor (2003)].

5.2.4 Equivalent neutral wind versus wind stress

The work here indicates that scatterometer winds appear to represent equivalent neutral winds. This is contrary to the conclusions drawn by Portabella and Stoffelen (2009), who found that ENW winds from the C-Band ERS scatterometer were statistically equivalent to true wind. The difference in results is likely due to the fact that the previous study had significant uncertainty due to the parameterizations used in the surface layer models necessary

to convert true wind to neutral wind, whereas this work relied upon the direct measurements available at the CLIMODE mooring. Although the results seen in Chapter 4 have yet to be replicated for C-band scatterometry, the collective conclusion of this work is that scatterometer winds are measurably different from stability-dependent winds, and in fact are much closer to ENW. This implies that, for future studies, researchers can be confident in their assumption of scatterometer ENW, but should potentially be concerned about the application of surface layer models to scatterometer retrievals to retrieve anemometer winds.

Although this dissertation supports the validity of scatterometer ENW, a direct scatterometer wind stress or friction velocity product might yet prove itself to be a valuable addition to the oceanographer's arsenal. As discussed in previous chapters, wind stress and radar backscatter are affected by wave properties and atmospheric stability in a similar fashion [Colton et al. (1995); Weissman (1990)]. The rarity of direct *in situ* stress measurements has limited the development of such an alternate scatterometer model function, but observations and results seen here, and specifically the dataset used in Chapter 4, provide fresh impetus for further efforts. Future work with additional direct eddy covariance flux measurement moorings in different regions and collocated scatterometer retrievals of various frequencies and resolutions should allow progress towards the validation of a scatterometer-derived stress product.

Bibliography

- Bailey, B., 2009: Personal communication, Apr. 3.
- Barthelmie, R. J. and S. C. Pryor, 2003: Can satellite sampling of offshore wind speeds realistically represent wind speed distributions? *Journal of Applied Meteorology*, **42**, 83–94.
- Beaucage, P., A. Glazer, W. Y. Choisnard, M. Bernier, R. Benoit, and G. Lafrance, 2007: Wind assessment in a coastal environment using synthetic aperture radar satellite imagery and a numerical weather prediction model. *Canadian Journal of Remote Sensing*, **33 (5)**, 368–377.
- Ben Ticha, M. B., 2007: Remotely sensed data fusion for offshore wind energy resource mapping. Ph.D. thesis, Ecole des Mines de Paris.
- Chelton, D. B., M. G. Schlax, M. H. Freilich, and R. F. Milliff, 2004: Satellite measurements reveal persistent small-scale features in ocean winds. *Science*, **303 (5660)**, 978–983.
- Colton, M. C., W. J. Plant, W. C. Keller, and G. L. Geernaert, 1995: Tower-based measurements of normalized radar cross-section from Lake Ontario - evidence of wind stress dependence. *Journal of Geophysical Research-Oceans*, **100 (C5)**, 8791–8813.
- Hughes, C. W. and C. Wilson, 2008: Wind work on the geostrophic ocean circulation: An observational study of the effect of small scales in the wind stress. *Journal of Geophysical Research-Oceans*, **113 (C2)**, doi:10.1029/2007JC004371.
- National Research Council, 2007: *Earth Science and Applications from Space: National Imperatives for the Next Decade and Beyond*. National Academies Press, Washington, D.C., ISBN: 0-309-66714-3.
- Portabella, M. and A. Stoffelen, 2009: On Scatterometer Ocean Stress. *Journal of Atmospheric and Oceanic Technology*, **26 (2)**, 368–382, doi:10.1175/2008JTECHO578.1.

Weissman, D. E., 1990: Dependence of the microwave radar cross-section on ocean surface variables - Comparison of measurements and theory using data from the Frontal Air-Sea Interaction Experiment. *Journal of Geophysical Research-Oceans*, **95 (C3)**, 3387–3398.